Magnetic bionanocomposites with low melting temperature: Fabrication, Characterization, and Application

Dissertation

zur Erlangung des akademischen Grades Doktor rerum naturalium

(Dr. rer. nat.)

vorgelegt dem Rat der Chemisch-Geowissenschaftlichen Fakultät der

Friedrich-Schiller-Universität Jena

Von M. Sc. Mengbo Zhou

geboren am 4. Mai 1986 in Guiyang, China

1. Gutachter: Prof. Dr. Thomas Heinze

2. Gutachter: Prof. Dr. Felix Schacher

Tag der öffentlichen Verteidigung: 13. Nov. 2019

Life in Jena is a travel in the train along the Saale river with a 4 years ticket valid for the Ph.D study. You see the sweet and bitterness through the window. The daily walking line is from Jenzig to Landgräfe. Finally I found that it is written on the table “Einsicht ist der erste Schritt zur Besserung“ (Insight is the first step for improvement).

List of abbreviations

AC, Alternating current;

AFM, atomic force microscopy;

AGU, anhydroglucose unit;

AMF, alternating magnetic field;

APIs, active pharmaceutical ingredients;

CA, contact angle;

CDI, *N,N′*-Carbonyldiimidazole;

CMD, carboxymethyl dextran;

DCC, dialkylcarbodiimide;

DMA, dimethylacetamide;

DMSO, dimethyl sulfoxide;

DMTA, dynamic mechanical thermal analysis;

DP, degree of polymerization;

DS, degree of substitution;

GFP, green fluorescent protein;

LCST, low critical solution temperature;

MNP, magnetic nanoparticle;

MRI, magnetic resonance imaging;

M_w, weight average molecular weight;

NBC, nanobiocomposites;

NMMO, N-methylmorpholine-N-oxide;

NMR, nuclear magnetic resonance;

PNIPAAm, poly(N-isopropylacrylamide);

PNIPAm, poly(N-isopropylamide);

RhB, rhodamine B;

SEC, size-exclusion-chromatography;

SEM, scanning electron microscope;

SHP, specific heating power;

Contents

List of figures

List of table

1. Introduction

Magnetic nanocomposites, mostly composed of polymer matrix and magnetic particles, can be applied for clinical diagnostics and therapies. They combine the advantages of enhanced area-specific localization, larger penetration depth in the body (> 10 cm), and high response time. Nowadays, magnetic nanocomposites are intensively studied in the field of hyperthermia[1-3], microfluidic devices[4-5], controlled release[6-7] and shape memory polymers[8]. Magnetically responsive drug delivery systems belong to exogenous stimuli-responsive materials, besides light, ultrasonic, pH value. Alternating current is an electric current, which periodically reverses direction. According to Ampère's circuital law, an alternating integrated magnetic field can be generated around a closed loop to the alternating electric current passing through the loop. Alternating current (AC) magnetic field or oscillating magnetic field is required for heating purpose, which is realized through two mechanisms: a) hysteresis loss for ferromagnetic particles and/or b) Neel and Brownian relaxation for superparamagnetic particles.[9-10]

Swellable hydrogel nanocomposites and thermally responsive lipids[8, 11] embedded with magnetite particles have been reported as magnetic remote controlled biomaterials. For example, poly(N-isopropylacrylamide) (PNIPAAm)[12] and poly(N-isopropylamide) (PNIPAm) based magnetic hydrogels[13-14] are usually used in the application. The PNIPAm hydrogels are thermosensitive and have a low critical solution temperature (LCST) usually around 32 °C. Above the LCST, the polymer collapse and active pharmaceutical ingredients (APIs) are squeezed out. Nevertheless, magnetic hydrogels have some shortcomings including low biocompatibility, poor biological degradability, long relaxation times and weak mechanical properties, which need to be improved.[12] Therefore in this work it is aimed to develop a new approach towards magnetically responsive biomaterials by exploitation of thermoplastic biopolymers.

Many efforts have been put to transfer non meltable polysaccharide in to meltable derivatives, because meltable polymer is easy to be processed. Unfortunately, the majority of the relevant biopolymers decompose before melting. In 2011, a method for the synthesis of pure dextran fatty acid esters by activation of the fatty acids with iminium chloride was reported.[15] The hydrophobic and completely bio-based dextran derivatives show adjustable thermoplastic behavior with a melting point in the range from 30 °C to about 140 °C depending on the detailed structure. The melting

temperature could be tailored by the type of substituent introduced, the amount of functionalization and the molecular weight of the polymer. For a biomedical propose, these derivatives are biocompatible and exhibit good adhesion on ceramics, metals, and polymer materials.

Therefore the task in this work is to use this class of biopolymers for the preparation of magnetically responsive biomaterials. Synthesis of proper starting materials, fabrication of the nanobiocomposites (NBC) and the magnetic and thermal behavior of this new nanocomposite were investigated to gain a "proof of principle" regarding to this approach. It could be shown that defined remote melting with an induced alternating magnetic field (AMF) of the biocompatible nanocomposites is possible. The composite disks were loaded with rhodamine B (RhB) and Green fluorescent protein (GFP) as model drugs, separately. Controlled release of the RhB was realized with high frequent AMF of 20 kA/m at 400 kHz, which shows that the cumulative release of RhB from magnetic composite was accelerated compared to the control sample without exposure to AMF. It was found that leaking can be avoided and a pulsatile release of GFP can be started while AMF was turned on.

Besides of controlled release, it was studied if it is possible to influence the surface properties of NBC by using magnetic fields. It will be investigated if local enrichment of particles and a structural, i.e., magnetic anisotropy could influence the surface properties of NBC. Surface topography can be influenced by the anisotropy or particle enrichment of magnetic particles near the surface of NBC. That could lead to macroscopical properties relevant for applications, like the specific absorption rate (heating behavior in an alternating current-magnetic field), surface roughness, wettability, *etc*. The NBC were characterized by scanning electron microscopy, vibrating sample magnetometer and static measurement of the contact angle with water drop.

The work carried out presents a promising magnetic responsive material in complementary to magnetic hydrogels. The results in this study bridge the gap between the medical application and fundamental research. However, the biodegradation mechanism of this material is not fully understood. Other aspects, such as loading capacity of drug and hemocompatibility are needed to be studied.

2. State of art

2.1. General aspects of polysaccharides and their derivatives

2.1.1. Polysaccharides

To pursue a sustainable and green society, polysaccharides and their derivatives have attracted great attention due to their biodegradability, renewability, and eco-sustainability. Polysaccharides have been used since ancient time, while the petroleum based synthetic polymers have been exploited and used on large scale only since 1950s. The wide range natural occurrence of polysaccharides can be found from plants, microorganisms, fungi, marine organisms, and animals as storage and structure forming macromolecules. The most common polysaccharides are cellulose, starch, chitin, dextran, curdlan and alginate.[16-18] Cellulose is the most abundant polymer in the world, whose annual amount of naturally produced is estimated around 1.5×10^{12} tons.[19] Chitin is the second largest most abundant polysaccharide ranking after cellulose, which are typically obtained from invertebrates like crabs, insects, and fungi.[20] Starch, whose components are divided into amylose and amylopectin, is one important energy source for human beings.[21]

In order to turn polysaccharide into other useful products, two concepts are widely investigated. One is fiber fabrication of cellulose through shape forming by regenerating it from a solvent. For example, cellulose fiber is regenerated from N-methylmorpholine-N-oxide (NMMO) process, whose product is called Lyocell. The other one is through chemical modification. In the chemical industry, heterogeneous reactions for polysaccharide ethers in water and base are usually carried out due to the cost reason of solvent. Dimethylacetamide/lithium chloride (DMAc/LiCl), ionic fluids, DMSO under some condition can yield homogeneous polysaccharide solutions, are widely used in the academic research. These conditions guarantee excellent control of the degree of substitution (DS) of hydroxyl group on the repeating unit of polymer, so they can be exploited for the preparation of soluble, partially substituted derivatives. They can lead to new patterns of substitution as well. A lot of research on homogenous reactions can be found in the literature.[22] DMAc/LiCl solvent system has been widely used to dissolve polysaccharide as it does not cause degradation and shows almost no interaction with acylation reagents. But until now the solving mechanism of

polysaccharides with DMAc/LiCl is not completely understood still unknown. One most reasonable model was proposed.[23] It is supposed that an ionic pair $[Li \cdot DMAc]^+Cl^-$ could push the intermolecular hydrogen bond aside and solve the polysaccharide.

Regioselectivity is an important issue in the functionalization of polysaccharide. Taking cellulose as an example, the most preferred hydroxyl group for the esterification reaction is the primary one, which is located on C-6, while the secondary hydroxyl groups on the C-2 and C-3 positions of the anhydroglucose unit (AGU) react slower due to their steric hindrance.[16]

2.1.2. Esterification of polysaccharide

The polysaccharides derivative can be mainly divided into two groups according to the type of chemical reaction on the hydroxyl group: esterification and etherification. The esterification is one the most versatile classes of transformation of polysaccharide, which have been widely researched.[22] Various pathways for the esterification of cellulose have been investigated. Some inorganic polysaccharide esters are widely found such as polysaccharide sulfate and phosphate.[24] But the focus of this thesis is the esterification of polysaccharides with organic acids. The commercial paths of polysaccharide esterification are carried out exclusively under heterogeneous conditions, at least at the beginning of the conversion. For example, the majority of cellulose acetate (about 900 000 t per year) is based on a route that includes the dissolution of the products formed.[25]

Furthermore, new methods with carboxylic acids after in situ activation have been developed for esterification of polysaccharides in homogeneous condition: respectively through Tosyl chloride, dialkylcarbodiimide (DCC)[26], *N,N′*-Carbonyldiimidazole (CDI).[27] In contrast to heterogeneous reaction, they can have better control of DS and of the solubility of partially substituted derivatives. Cellulose esters were prepared by heterogeneous esterification in Pyridine and tosyl chloride with unsaturated or saturated long chain organic acids.[28] Acylation reactions of starch and cellulose via transesterification with methyl esters of palmitic and stearic acid were reported; the reaction was achieved in a double-screw device without solvent at a temperature ranging between 180 and 230 °C.[29] Dextran was enzymatically derivatized with vinyl acrylate supported by the catalytic activity of Proleather FG-F and lipase AY, a protease and lipase from *Bacillus* sp. and *Candida rugosa,* respectively in anhydrous DMSO.

Product with DS of up to 0.37 was reported.[30] Under catalyst of NaOH and KOH are used as catalyst to synthesize cellulose esters reacted with vinyl acetate, vinyl propionate, and vinyl butyrate in DMSO.[31] Acylation with carboxylic acid chlorides or anhydrides on cellulose and starch can generate thermoplastic products, which will be explained in detail in the coming part.

2.1.3. Thermoplastic polysaccharide derivatives by esterification

The intra- and intermolecular hydrogen bond between the hydroxyl groups and oxygen atoms of the ring and the glycosidic bond build up the rigidity and stiffness of polysaccharides, so they are not thermoplastic. Even a lot of polysaccharide derivatives are not thermoplastic. From a technical point of view, thermoplastic polysaccharides are of great interests, because they are easy to be processed by extrusion and molding into different forms. This means that they can be used for manufacturing of many kinds of thermo-processable products, such as films, bags (for shopping or waste) for packaging, and other one-off products.

One of widely used method to produce thermoplastic products is plasticization of starch under specific extrusion conditions and in the presence of plasticizers, such as glycerol and water, into thermoplastic starch (TPS).[32-33] Due to the moisture sensitivity and critical ageing in TPS, it has led to the necessity to blend TPS with other polymers, polyethylene polycaprolactone (PCL), polylactic acid (PLA), polyhydroxybutyrate-co-valerate (PHBV), and polyesteramide, on one hand.[34]

On the other hand, chemical modification of polysaccharides results in a diverse product and new functionalities. Esterification is one of these important methods. Typical cellulose derivatives are cellulose acetate, cellulose acetobutyrate, benzyl cellulose shown in Table 1. For example, cellulose acetate is produced by conversion of cellulose with a mixture of acetic acid and acetic anhydride in presence of sulfuric acid as a catalyst, which can form acetyl sulfuric acid during the acetylation reaction. By derivatising the hydroxyl groups, intra- and intermolecular hydrogen bond between the hydroxyl groups in positions 2, 3 and 6 of the AGU can be broken. As a result, a thermoplastic polysaccharide product can be obtained. As the level of substitution increases, however, the biodegradability is reduced because obviously a certain number of non-substituted glucose units must be present for the sterically demanding enzyme attack.[35-36] Approaches enabling effective thermoplasticization and further incorporation

of material functionalities into structural polysaccharides was reviewed by Teramoto[37], including blending of simple derivatives with synthetic polymers, and graft copolymerization. Cellulose triacetate and diacetate with degree of polymerization (DP) values in the range from 100 to 360, are produced for various applications, such as eyewear frames, textile fiber, filter tow, food packaging *etc*.[38] Long alkyl groups can be introduced into the polymer backbone to have an internal softening effect and to decrease the melting point. An internal plasticizing effect is caused by the covalently bound long chain fatty acids by ester linkages. The advantage is clearly that no plasticizer is needed to add in. Cellulose fatty esters were synthesized by using the acid chloride in the presence of pyridine. The mechanic properties of cellulose fatty esters studied by dynamic mechanical thermal analysis (DMTA) was reported.[39] The partially substituted cellulose esters behave in a very different way than fully substituted cellulose esters on the T_g, the thermal expansion coefficient, tan δ, and the dynamic elastic modulus. T_g and elastic modulus vary with the number of carbon atoms in the linear acyl group for partially substituted cellulose esters, but they remain constant for the fully substituted cellulose esters.

Besides cellulose, long chain fatty acid starch esters have also been reported. Conversion of starch with acid chlorides in organic solvents in the presence of a base (for example, pyridine) is the method of choice for the preparation of long chain aliphatic esters. [40] However, these products are not fully meltable and they are not transparent. Liebert *et al*, developed chloride-esterification approach in imidazole as an alternative reaction media, which results in a meltable and transparent starch ester. [41] Winkler *et al*. reported that starch laurates (DS > 2) were obtained through transesterification of fatty acid vinyl esters in DMSO. [42] In these starch long chain fatty esters, an internal plasticizing effect is caused by the covalently bound long chain fatty ester groups. The advantage is clearly that no plasticizer is needed to add into polymers.

Table 1. Some thermoplastic polysaccharide derivatives and their structure.

Derivatives	Repeating unit	R group	Reference
Cellulose acetate	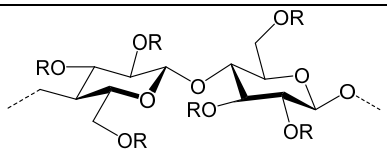	H, or 	36
Cellulose acetate butyrate	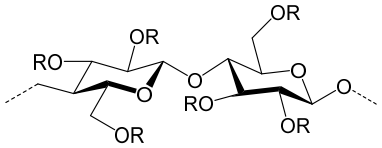	H, 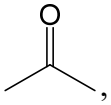 , 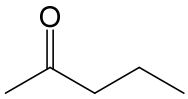	44
Starch palmitate	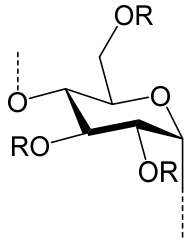	$CO(CH_2)_{14}CH_3$	42
Dextran myristate	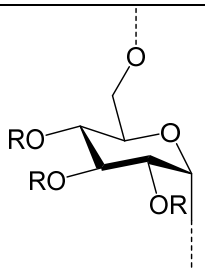	$CO(CH_2)_{12}CH_3$	15

2.2. Polymers with low melting temperature nearly human body temperature

2.2.1. Overview of polymers with low melting temperature

Engineering polymers are usually required to have high melting temperature in order to have heat stability. That is to say, the T_m is much higher than the continuous service temperature. For example, the polymers such as polyethylene and propylene have T_m around 100 and 160 °C, respectively. Some high performance polymers have even high T_m, like polyether ether ketone (PEEK) with T_m of 340 °C.[43] The above mentioned cellulose acetates (2.1.3.) usually have melting temperature of 200 °C.

However, in industry, some polymers with low melting temperature such as: special polyolefins with melting range between 40 and 50 °C, which are applied in fields of adhesive modifier, resin modifier, and wax modifier[44] as well as ethylene/vinyl acetate (EVA) copolymers are used for sealants in meat and dairy packaging, footwear, wire, and cable insulation.[45] However, these polymers are not biocompatible and not suitable for biomedical application.

In the academic research field, polymers with low melting temperature have been reported, which are not used for structuring materials due to weak mechanic properties. But they can be developed for some niche products, such as scaffolds for tissue engineering that are based on poly(benzyloxymethyl glycolide-co-ε-caprolactone),[46] and shape memory material as smart punctual plugs based on polylactide.[47] High functionalized meltable long chain aliphatic acid ester of cellulose was synthesized by mixing carboxylic acid with trifluoroacetic acid anhydride (TFAA)as an impeller.[48-49] Esterification of starch with long-chain aliphatic carboxylic acids using the corresponding chlorides are realized with in situ activation with tosyl chloride and CDI. But the products obtained with both above-mentioned methods do not have melting range close to 40 °C.[50] In the coming subsection it will explain why dextran is chosen for the starting material.

2.2.2. Dextran and its derivatives

Scheibler gave the name „Dextran" in 1874, when he found the carbohydrates having a positive optical rotation in thickening cane sugar and beet sugar. [51] Dextran consists of an α-(1→6)-linked D-glucose varied from 50 % to 97 % in main chain with varying proportions of linkages and branches depending on the strain of bacteria applied. Possible linkages are α-(1→2)-, α-(1→3)- and α-(1→4) branches. [52] It can be produced by fermentation either with *Leuconostoc mesenteroides* strains and other lactic acid bacteria or with certain *Gluconobacter oxydans* strains. [53] *Leuconostoc mesenteroides* strain NRRL B-512F is used for most important commercial dextran production, which has a relatively low level (about 5 %) α-(1→3) branch linkage detected by methylation [54] Major producers of dextran apply the batch-wise culture *Leuconostoc mesenteroides* NRRL B512(F) or B512 strains in the presence of sucrose. For clinical and technical dextran, the partial hydrolysis and further fractionalization of native dextran gives products with the desired molecular sizes. [55]

Dextran has an amorphous structure. Dextran is used for medical application. A 6 or 10 % aqueous solution (40,000–100,000 g/mol) are at present available for replacing moderate blood losses. It can substitute blood proteins, e.g. albumins, in providing colloid osmotic pressure to pull fluid from the interstitial space into the plasma. The high percentage of α-(1→6)-glycosidic linkages is responsible for the biological stability in the human bloodstream. Because of the narrow molecular weight distribution, specific fractions are used as size-exclusion-chromatography (SEC) standard for molecular weight determination.[16] Dextran-coated iron oxide nanoparticles can be versatile platforms for targeted molecular imaging, molecular diagnostics, and therapy.[56]

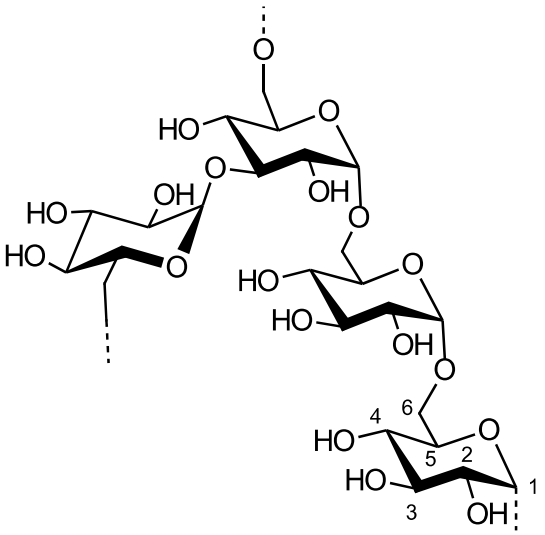

Figure 1. Part of α- (1→6)-linked glucose main chain of dextran (Leuconostoc mesenteroides NRRL B-512F strain) with branching of α-(1→3) linkage.

Due to its biocompatible-, biodegradable-, non-immunogenic-, and non-antigenic properties and pure structure, dextran has been chemically functionalized into versatile products for medical and biomedical application.[57] The modification is on the three secondary hydroxyl groups at C2, C3 and C4 position in the glucose unit. For example, dextran sulfate sodium salt (DS = 2.3), a water soluble product, is an available product by Sigma Aldrich, e.g. It is used to accelerate hybridization rates of nucleic acids.[58] Another example of dextran derivative is carboxymethyl dextran (CMD) that can be obtained in isopropanol/water using monochloroacetic acid (MCA) under strong alkaline conditions (Eg. 3.8M aqueous NaOH). It may be used as a matrix component to prepare surfaces for cell adherence and culture and in the construction of polymer membranes used in the development of biomaterials/biostructures for applications such as drug delivery. Coating of CMD on iron oxides has been widely reported.[59-60] Dextran alkyl carbonates were synthesized applying ethyl chloroformate, butyl chloroformate, butyl fluoroformate.[61] Spermine modified acetalated-dextran was reported to be used to efficiently encapsulate siRNA.[62]

2.2.3. Dextran fatty acid esters with low melting temperature

The above mentioned biocompatible-, biodegradable-, non-immunogenic-, and non-antigenic properties are the reasons why dextran is studied in this work as matrix material for magnetically responsive biomaterials. Fractionated dextran has narrow molecular weight distribution and more defined structure. Therefore, dextran could be a

suitable starting material to obtain a biopolymer with low and narrow melting range. To achieve the aim of this work "meltable polysaccharide derivatives", esterification of dextran is the chosen strategy

Esters with short side chain, for example, dextran acetate, propionate and butyrate were esterified in dimethyl sulfoxide (DMSO) with acetic anhydride, propionic anhydride, and butyric anhydride. It was found that dextran esters having the low DS around 1.0 and constituting of short carbohydrate chains showed the best and significant enzymatic degradation and could be used as a promising carrier for specific colon drug delivery system.[63] However, the products from above-mentioned acylation do not have melting point in the range of 40 and 42 °C. Furthermore these methods have some drawbacks, when long chain acylation of dextran is needed, such as decrease in reactivity, minor solubility of the acyl anhydride, narrow availability of the anhydrides and loss of half of the acid. Therefore, other methods can be applied for esterification of dextran with fatty acid. Synthesis of long chain fatty acid esters (LCE) of polysaccharides involving acid chlorides in pyridine is a conventional method,[40] but these methods results in incomplete meltable and incompatible products because of side reactions. Some in situ activating agents have been reported to esterification of dextran as introduced in the part of 2.1.2, including *N,N′*-dicyclohexylcarbodiimide (DCC)[64] and *N,N′*-Carbonyldiimidazole (CDI)[27, 65] In comparison to DCC method, the application of CDI is much more efficient, less toxic, less side reactions and allows the use of DMSO, which is a good solvent for dextran and most of the carboxylic acids. During conversion the reactive imidazolide of the acid is generated and only CO_2 and imidazole are formed as by-products, so it is especially useful for the preparation of derivatives for biological application. For example, dextran was conjugated with poorly water-soluble drugs (ibuprofen, naproxen) via in situ activation of the carboxylic groups with CDI.[66]

It was reported by Liebert *etc.* in 2011 that a series of pure and meltable dextran fatty acid esters can be achieved with adjustable melting temperature from 30 to 140 °C.[15] The melting temperature of selected dextran ester can be fine-tuned in the range 40 – 42 °C by controlling the DS of fatty acid ester groups. The esterification of the polysaccharide by activation of the fatty acids with iminium chloride guaranteed mild reaction conditions leading to pure products as confirmed by Fourier-transform infrared (FTIR)- and nuclear magnetic resonance (NMR) spectroscopy. The melting temperature

of dextran ester is dependent on the type of substitute introduced, the degree of substitution, and the molecular weight of the polymer. Therefore, it is possible to make dextran ester with desired melting temperature. These materials with melting temperature near human body temperature could be very interesting for medical application because of the biocompatibility with cells.

The following reasons are explained why dextran ester synthesized with iminium chloride method is used in this work compared to to other esterification methods: First is the purity of product due to the gaseous by-product, which generates homogeneous and completely transparent melt. Secondly, polymer with melting temperature slightly above the human body temperature is focused. Because of the narrow molecular weight distribution, dextran is chosen for production of thermoplastic products for narrow melting temperature range rather than starch. And due to the low melting temperature the polymer undergoes a phase transition when an external stimulus generating heat is applied, for example for the controlled release application as matrix material. Therefore it is highly motivated to discover the use of these dextran fatty acid esters as polymer matrix for magnetic composites.

2.3 Magnetically responsive materials

Magnetic responsive materials can be divided into two main categories according to structure: one is composite material, in which the magnetic particles are embedded and dispersed mostly in a polymer matrix, and another one is the core-shell structure, in which the magnetic particle is coated with polymer shell.[67] In the magnetic responsive polymer composite materials, the polymer matrices bind the particles together, absorb and transfer the external load, and give the shape to the composite. The matrices are versatile, which can be fluids, elastomers, and gels, *etc*.

Due to the magnetic moment, chemical stability, and low toxicity, magnetite- (Fe_3O_4) and maghemite (γ-Fe_2O_3) nanoparticles have attracted much interest for both the fundamental investigations and biomedical application. Iron oxides (either Fe_3O_4 or γ-Fe_2O_3) can be synthesized with wet chemical method through the co-precipitation of Fe^{2+} and Fe^{3+} aqueous salt solutions by addition of a base. Compared to physical methods such as gas phase deposition and electron beam lithography[68], the wet chemical routes to magnetic nanoparticles are simpler, more tractable and more efficient with good control over size, composition and sometimes even the shape of the nanoparticles. The control of size, shape, and composition of nanoparticles depends on the type of salts used (e.g. chloride, sulphate, nitrate, perchlorate), ionic strength of the media, pH value and the ratio of Fe^{2+} and Fe^{3+}.[69] With size in the range of 6–15 nm, the iron oxide nanoparticle can be considered as a single magnetic domain, which do not retain any magnetic moment after removal of magnetic field.[70] This is called superparamagnetic behavior with high magnetic susceptibility. Because of their unique mesoscopic physical, chemical, thermal, and mechanical properties, superparamagnetic nanoparticles offer a high potential for several biomedical applications, such as: magnetic resonance imaging, hyperthermia, cellular therapy, tissue repair, drug delivery.[1] The major drawback of this wet chemical method is the broad particle size distribution.

The important property of the magnetic nanoparticle in this work is the specific heating power (SHP) that strongly depends on the size, the size distribution, and the micro-structure of the particles as well as on the alternating magnetic field amplitude and the frequency *f*.[71] Magnetic particles with optimal SHP are important for melting purpose of polymer under AMF. Furthermore, it has been known for a long time that the

magnetic nanoparticle can be orientated in a magnetic field in the viscous polymer matrix. However, the influence of magnetic orientation on the heating ability after magnetic treatment is unknown.

Magnetically responsive composites can be used for bearings and vibration absorbance, drug targeting, automotive bushings, magnetic tapes, magnetic gums, soft actuators, micromanipulators, artificial muscles, and suspension devices.[72] Following are several types of magnetically-active composites discussed.

Magnetorheological (MR) fluids are conventionally carbonyl iron particles suspended in mineral and silicone oils, synthetic hydrocarbons and water. Carbonyl iron is a highly pure iron, which is prepared by chemical decomposition of purified iron pentacarbonyl. They can exhibit changes in apparent viscosity of several orders of magnitude for applied magnetic flux densities of order of magnitude 1 T. With this property, they are used to control the vibration or to transfer the torque in vibration damper and shocker absorber, e.g..[73] Magnetorheological elastomers, providing a field-dependent material property to the material, e.g., a controllable modulus and damping, are found in application such as vibration absorber and vibration isolator.[74] Ferrogels, composed of magnetic particles and usually hydrogels, can respond to external magnetic fields in a variety of ways that include elongating, contracting and altering swelling properties.[75] Core-shell structured magnetic particles are found in field of cell separation[1], magnetic resonance imaging (MRI) contrast agents,[76] and hyperthermia.[77]

Magnetically responsive materials/composites must be distinguished from the term “soft magnetic composites” (SMCs), which are used in electromagnetic applications, can be described as ferromagnetic powder particles surrounded by an electrical insulating film.[78]

2.3.1. Magnetic composites based on polysaccharides

Magnetic particles combined polysaccharides are mainly used in biomedical field to improve the stability, biocompatibility, and biodegradability in many cases.[79] For instance, use of unmodified polysaccharide coated MNPs for imaging and gene delivery. In comparison with the non-polysaccharide coated MNPs, they have many advantages such as higher biocompatibility with the human body fluids; the elimination by white corpuscles from liver would be avoided and provides a steric barrier thereby preventing

agglomeration.[80] Fabrication of cellulose nanocrystals (CNCs) magneto-responsive self-standing films was reported for biomedical and magneto-optical components.[81] Modified polysaccharides are widely used as well, e.g., carboxymethyl cellulose (CMC) can be used as stabilizer for superparamagnetic Fe_3O_4 and act as templates for the growth of nanosized Fe_3O_4.[82] Maleilated carboxymethyl chitosan (DS=0.6) based hydrogels was investigated for magnetically assisted bioseparation in water remediation process.[83]

2.3.2. Magnetic composites for controlled release

Conventional parenteral drug delivery systems, typically including intravenous injection, occasionally cause a high plasma drug concentration, which could be close to the minimum toxic concentration. Therefore, repetitive administration is sometimes required due to the short duration of action from traditional systems.[84] To avoid the problems from conventional systems, parenteral controlled-release drug delivery systems are designed to achieve consistent, predictable or desired drug release profiles. Controlled release drug delivery can be defined as the use of whatever means possible, be it chemical, physiochemical, or mechanical, to regulate a drug´s access rate to the body´s central compartment or in some cases, directly to the involved tissues. It is desirable to improve the temporal and spatial control of drug delivery to avoid an initial fast release and a slow release later on. They can be administered typically via a parenteral route either by subcutaneous injection, intramuscular injection, or injection to other specific sites such as intra-articulate injection.[85-86] Suspensions, emulsions, liposomes, microparticles and implants are identified as parenteral controlled release drug delivery systems.[87] The systems are useful and necessary when drug candidates have poor absorption by other routes of administration and short half-lives, such as when peptides and proteins are used. Additionally, they offer benefits for patients who have difficulty with oral drug administration or are unconscious.

Based on the release mechanism, exogenous stimuli-responsive drug delivery can be divided into temperature-sensitive system[88], magnetically responsive system[13], ultrasound triggered system[89], light-[90] and electrosresponsive system[91], while endogenous stimuli-responsive drug delivery are pH-sensitive system[92] and enzyme-sensitive system.[93]

Among of those above mentioned techniques of controlled release, magnetic responsive systems combine the advantages of enhanced area-specific localization, larger penetration depth in the body (> 10 cm), and high response time. The temperature rise in magnetic composite is realized by using the energy absorbed from the alternating (or oscillating) magnetic field and transformed into heat by means of a special target material. Heat can be generated on the sites, where magnetic particles are loaded with little absorption of energy into body tissue when high frequency alternating magnetic field is used.[94] The mechanisms can be described as reversal of the magnetization inside a crystal lattice and rotation of the magnetic material relative to its surroundings understood as magnetic hysteresis.[95]

With heating generated by alternating magnetic field, the structure can change themselves allowing release of loaded molecules. Two types of systems have been reported according to the dimension: first one is particulate material (nano- and microsize) parenteral administration.[96] The applications of magnetic nanocapsules[97] are mainly found in in medicine and biology area, including purification of proteins[79], contrast agents for magnetic resonance imaging,[98] and hyperthermic treatments of tumors.[99] The second type is macroscopic materials for implantable devices.[100-101]

In the first system, magnetic guidance is typically obtained by focusing an extracorporeal magnetic field on the biological target during the injection of a magnetically responsive nanocarrier. This concept has demonstrated great potential in experimental cancer therapy because of improved drug accumulation inside solid-tumor models. Candidate nanosystems for such a therapeutic approach are core-shell nanoparticles (a magnetic core made of magnetite (Fe_3O_4) coated with silica or polymer),[102-103] magnetoliposomes (Fe_3O_4) or maghemite (Fe_2O_3) nanocrystals encapsulated in liposomes)[104], zwitterionic core-shell hybrid nanoparticles consisting of a core of iron oxide multicore nanoparticles[105] and porous metallic nanocapsules.[106] Most core-shell nanoparticles have shown promising results *in vitro*, yet only some of them have demonstrated improved tumor accumulation and anticancer pharmacological efficacy in various *in vivo* models.[9] Other examples for controlled release with nanoparticles, like phase-change materials made of 1-tetradecanol and dodecanoic acid are capable of encapsulating both hydrophobic and hydrophilic compounds. The compounds can be released after the hydrophobic matrix melted through an external

heating.[11] Polymersomes are in general prepared from macromolecular amphiphiles of various architectures including diblock copolymers, for example, poly(ethylethylene)-b-poly(ethylene glycol) (PEE-PEG).[107] The main drawbacks of NPs are related to the small amount of drug that can be linked to each NP, the possibility of drug deactivation once it is chemically bound to the NP, and the possibility of its immediate uncontrollable passive release (burst effect).[108]

Magnetic responsive polymer composite materials, investigated as implant devices for controlled release, can be for instantly coated on the artificial implantation. The main advantage of the macroscopic material is that a larger amount of drug can be loaded, in comparison to that carried by magnetic NPs in dispersion.[102] Magnetic hydrogels are one of mostly studied macroscopic materials for this application. Composites of poly(N-isopropylamide) (PNIPAM) and magnetite nanoparticles have been studied by Satarkar *et al*. for pulsatile drug release.[7] The polymer undergoes a transition from a hydrophilic to a hydrophobic structure due to the weakening of hydrogen bonding at the low critical solution temperature (LCST).[109] The LCST can be adjusted to 42 °C by modification on the molecular structure of PNIPAM. When the alternating magnetic field is turned on, heat is generated mainly though the magnetic hysteresis of embedded nanoparticles. If resulting temperatures are above LCST, the gel will collapse leading to expulsion of water. The drug can be squeezed out of the polymer matrix. When the AMF is turned off, i.e., the temperature decreases below LCST, the polymer network swells. So the release of drug is slow down. The magnetic hydrogels may have some shortcomings including poor biological degradability, long relaxation times of 1 to 2 hours for collapsing and swelling back.[6] Moreover, PNIPAM based systems have low biocompatibility because the NIPAM monomer is carcinogenic and teratogenic.[109] An alternative strategy is to combine phase transition materials into magnetic release system. The drug can be encapsulated without leaking and losing the activity. The thermoresponsive switch is based on increasing the diffusion coefficient of a drug in a polymer matrix by increasing the temperature. Externally heating results in enhanced diffusion. This means an on-demand release is possible. Several phase transition materials system have been reported, including monoglyceride-based thermoresponsive drug delivery system[110], polymer based system like poly(methyl methacrylate) (PMMA) implant[111], and poly(D, L-lactic acid) drug carrier.[112] However, these materials have some problems. PMMA implants are non-biodegradable in the human body.[113] For the

poly(lactic acid) polymer, one of the likely scenarios is that the formation of small chain carboxylic acids leads to local pH changes that cause an inflammatory response.[114]

The bio-based dextran esters with melting temperature nearly human body temperature and pure structure could be a candidate for the phase transition material system. The polymer is biocompatible and with adjustable melting in the range from 40 to 42 °C, which can be combined with magnetite nanoparticles. The thermoplastic magnetic composites may have a melting range close to human body temperature and can be easily shaped into disk or coating film under melting.

2.3.3. Switchable magnetic composite surface wettability

Magnetic switchable surfaces between hydrophobic and hydrophilic are of interest for anti-fouling and separation membranes.[115] The wetting property of a surface can be defined according to the contact angle (CA) "θ", which forms a liquid droplet on the three phase contact line (interface of three media as shown in Fig. 2). The surface tension, noted γ, is the tension which exists at the interface of two systems (solid/liquid, liquid/liquid, solid/gas). It is expressed in energy per unit of area (mJ/m^2). From this definition, it is possible to identify three forces acting on the three phase contact line: γ_{lv} (liquid surface stress/gas), γ_{sl} (liquid/solid surface stress) and γ_{sv} (solid surface stress/gas). The three forces are represented in Fig.2. In Practice, a surface is regarded as hydrophilic when the contact angle, which forms a drop with this one, is lower than 90°. In the opposite case (the contact angle is higher than 90°), the surface is hydrophobic.[115]

At the equilibrium state:

$$\gamma_{lv} \cos\theta + \gamma_{sl} = \gamma_{sv}$$

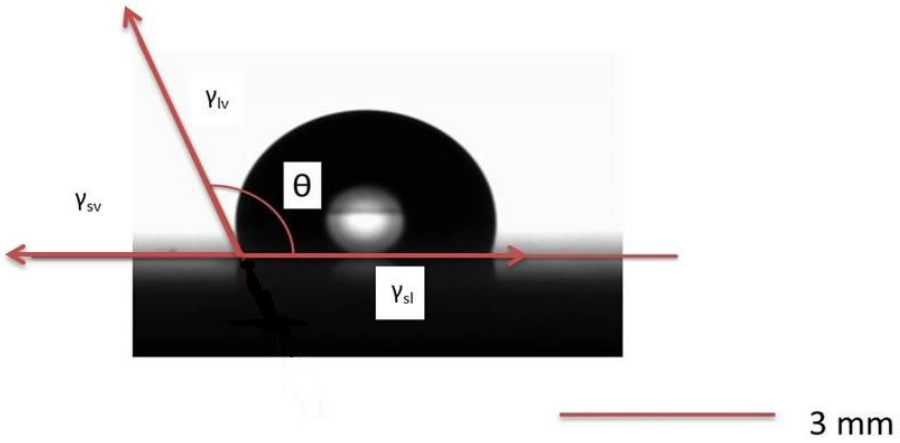

Figure 2. A picture of a sessile-drop contact angle system.

In practice, two types of CA values are used: static and dynamic CAs. Static CAs are measured when a droplet is standing on the surface and the three-phase contact line is not moving. Conversely, when the three-phase boundary is moving, dynamic CAs can be measured. The chemical compositions determine the surface free energy and the surface topographic structure are two important factor that influence the wettability.[116]

Many switchable surface wettability have been achieved through different stimuli, such as: temperature[117], light[118], mechanic[119], chemical[120] have been investigated. A lot of works are good summarized in the reviews.[72, 121] But there are few literatures are found in the field of magnetic switchable surface techniques. Katz, *et al*, found that the magnetic nanoparticles consisting of undecanoate-capped magnetite (average diameter 4.5 nm; saturated magnetization, *M*s, 38.5 emu/g) are used to control and switch the hydrophobic or hydrophilic properties of the electrode surface.[122] In the second example, it was reported that a superhydrophobic iron surface (fluoroalkylsilane coated) that has a tunable adhesive force with the superparamagnetic microdroplet (aqueous solution of Fe_3O_4 nanoparticles) as a function of the magnetic field.[123] After magnetization the adhesion on the surface was increased, since the superparamagnetic microdroplet became magnetized. In another example, magnetic micropillars with a height of 43 μm, a diameter of 18 μm, and a spacing of 22 μm were obtained by soft molding on the polydimethylsiloxane (PDMS) with carbonyl iron particles. Changing the pattern geometry (tilting) causes changes in the roll-off angle (ROA) of water droplets on the surface. The ROA corresponds to the tilting angle at which the droplet rolls off the

surface.[124] Gels sensitive to magnetic fields were obtained by incorporating colloidal magnetic particles into poly(N-isopropylacrylamide-co-N,N-dimethylacrylamide). The gel beads formed straight chainlike structures in uniform magnetic fields, while they aggregated in nonhomogeneous fields. The rapid and controllable shape changes of these gels would be expected to mimic muscular contraction.[125] However, so far as it found in the literatures, techniques on magnetic switchable surface from a polysaccharide based polymer was not reported. In the part of 3.5, it will investigate the possibility to change the surface properties of dextran ester based magnetic composite with alternating magnetic field.

3. Results and Discussion

3.1. Magnetic responsive composites

Dextran is not thermoplastic because of inter- and intramolecular hydrogen bond network. Esterification with fatty acids is a path to convert dextran into a thermoplastic and processable derivative, since the introduction of a fatty acid weakens the interaction between the macromolecules and acts as inherent plasticizer. The focus of this part is the development of the dextran esters particularly with low melting temperature. The routine to synthesize pure and meltable dextran esters and its influencing factors on the melting temperature of dextran esters will be described in the part 3.1.1. Based on these polymers and the magnetic nanoparticle described in the part of 3.1.2, a magnetic composite system will be made as discussed in the part of 3.1.3. It is going to describe the fabrication and characterization of magnetic dextran ester composites, including their thermal, magnetic, biocompatibility, and rheological properties.

3.1.1. Meltable dextran fatty acid esters

Synthesis

Esterification of dextran can be achieved by reacting of the polysaccharide dissolved in *N,N*-dimethylacetamide (DMAc)/LiCl with iminium chlorides of fatty acids [15]. The iminium chlorides can be easily prepared in an one pot reaction by conversion of *N,N*-dimethylformamide (DMF) with oxalyl chloride and subsequently reacted with the fatty acid (Fig. 3). Both the activation of the fatty acid and the esterification occur under mild and efficient conditions resulting in pure products of defined properties. The reaction conditions and results achieved by this path are summarized in Table 3.1 Products with degree of substitution (DS) in the range from 0.92 to 2.76 were accessible. Dextran esters (**DE**) obtained with dextran with M_w 6,000 g/mol and M_w 15,000 g/mol are also soluble in organic solvents like chloroform, toluene, and THF. Dextran lauric ester (**DE01**) and dextran myristic ester (**DE4**) are additionally soluble in methanol and isopropanol. It is assumed that dextran esters (**DE01 and DE04**) of moderate DS (around 1) have a sufficient number of hydroxyl groups and, therefore, can interact with polar solvent making them soluble in the alcohols. Higher DS of fatty acid groups tend to increase the solubility in chloroform, toluene, and THF. In contrast, esters prepared from a dextran with M_w 60,000 g/mol (e.g., **DE11**) do not dissolve

completely in chloroform and do not melt homogeneously. This is may be attributed to the fact that the starting polymer is not fully soluble in DMAc/LiCl leading to an inhomogeneous reaction. Therefore, the dextran esters with higher molecular weight (> 60,000 g/mol) were not investigated in detail. The values of molecular weight of the dextran esters determined by SEC are summarized in Table 2. It can be seen that degradation of the polymer during the conversion is moderate. The M_w values increase as the DS values increase because more fatty acids are bond to the dextran backbone. The polydispersity index (PDI) of dextran esters is between 1.2 and 1.7 (Table 2). The melting point of **DE06** and **DE09** are nearly above the human body temperature, so they are the proper material for the composite matrix. **DE12** was repeated in the same reaction condition as **DE06**. **DE13 – 15** were repeated in same reaction condition as **DE09**. The products have similar melting point and DS compared to **DE06** and **DE0**9, except that **DE15** has T_m with 120 °C. In the case of dextran myristate (**DE06**) at molar ratio of 1:5, ≈ 55% of the carboxylic acid is converted to the corresponding ester.

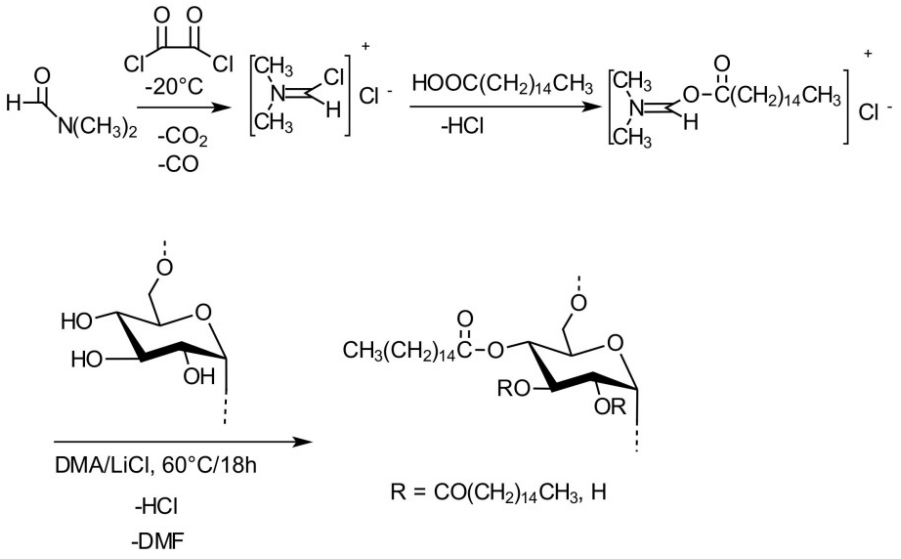

Figure 3. Reaction scheme of the conversion of dextran with palmitic acid activated with iminium chloride

Table 2. Summary of reaction conditions and products characterization of dextran esters prepared by esterification of dextran (M_w 6,000 g/mol) with different fatty acids activated as iminium chlorides.

Reaction condition			Products			
No.	Carboxylic acid (C-number)	Molar ratio [a]	DS	Solubility	Melting temperature (°C) [b]	M_w (g/mol) /PDI
DE1	Lauric (12)-	1:2	1.06	$CHCl_3$, THF, methanol, isopropanol	60 – 70	2,090 /1.21
DE2	Lauric (12)-	1:3	1.47 [c]	Toluene, $CHCl_3$, THF	90 – 98	12,300/1.43
DE3	Lauric (12)-	1:5	2.51	Toluene, $CHCl_3$, THF	30 – 40	21,500/1.68
DE4	Myristic (14)-	1:2	0.98	Toluene, $CHCl_3$, THF, methanol, isopropanol	70 – 75	4,970/1.21
DE5	Myristic (14)-	1:3	1.50	Toluene, $CHCl_3$, THF	96 – 105	12,800/1.4
DE6	Myristic (14)-	1:5	2.56	Toluene, $CHCl_3$, THF, hexane	40 – 45	22,200/1.43
DE12	Myristic (14)-	1:5	2,76	Toluene, $CHCl_3$, THF, hexane	40 – 45	-
DE7	Palmitic (16)-	1:2	1.42	Toluene, $CHCl_3$, THF	100 – 105	15,540/1.25
DE8	Palmitic (16)-	1:3	0.92	Toluene, $CHCl_3$, THF	130 – 140	7,290/1.22
DE9	Palmitic	1:5	2.69	Toluene,	45 – 50	19,200/1.45

	(16)-			$CHCl_3$, THF		
DE13	Palmitic	1:5	2.6	Toluene,	47 – 50	-
	(16)-			$CHCl_3$, THF		
DE14	Palmitic	1:5	2.63	Toluene,	45 - 48	-
	(16)-			$CHCl_3$, THF		
DE15	Palmitic	1:5	0.83	Toluene,	120	-
	(16)-			$CHCl_3$, THF		
DE10 [d]	Palmitic	1:5	1.59 [c]	Toluene,	88 – 95	44,800/1.46
	(16)-			$CHCl_3$, THF		
DE11 [e]	Palmitic	1:5	1.25 [c]	$CHCl_3$ [f]	100 – 105[g]	101,000/ 1.15
	(16)-					

[a] molar ratio of anhydroglucose unit/fatty acid, lauric acid (LA), myristic acid (MA), palmitic acid (PA); [b] determined with hot stage microscope, onset- and clarification temperature; [c] determined with elemental analysis; [d] dextran M_w of 15,000 and [e] 60,000 g/mol; [f] **DE11** does not dissolve completely; [g] incomplete melt.

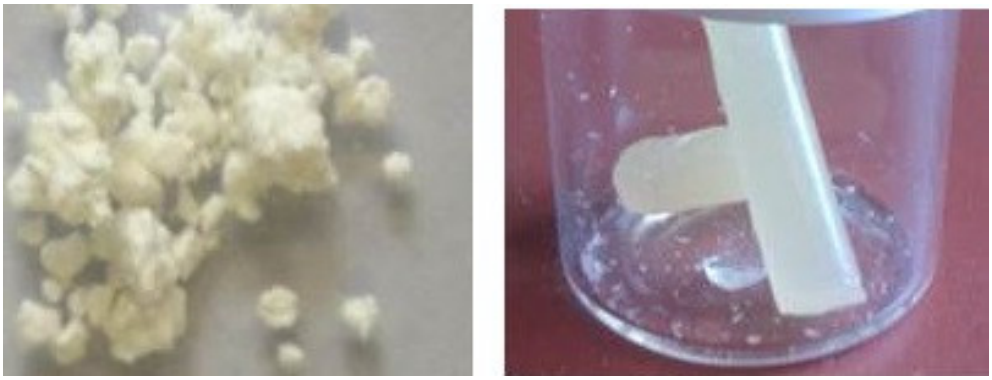

Figure 4. Dextran fatty acid ester (DE09, DS 2.69) in powder form before thermal molding and in stick form after thermal molding

Characterization

Dextran esters are free of chlorine as elucidated by elemental analysis. FTIR spectra show that after esterification stretch vibration of carbonyl group was found between 1740 and 1750 cm^{-1} and no stretch vibration of carbonyl group of the fatty acid at 1700

cm^{-1} appear, confirming the structure and the purity of the dextran esters (Fig. 5). Signals for hydroxyl groups were found between 3470 and 3510 cm^{-1}. For more detailed structure analysis with NMR, the dextran esters can be peracetylated. FTIR spectra reveal the completeness of the peracetylation by disappearance of the signals in the area above 3400 cm^{-1} (Fig. 5). Well-resolved NMR spectra could be obtained with these samples. Representative $^{1}H/^{13}C$ heteronuclear single quantum coherence (HSQC) spectrum elucidates the structure of peracetylated dextran myristic ester (**DE6**, Fig. 6). The proton signal (δ) of the anhydroglucose unit (AGU) can be found between 3.5 and 5.6 ppm. The signals of the hydrogen atoms of the fatty acid ester and acetic acid ester are located between 0.5 and 2.6 ppm. The DS of fatty acid group was calculated from the ^{1}H NMR spectra of peracetylated samples:

$$DS_{\text{fatty acid}} = 3 - (7 \times I_{H,\text{ acetyl}})/ (3 \times I_{H,\text{ AGU}}) \quad (3.1)$$

In the ^{13}C NMR spectrum, signals for the ester moiety are found between 12 and 35 ppm (aliphatic group) and 172 ppm (carbonyl group). The signal of C-1 atom after esterification at O-2 is located at δ = 96 ppm. Further signals of the AGU carbon atoms are detected between 65 and 73 ppm. All signals of proton- and carbon atoms can be completely assigned via the cross peaks in the spectrum. The product contains no substructures along the polymer backbone and no by-products. No signal is found at 46 ppm indicating the absence of impurities like desoxychloro moieties that might be formed by side reaction. No additional peaks are present confirming that only the goal structure was obtained.

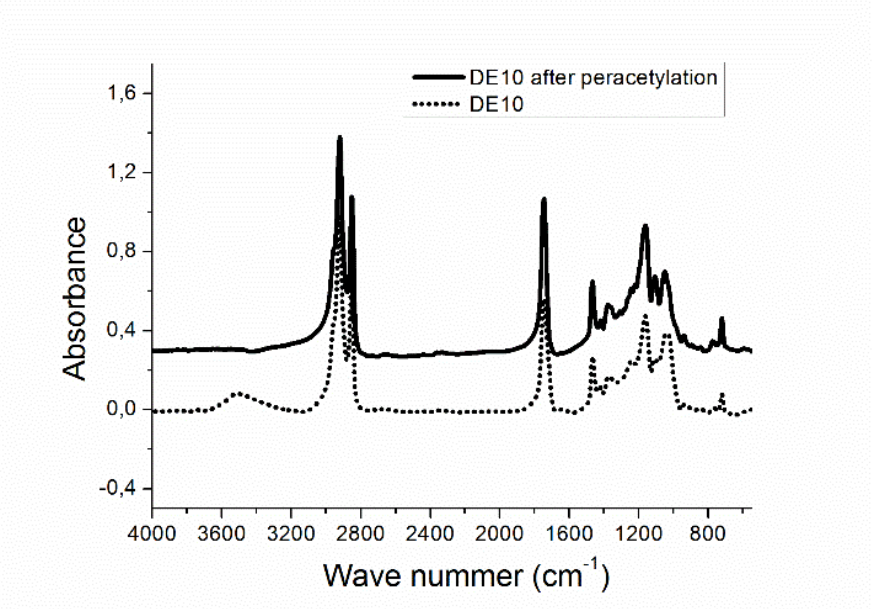

Figure 5. FTIR spectra of dextran palmitic ester DE10 before and after peracetylation

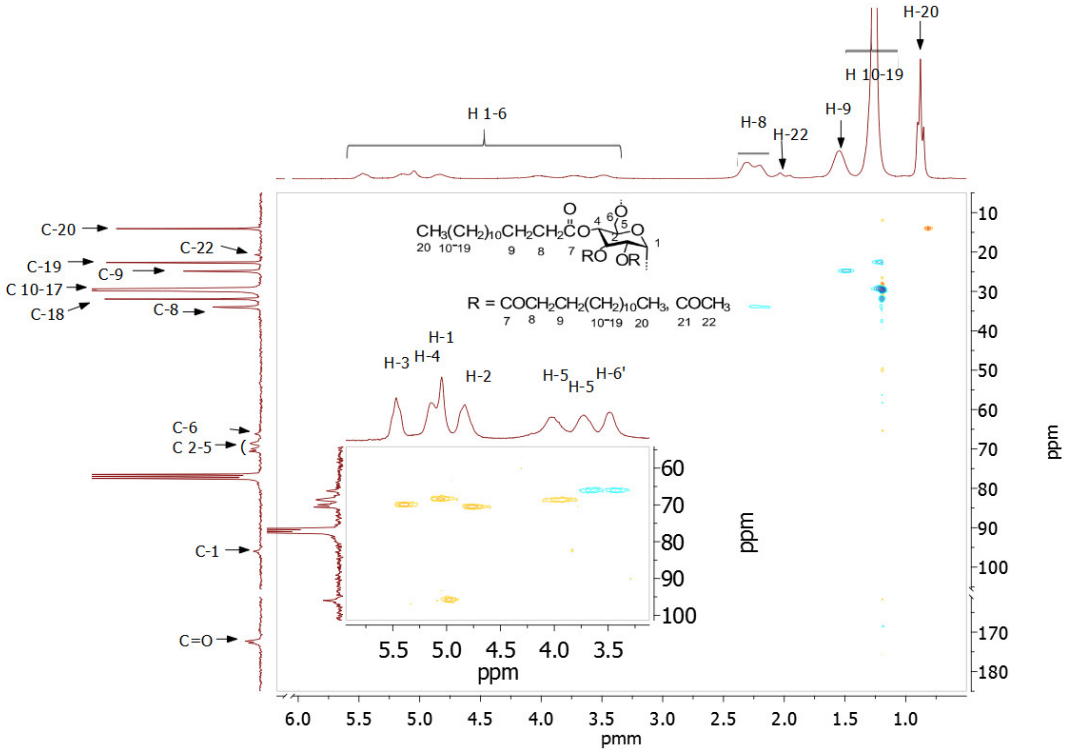

Figure 6. Representative HSQC NMR spectrum of peracetylated dextran myristic ester (DE6, DS = 2.56) in $CDCl_3$.

3.1.2. Magnetic nanoparticles

The magnetic nanoparticle (MNPs) used in this work should form homogeneous nanocomposites with the highly functionalized dextran esters. Magnetic nanoparticles were prepared from a $FeCl_2/FeCl_3$ solution by a basic precipitation process [71] (Fig. 7). It generates bigger MNPs (mean diameter 15.2 nm above the superparamagnetic limit) that have larger specific heating power at "high" magnetic field amplitude (Example: 20 kA/m).

$$Fe^{2+} + 2Fe^{3+} + 8OH^- \rightarrow Fe_3O_4 + 4H_2O$$

Figure 7. Formulae of wet chemical precipitation in alkaline media ($NaHCO_3$)

Preparation of the particles in the solution under optimum synthetic conditions takes place by the formation of tiny crystalline nuclei in a supersaturated medium, followed by crystal growth. The latter process is controlled by mass transport and by the surface equilibrium of addition and removal of individual monomers, i.e., atoms, ions, or molecules. Hereby, the driving force for monomer removal (dissolution) increases with decreasing particle size. Thus, within an ensemble of particles with slightly different sizes, the large particles will grow at the cost of the small ones. This mechanism is called Ostwald ripening and is generally believed to be the main path of crystal growth.[1, 126]

The MNPs tend to agglomerate due to the high surface energy and magnetic interaction. Oleic acid was chosen to hydrophobilize the particle surface, which stabilizes the MNPs. Surface modification was achieved by mixing of the particles with oleic acid in a ball mill. Modification of iron oxide nanoparticle with carboxylic acid results from the interactions between the carboxylic/carboxylate moieties and the surface metal ion. Dried particles were investigated by TEM measurements (see Fig. 8). The powders consist of multicore particles with a mean crystallite size of about 15 nm. The coercivity (H_C) of unmodified MNPs is 3.06 kA/m and the specific saturation magnetization (M_S) is 74.8 Am^2/kg. The M_S-value lies between those of magnetite (Fe_3O_4) and maghemite (γ-Fe_2O_3) nanoparticles. After oleic acid modification the MNPs show decreased H_C-values of 2.5 kA/m and M_S of 68.8 Am^2/kg measured by means of VSM. From M_S measurements the content of oleic acid was calculated which is in the range of 8 wt. %.

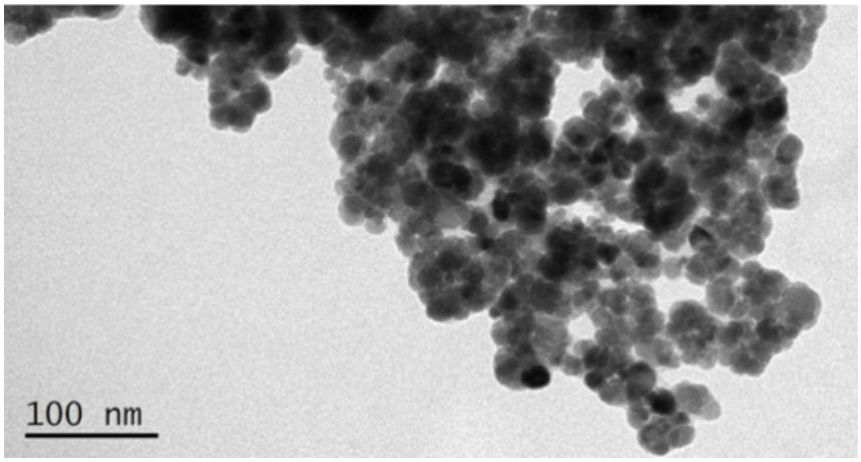

Figure 8. Transmission electron microscopy (TEM) image of oleic acid coated MNP

3.1.3. Meltable nanobiocomposites

In this subsection it deals the preparation of meltable nanobiocomposites (NBC). Because of high (DS), dextran palmitate and dextran myristate (**DE6** and **DE9**, Table 2), showing melting points in the region of body temperature suitable for applications in the biological field, were chosen for fabrication of magnetic hybrid material and were applied for the following experiments. The composite should show a homogeneous heating response under alternating magnetic field, otherwise it would fail to melt the sample at the same time. In order to find out an optimized method to preparation the composite, three different approaches were investigated for fabrication of homogeneous magnetic nanocomposites:

a) mixing of the polymer and the nanoparticles, followed by melt extrusion with a lab extruder and fixation of the material with an applicator on glass;

b) dissolution/suspension of the polymer and the nanoparticles in THF and film formation on glass with the help of a spin coating;

c) dissolution/suspension combined with solution casting and subsequent coating with lab applicator on microscope slide after melting. (Fig. 9)

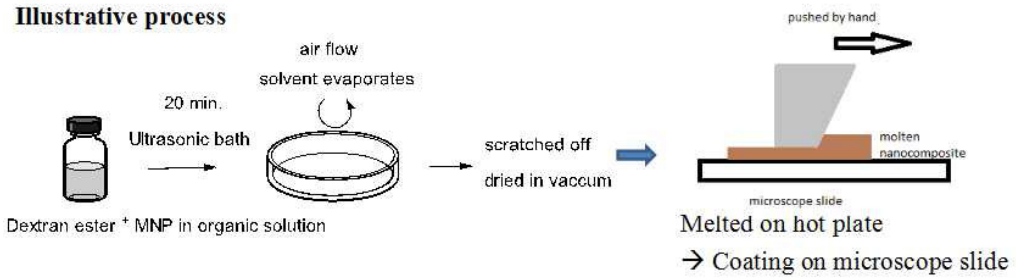

Figure 9. Illustrative process of solution casting method in fabrication of composite and coating process with lab applicator.

Due to the fact that TEM experiments (unsuitable spatial particle distribution, limited contrast, thermal instability of matrix) are not a suitable technique to visualize the particle distribution in the composites, SEM experiments were carried out on a sliced sample. In case of method a) agglomerates and irregular particles with size distribution of about 10 µm were found in the nanocomposite by SEM (Fig. 10). Although extrusion is often used for the preparation of nanocomposite[20, 21], it seems not a proper process here. The reason may due to the limitation of the shear force of the lab extruder.

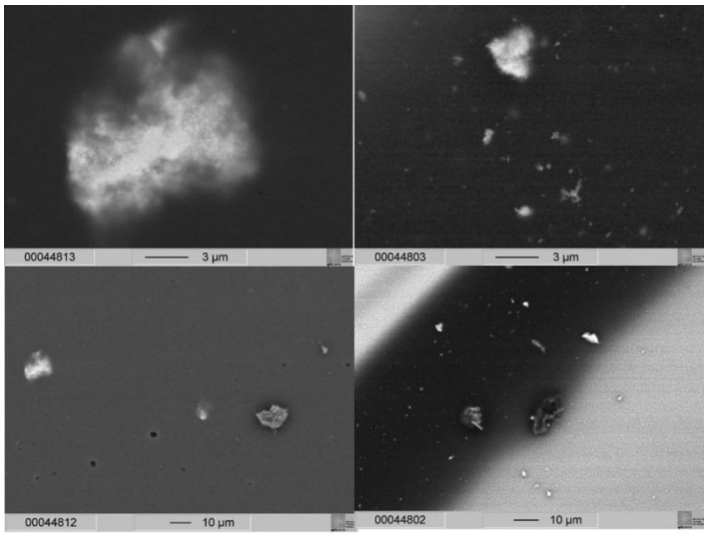

Figure 10. SEM images: (left) extruded sample obtained by method a) (DE9, 2% MNP) and (right) sample prepared by spin coating according to method b) at scale of 3 and 10 µm; 2 wt % MNP indicates that the weight percent of MNP in nanocomposite is 2%.

Samples prepared by method b) do also not contain a homogeneous distribution layer of MNPs in the polymer matrix (Fig. 10). It seems that aggregation occurs in the spin coating step. On the contrary, method c) gives a uniform dispersion of MNPs in the

polymer matrix especially when ultrasound is applied to the suspensions (Fig. 11). The MNPs and some small agglomerates with a size in the range between 100 nm and 1 µm are uniformly distributed in the polymer matrix in case of sample **DE9** with 2 wt. % MNP (Fig. 11). They show that the particles are also evenly distributed over the cross-sectional of the material, which means that the MNPs are interlocked in the polymer because of their high melt viscosity during the sample preparation. These SEM results showed that method c) was suitable for the preparation of homogeneous nanocomposites and was consequently used for the fabrication of samples for subsequent characterization and alternating magnetic field heating experiments.

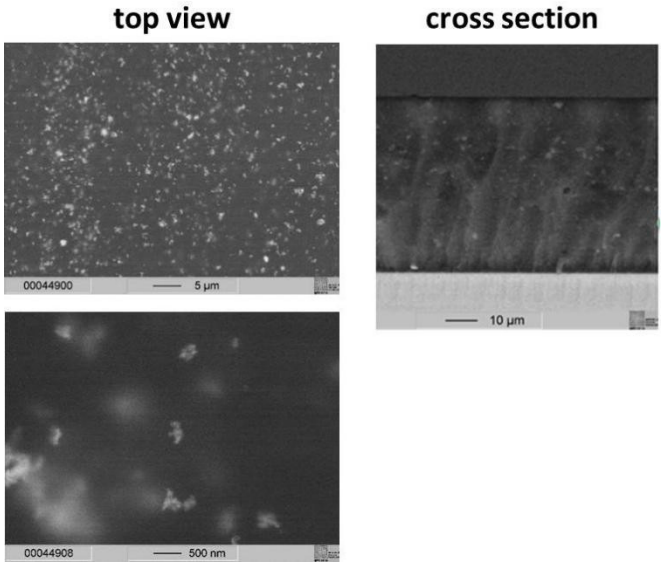

Figure 11. SEM images of bionanocomposite obtained by method c) at different scale bars of 5 µm and 500 nm: 2 wt. % MNP (left); cryo cross section of the sample with a scale bar of 10 µm with 2 wt. % MNP (right).

The rheological behavior dextran palmitate and dextran palmitate (1% MNP loaded) in dependence on temperature are very close to each other as shown in Fig. 12. This means that the addition of 1 % MNP has no influence on the viscosity. It is better to heated up the polymer or composite above 70 °C to have a low viscosity in the coating process.

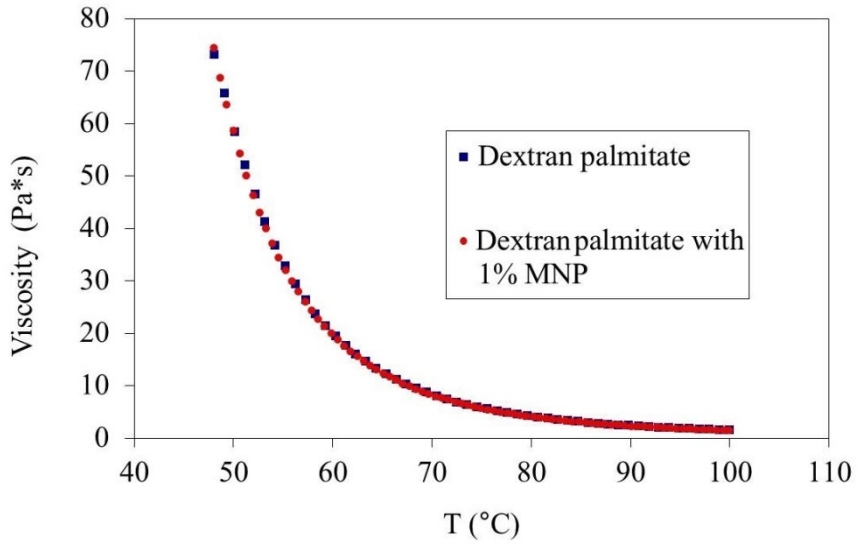

Figure 12. Viscosity of dextran palmitate and dextran palmitate (1% MNP loaded) measured with rotational rheometer.

DSC measurements were carried out to evaluate if the embedment of particles modify the thermal behavior of the dextran esters. The first heating curve of dextran palmitic ester (**DE9**) and nanocomposite obtained with this sample (1 and 2 wt. % MNP) is shown in Fig. 13. An endothermic peak is found at 39 °C for dextran palmitic ester and two addition peaks at 50 °C and 56 °C. This is the area of the optically determined melting region. Detailed assignment of these peaks is not possible yet. Nevertheless, the DSC measurements of the nanocomposites of **DE9** show the same signals, which means the presence of the MNP does not affect the thermal behavior of dextran ester. A slight difference in the peak intensity may indicate a slower heat transport in case of the sample without the particles which could have the observed effect. A further explanation might be that the observed thermally initiated structure transitions can be influenced by the MNPs, i.e. they act as nucleation centers.

Typical magnetization curves of composite (0.05%, 0.3%, 0.7% and 2% MNP) can be seen in Fig. 14. The magnetic particle is not completely superparamagnetic. Magnetization saturation of composite (2% MNP) is about 1.5 Am2/kg).

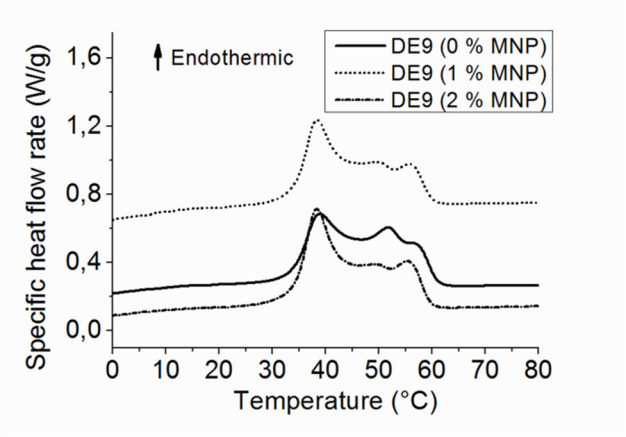

Figure 13. Thermal behavior of dextran palmitic ester and NBC characterized by DSC.

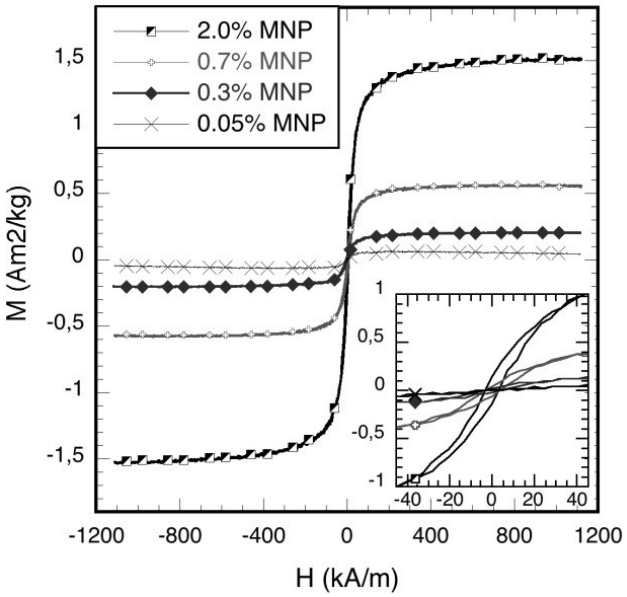

Figure 14. Typical magnetization curves vs static magnetic field of dextran palmitate composites.

In order to investigate the biocompatibility of the composite, human microvascular endothelial cells (HBMEC) as blood-brain barrier-representing model[127] were seeded on glass slides covered by increasing concentrations of magnetic nanoparticles embedded within dextran palmitate. Microscopic investigations of fluorescently stained cells reveal that these sensitive cells attach to the DE9 surface in a well-distributed manner and show a regular cellular growth compared to control cells cultured on glass cover slips without any composite coating (Fig. 15). Phalloidin-based staining of F-actin indicates that the cell morphology is not influenced and cell-cell contacts do not appear

disrupted in the presence of DE9 with particle concentrations between 0.5 and 2.0%. Furthermore, similar numbers of cells recovered from the dextran-coated surface exclude a composite-associated harmful effect on cell viability and proliferation. Taken together these results confirm a biocompatible nature of this composite containing up to 2.0% magnetic particles.

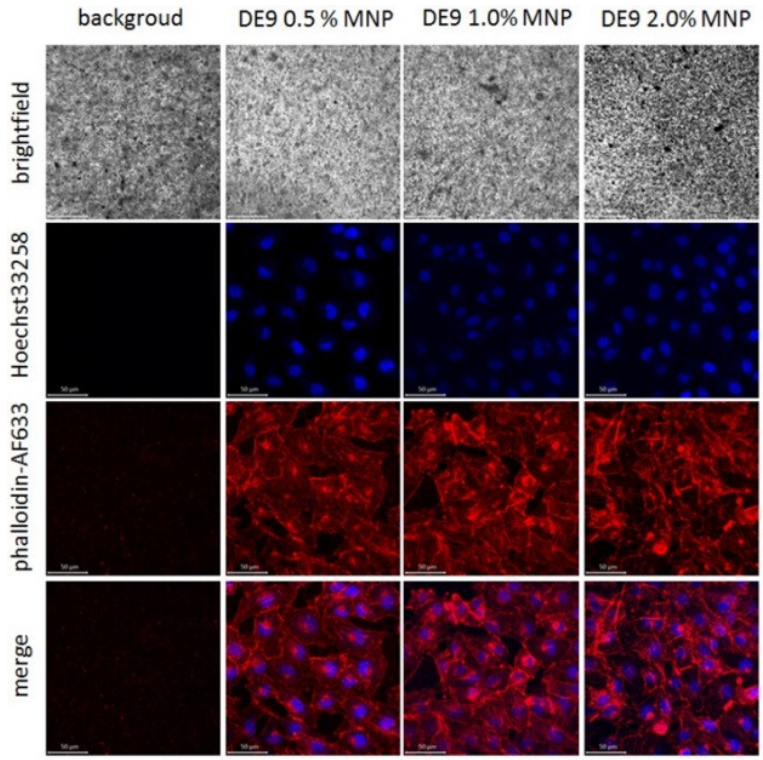

Figure 15. Upon fixation and permeabilization nuclei and F-actin of HBMEC were good distributed on dextran palmitate (DE9) containing magnetic particle concentrations of 0.5%, 1.0%, and 2.0% immobilized on glass cover slips showing a regular cellular growth compared to control cells cultured on glass coverslips without any composite coating. Scale bars indicate 50µm.

3.2. Mobility of nanoparticle in composite

The movement of magnetic particle is dependent on the external magnetic field, namely a static gradient magnetic field or alternating magnetic field. As introduced in the last part, the magnetic particles are embedded in a high viscous polymer matrix, even when the polymer is in a molten state. This part it is aimed to firstly describe how does the

viscous polymer matrix influence the mobility of magnetic particles in a magnetic field, and secondly find out the correlation between the mobility and viscosity.

3.2.1. Mobility of magnetic particle in static magnetic field

A static magnetic field can be used to study the mobility of MNP in the polymer matrix because it is one simple method. The particle themselves cannot move in a static magnetic field when the polymer is in a solid state. They can move when the polymer is a in molten state. This can be understood as a lateral movement, by ignoring of the attraction force between the magnetic particles.

In samples with a low particle concentration of < 0.2%, microscopic observations of the movement of single particles in the matrix are possible. The melting of polymer was realized with external heating plate at temperature of 100 °C. Red marked magnetic particles 1 and 2 have velocity up to 0.25 µm/s, which was calculated by dividing the distance over 45 sec observed by a microscope shown in Fig. 16. The experiments showed that MNP could be moved inside the molten matrix by application of an external static magnetic field (NdFeB magnet, high field gradient about 90 T/m). The results are in accordance to the viscosity measured with rotational rheometer in the part of 3.1.3. In the sample with high particle concentration, the observation of magnetic particle was difficult due to the overlapping.

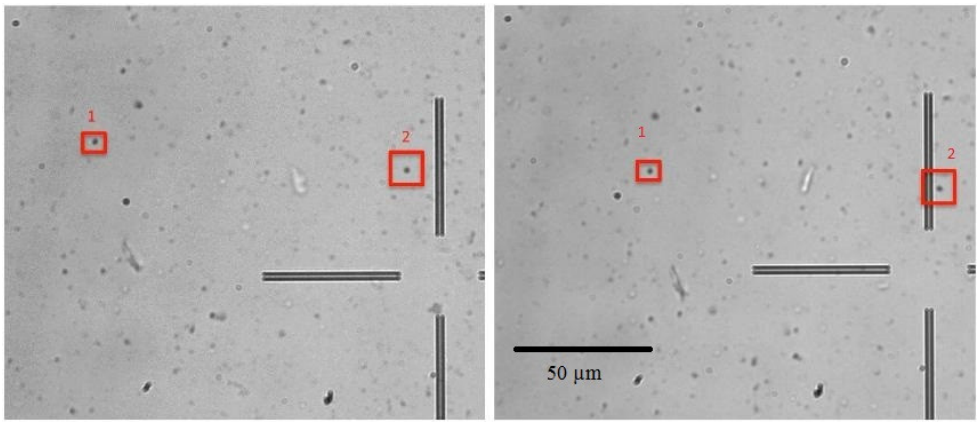

Figure 16. Microscopic fixed image of single particle in the polymer (left) at 0 s and after 45 s (right, scale bar: 50 µm)

3.2.2. Mobility of magnetic particle with AC susceptometry and Mössbauer

The mobility of magnetic particles is studied in an alternating magnetic field. It is going to study magnetic relaxation processes (Brownian and Neel relaxation). This property is

related to the potential usability of new composite systems in regards to their heating abilities, which determines the systems' energy uptake in the magnetic field.

It is possible to determine the mobility of the nanoparticles (or agglomerates) moving in the liquid polymer melt with measurements of the magnetic AC-susceptibility. The imaginary part χ'' of the magnetic susceptibility of 1% MNPs in the dextran myristate-based biopolymer in the temperature range of 20 – 120 °C is shown in Fig. 17. The imaginary part χ'' is related to how much energy dissipated into the polymer matrix by relaxation process. For temperatures below the melting region, χ'' is found to be relatively constant, with no considerable frequency dependence being observable. The frequency independent signal is presumably caused by slow Néel relaxation processes with a broad distribution of relaxation times, which is also indicated by a slight increase of the "background" signal towards higher frequencies. This means no Brownian process was taking place indicating that there is no particle rotation in the polymer matrix.

$$f = \frac{k_B \mathrm{T}}{8\pi^2 \eta {R_H}^3} \qquad (3.2)$$

In the equation 3.2, f is the Brownian rotation frequency, η is the fluid´s dynamic viscosity, R_H is the average hydrodynamic radius of the particles, k_B is the Boltzmann constant. As the temperature rises up, the viscosity decrease, as a result, the frequency f increases.

When reaching temperatures far above the melting region (green line 40 °C), a broad peak emerges at the low frequency regime, moving towards higher frequencies with increasing temperature as found in Fig. 17. In case with frequency of 0.05 Hz at 120 °C, the Brownian relaxation reaches a peak. Obtaining by experimental data the polymer viscosity is about 0.5 Pa·s at 120 °C (part 3.1.3). This means that magnetic particles could rotate themselves at frequency of 0.05 Hz in such viscous matrix. Brownian relaxation starts to occur at 313 K (close to the melting point of polymer). No imaginary part χ'' was found below 40 °C indicating that no Brownian relaxation was taking place. This could be the evidence that magnetic particles are blocked in the polymer matrix under their melting temperature.

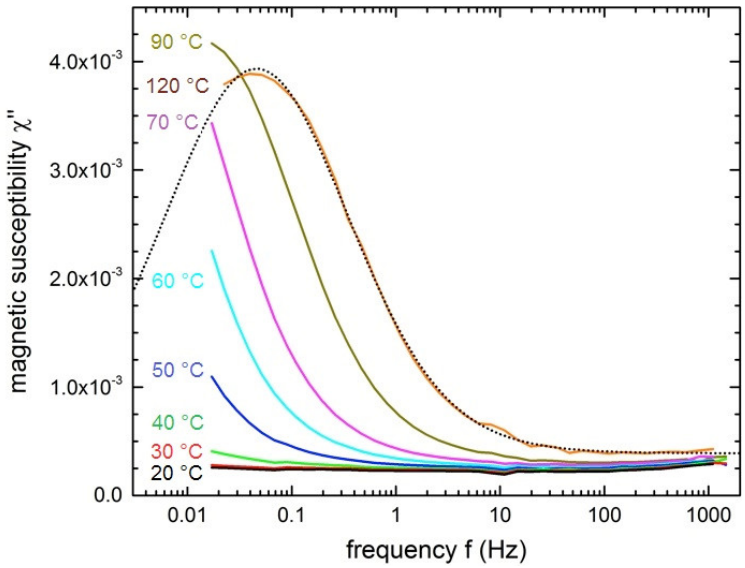

Figure 17. Imaginary component χ'' of the AC magnetic susceptibility of dextran myristate based sample at temperatures of 293 – 393 K (solid lines). The dashed line corresponds to the theoretical Debye fitting model at 393 K.

The average particle diameter can be calculated by ACS according to equation (3.2). By adapting the parameters (viscosity 0.5 Pas at 393 K) it results in an average particle diameter of ca. 64 nm (according to equation 3.2). Considering the size of about 30 to 80 nm of the "raspberry" multicore particles determined by SEM, this indicates that relaxation in the liquid polymer melt is dominated by the movement of separate particles rather than large agglomerates. However, one has to keep in mind that agglomerates with larger hydrodynamic diameters would display a much higher relaxation time. Due to the high viscosity of the polymer melt, the relaxation times of agglomerates are assumed to be outside of the accessible measurement range using AC-susceptometry. A magnetic composite system with low viscous medium, for example, a ferrofluid system consisting 70 vol.% glycerol solution was measured with same ACS method, showing that the Brownian frequency is about 800 Hz at 40 °C when the viscosity is about 10 mPas.[129] The difference on frequency between the two systems is about times of 1.6 x 10^4, which is largely due to the difference on matrix viscosity. Yet, it has to be mentioned that the magnetic particle size in two systems are different, which is in cubic reciprocal to the frequency.

Not only the viscosity, but also the polymer network could have influence on the mobility of magnetic particle. For example, it was reported in the literature that the mesh size of hydrogels could influence the mobility of magnetic particle. When the

magnetic particle size is bigger the mesh size of hydrogel, the rotation movement is strongly constrained by the polymer network.[130]

3.3. Heating behavior of nanobiocomposite with an alternating magnetic field

The heating behavior of nanobiocomposite with an alternating magnetic field will be discussed. First the influence of magnetic particle content and geometry of composite sample on the heating ability with AMF is discussed. In the following, it is described that the heating ability of nanobiocomposite can be influenced after being melted with a heating plate and placed in an external static magnetic field, i.e., a texturing effect of composite materials takes place with external static magnetic field.

3.3.1. Heating behavior of the nanobiocomposite with an alternating magnetic field (AMF)

Nanobiocomposite with different geometry (film, disc, and granules dispersed in gelatin) were prepared by melting the sample in corresponding molds in Fig. 18. The heating response to AMF of magnetic nanocomposite on object glass with different thickness and MNP content was studied in detail (Table 3). Nanocomposite coatings on microscope slide (prepared according to method c in part of 3.1.3) were placed in the middle of a coil in air at room temperature and subjected to an alternating magnetic field of 20 kA/m and frequency of 400 kHz for 5 min. The surface temperature of the films was monitored by IR thermography using a thermographic camera. Three points on the surface of magnetic nanocomposite were averaged and the effect of waste heat by the AMF generator was removed by subtraction with control sample (**C7**, Table 3). It can be seen that a uniform heating response of sample **C2** on application of AMF is generated due to the good dispersion of MNP in the composite layer in Fig. 19. AMF for 60, 180, and 300 s on sample **C2** increases the surface temperature of 3, 6, and 9 °C, respectively. The heating response of nanocomposite coating is strongly dependent on the thickness of the layer. AMF treatment for 4 min yields an increase of the temperature of 25 °C in case of a layer thickness of 600 µm (**C1**), 7 °C at 50 µm (**C2**) and only 1 °C for a layer of 5 µm thickness in Fig. 19. The maximal increase of temperature after 5 min and the corresponding heating rates (after the subtraction of control sample) measured on the coating films without MNP are listed in Table 3. The reason why thickness influences the heating drastically is heat dissipation. Heat is dissipated through conduction to the glass substrate and convection to air. The influence

of the humidity can be neglected because the difference between air and steam is low in comparison to the substrate effect (see thermal conductivity coefficients). Heat dissipation increases as the sample thickness decreases, because the ratio of the surface area to volume increases. When the MNP loading is below 1 wt. % (**C5, C6**), there is no significant heating response for samples with thickness of 50 µm (Table 3.). In this set of experiments, the films on glass do not melt by application of AMF.

Samples of the nanocomposite with a disk shape were prepared to diminish heat dissipation compared to the films on glass (see Fig. 20.). The thermoplastic nanocomposite can be shaped by casting into a cylindrical mold. Disks made from sample **C8** and **C9** with thickness of 1.4 mm and radius of 8 mm were studied. For AMF measurements, the disk samples were placed on a polystyrene holder in the middle of coil. As shown in the Fig. 20. , it took 160 s to heat such a disk-type sample of **C8** above the melting temperature (50 °C) of the dextran ester. In case of a comparable sample of **C9**, it took only 120 s (melting temperature 45°C). Obviously, these samples have a much better heating rate than the films (Table 3). After AMF was switched off, the nanocomposites were quickly cooled by air and the temperature dropped down under the melting temperature within 2 min (see Fig. 20. right). These data confirm that the material is in principle very well suitable for remote melting, e.g., in controlled release applications. In a further experiment, the nanocomposite was dispersed in gelatin (sample **C10**) to obtain a model system comparable to a biological surrounding (see Fig. 18d). The specific absorption rate of the nanocomposite **C10** (10 wt. % in gelatin) was determined as 6.3 W/g with a fiber optic sensor on a bulk shaped sample (Fig. 20. purple), which was subjected to AMF (20 kA/m, 400 kHz). A plateau at 55 °C was found and lasted for about 80 s. The temperature went to 54 °C until the field was turned off. The heating rate is smaller compared to disk sample, because the heat was absorbed by water. Nevertheless, even in this set up melting of the composite was readily achieved.

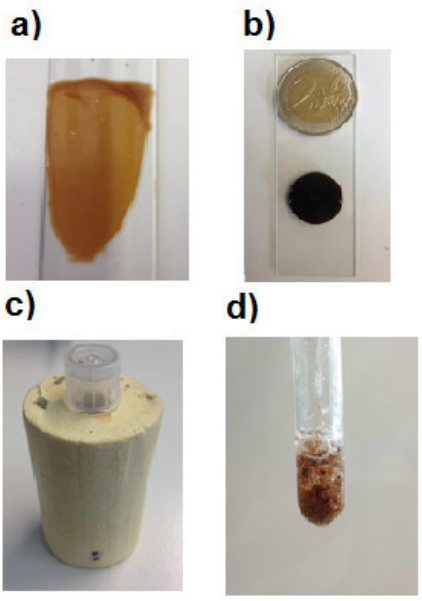

Figure 18. (a) Composite film (DE9, 2% MNP, 50 µm) on object glass; (b) disk shape sample; nanocomposite granules dispersed within gelatin in a glass tube and in polystyrene isolation for AMF (c & d).

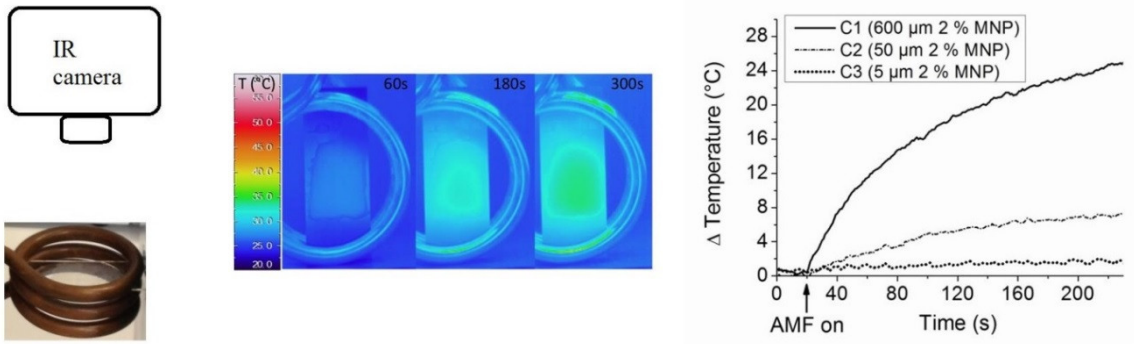

Figure 19. IR thermography of a film prepared from sample C2 (Dextran palmitate, DE9, DS = 2.69 with 2 wt. % MNP and 50 µm thickness, coated on glass) after 60, 180, and 300 seconds in an alternating magnetic field (AMF, left); The graph (right) shows the surface temperature subtracted by control sample **C7** of the nanocomposite films **C1 – C3** subjected to continuous AMF. The temperature was measured every second by the IR camera ($N = 3$).

Table 3. Summary of composition and geometry of nanobiocomposites fabricated by solution casting, and their maximal heating response by IR thermography on alternating magnetic field heating

No.	Composition	Thickness (µm)	Sample geometry	Maximal ΔT (°C)*	Heating rate (10^{-3} °C/s)**
C1	**DE9** + 2 wt. % MNP	600 ± 20	film	25	114
C2	**DE9** + 2 wt. % MNP	50 ± 3	film	7	32
C3	**DE9** + 2 wt. % MNP	5 ± 1	film	1	5
C4	**DE9** + 1 wt. % MNP	50 ± 3	film	4	14
C5	**DE9** + 0.3 wt. % MNP	50 ± 3	film	1	4
C6	**DE9** + 0.05 wt. % MNP	50 ± 3	film	0	0
C7	**DE9** (control sample)	50 ± 3	film	0	0
C8	**DE9** + 2 wt. % MNP	1400 ± 50	Disk (r = 8 mm)	38	136
C9	**DE6** + 2 wt. % MNP	1400 ± 50	Disk (r = 8 mm)	33	138
C10	0.1 g **DE9** + 2 wt. % MNP in 0.9 gelatin	-	Granules (< 1 µm)	30	88

3.3.2. Heating behavior of the nanobiocomposite in an AMF after texturing in a static magnetic field

The magnetic particles are fixed in the polymer matrix below the melting temperature, but the mobility of particle can be gained when the polymer is in a viscous state with an external static magnet discussed in the 3.1.3. It is occurs to samples with a higher particle concentration (> 0.5%) a “magnetic texturing” of the composite under a static field. The particles are fixed again, when the polymer is cooled down to room temperature. This would give a difference on the heating ability of the composite, since the distribution and orientation of magnetic particle were changed. In this part it is aimed to understand how the texturing in the composite has an influence on heating

ability in an AMF. As heating sources a Peltier element (thermoelectric effect) and alternating magnetic field are used, separately.

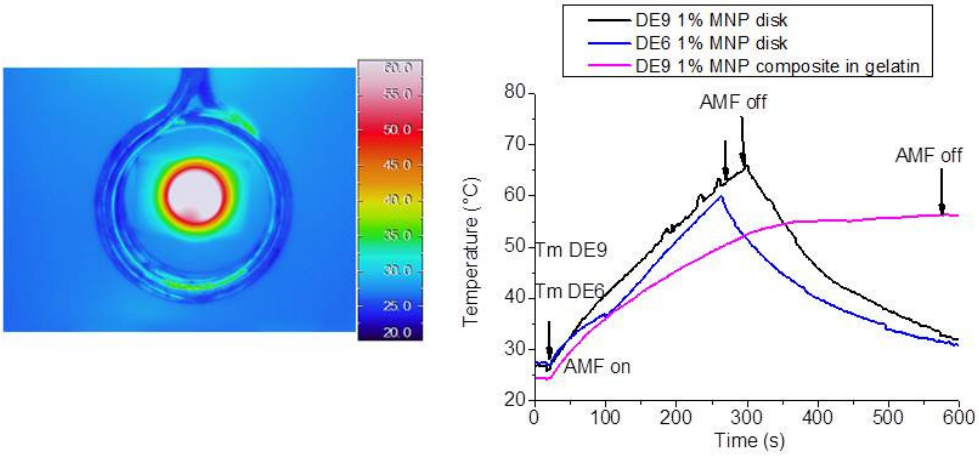

Figure 20. IR thermography of sample C8 (dextran palmitate nanocomposite disk with 2 wt. % MNP, disk with a thickness of 1400 µm and r = 8 mm) after 240 seconds in AMF (left); surface temperature of bionanocomposite disks of samples C8 and C9 (1400 µm thickness and radius of 8 mm) in comparison to sample **C10** (bionanocomposite granules dispersed in gelatin) subjected to continuous AMF (right). The surface temperature of samples **C8** and **C9** was measured every second by an IR camera (N = 3). The temperature in the gelatin was measured with a fiberoptical sensor every second.

The increased of heating rate on the surface of one magnetic composite (2% MNP, 100 µm thickness) recorded by IR-camera before and after the magnetic texturing can be seen in Fig. 21. On the right axis, "#" is the frequency of occurrence of pixels on the surface of composite layer. The temperature values are average values from three points of about 0.3 mm size. Magnetic field was perpendicular to the composite layer. Before being placed in the magnetic field, the heating behavior in AMF is rather homogenous on the sample. In contrast to that, an enhanced heating appeared after the sample was exposed to an external permanent magnet heated with a Peltier element. A red "hot-spot" area was found in the sample, which is 4 °C higher than the rest area. The reason is that a magnet was put above this area when the polymer was in molten state, resulting in an agglomeration and orientation of magnetic particles.

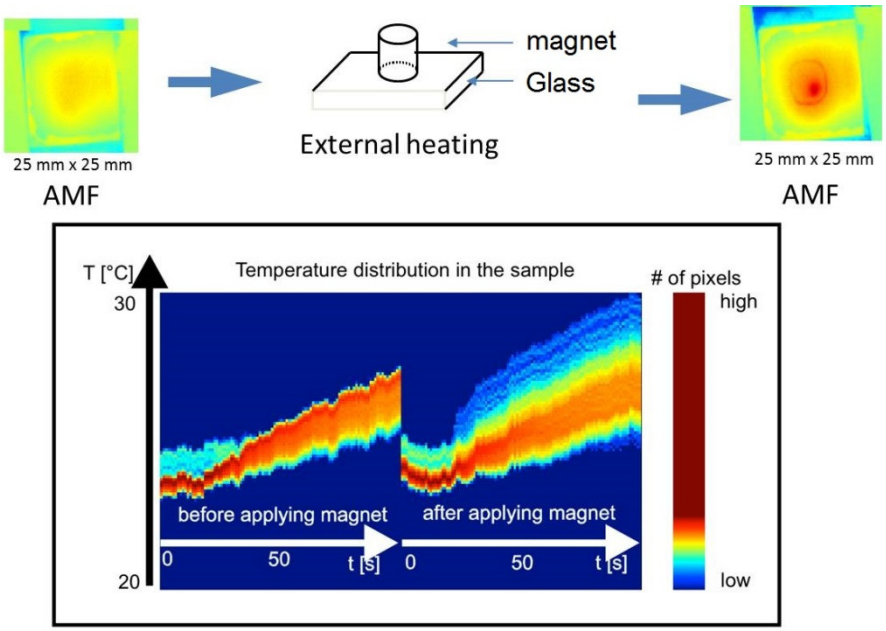

Figure 21. Surface temperature of the composite in a Peltier element before and after texturing in a static magnetic field under external heating. "#" is the frequency of occurrence of pixels on the surface of composite layer. Magnetic field is applied perpendicular to the composite layer.

This strengthening effect on heating rate can be also realized with alternating magnetic field, instead of a Peltier-element. The composite (2% MNP, 600 µm thickness) was heated up over its melting temperature with AMF. Then AMF was turned off to avoid the heating on the NdFeB magnet, when the magnet was placed close to the composite coating.

The increased surface temperature of this sample before and after the magnetic field can be clearly seen in Fig. 22. After being treated with a NdFeB magnet, the AMF heating response of this magnetic composite changed itself into a different manner. A hot-spot area can be found on its surface. The difference of temperature between the two pictures (with texturing and without texturing) is 12 °C after 90 s AMF was started. Because of the bigger thickness, the surface temperature on this sample is even higher than last sample. The temperature values are averaged values from three points of about 0.3 mm size. Magnetic field was perpendicular to the composite layer.

It is important to note that the inhomogeneity of distribution of MNP in this thermoplastic polymer can be maintained, when the polymer is in solid state. When the

composite is molten and no external magnetic field is present, for example, between 42 and 45 °C (typical application temperature for hyperthermia) [131], the magnetic particles would not move due to gravity, since they are trapped in such high viscous system. While in the ferrofluid system, the magnetic particles are expected to be dispersed homogeneously again after the external magnetic field is removed. This phenomenon can be explained by the polymer compact structure, which is different to ferrofluid system. The Brownian relaxation is prone to happen, when the mesh-size of hydrogel is bigger than the size of magnetic particle.[130]

Increased heating rates of magnetic fluids are an important challenge in order to minimize dosages of magnetic fluids needed to reach therapeutic temperatures in magnetic fluid hyperthermia. For example, it was reported that the heating rate can be improved by using monodisperse magnetite particles.[132] This finding on this hot-spot heating effect after being placed with an external magnetic field could be alternative solution for improving of heating rate. Namely, the position, where the heating rate is needed to be increased, can be adjustable by an external magnetic field. Moreover, the position of hot-spot heating area can be changed by moving the external magnetic field to expected position when the composite is in molten state. This changeable heating hot-spot with increasing heating rate could be very useful for hyperthermia.

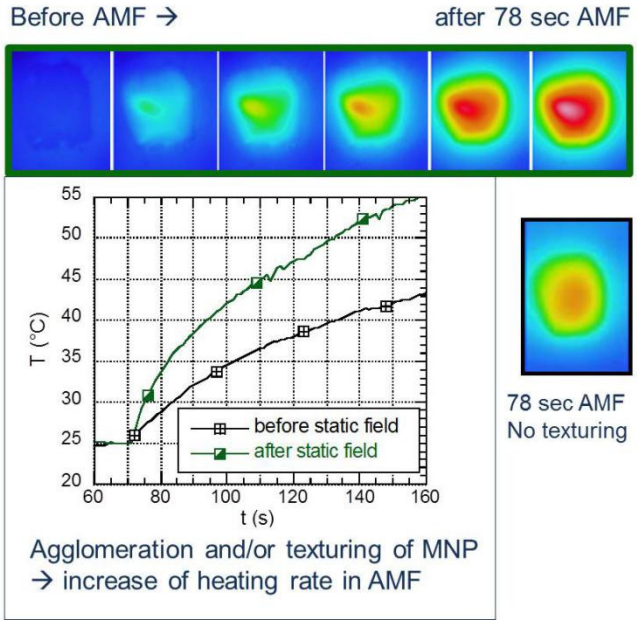

Figure 22. Surface temperature of the composite in an AMF before and after texturing in an alternating magnetic field.

The structural reason for the changes on heating ability could be the orientation of MNP and agglomerates i.e. increase of the local MNP concentration. The “increase of the local MNP concentration” can be seen in optical micrographs and by pixel analysis (in-plane direction of pixel structures; no particles analysis) in Fig. 23. The image before texturing reveals no preferred direction of pixel structures, i.e. there is no particle texturing caused by formation of the composite films. The texturing axis corresponds roughly with the direction of the field gradient. The magnetic field was not exact parallel to “y” direction. Thus, the peak of maximum amount of particle is about deviation of 20° in “y” direction.

3.4. Controlled release of model drugs from meltable nanobiocomposites

Meltable nanobiocomposites composed of biocompatible dextran fatty acid ester and MNPs melting close to human body temperature were prepared and loaded with green fluorescent protein (GFP) or Rhodamine B (RhB) as model drugs to evaluate their potential use as drug delivery system. It is highly motivated to study the release of the model drugs from the magnetic NBC influenced by high frequent alternating magnetic field (AMF, 20 kA/m at 400 kHz). Moreover, on-demand release would be very interesting with applying the external AMF.

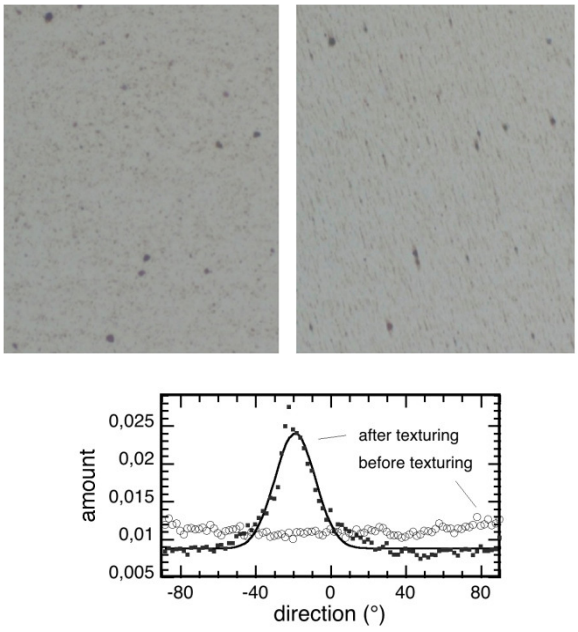

Figure 23. Proof of particle texturing in a static magnetic field under external heating at 80°C/5min: Optical image before (left) and after (right) texturing (size ca. 205 x 260 µm) and corresponding pixel analysis (0° = y-direction).

3.4.1. Nanobiocomposites for control release

In the previous chapters, it was found that esterification of dextran with fatty acids is a path to convert the biopolymer into a thermoplastic material. The thermoplastic constitutes a matrix polymer for the preparation of remote controlled release systems that can be load with magnetic nanoparticles. It is possible that the NBC undergoes a softening / melting above human body temperature under exposure of an alternating magnetic field (AMF), leading to an accelerated release of drugs loaded. Dextran myristic- and dextran palmitic acid ester with degree of substitution (DS) of 2.76 and 2.69 (**DE6** and **DE9**), respectively, were chosen as polymer matrix, because they are solids at 37 °C showing softening (melting) above human body temperature.

On the contrary to hydrogels, the dextran esters are composed of high DS of long hydrocarbon chains. Thus, they are hydrophobic and insoluble in biological matrices. The incorporation of lipophilic MNPs (with oleic acid shell) and of lipophilic drugs should easy to be carry out.

In order to study the influence of the kind of heating (AMF or by water bath) of the NBC with respect to heating rate and accessible temperature, heating tests under certain "geometrical" arrangements (Table 4) were carried out. It was turned out that the temperature of a NBC disk floating in 0.5 mL water can be easily increased by AFM (Fig. 24). The reached temperature has surpassed the melting range of the NBC after about 6 min. Therefore the AMF heating time was set as 12 min in order to melt the NBC. After cooling, the NBC solidified and it could be molten again by increasing the temperature applying AFM.

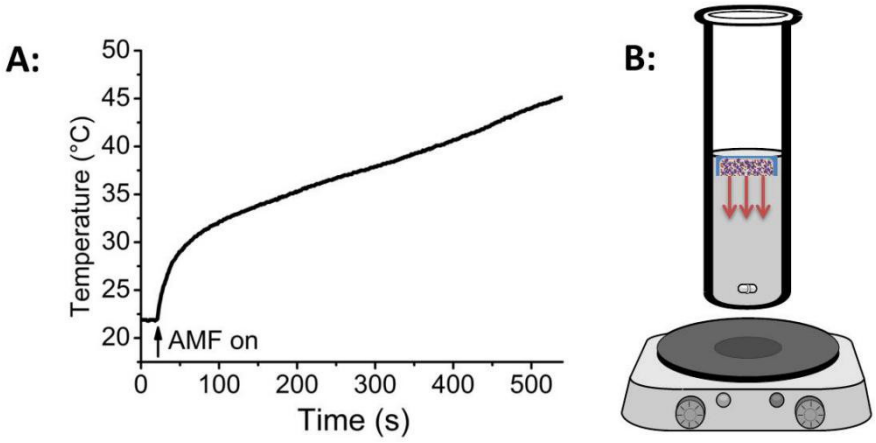

Figure 24. Temperature increase (measured with a fiber optical sensor) in the biocomposite disk (1 wt.% MNP) surrounded by 0.5 mL water and subjected to continuous alternating magnetic field (strength of 20 kA/m and frequency of 400 kHz). AMF was turned on at 20 second. B: Arrow represents the diffusion of RhB under external heating and stirring. The composite is filled in a blister pack with diffusion one side due to blister.

3.4.2. Calibration of concentration with spectrometric methods

Green fluorescent protein (GFP) and rhodamine B (RhB) are used as model drugs to be released in PBS solution by application of AMF. Therefore it is important to know how much model drugs are released in the aliquot. The method is to use stock solution of corresponding model drugs with known concentration to do the calibration curve. The characteristic absorbance at 544 nm of RhB with UV-vis spectrometer and emission intensity of GFP at 510 nm with fluorescence spectrometer can well be linearly correlated to the concentration of stock GFP and RhB solution. The released mass of GFP and RhB in PBS solution was obtained by calculating the concentration in a known volume. Thus, the GFP concentration was determined with good precision.

Rhodamine B (Fig. 25): (No heating: $y = 0.1118x + 0.0015$, determination coefficient $R^2 = 0.9976$; after heating at 45 °C, measured at 25 °C: $y = 0.1096x - 0.0367$, $R^2 = 0.9864$. x: concentration (10^{-6} mol/L), y: absorbance at 544 nm).

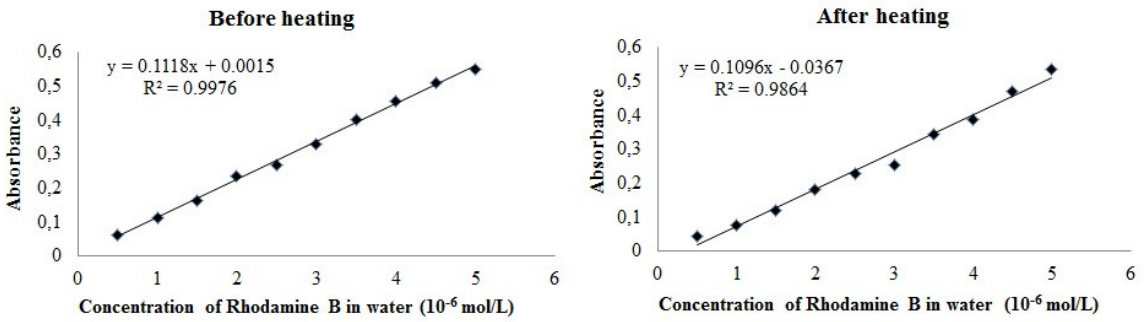

Figure 25. Calibration curve calculated from the absorbance at wavelength 544 nm as a function of the concentration of Rhodamine B.

Green fluorescent protein (Fig. 26): (No heating: y = 22.194x + 15.831, determination coefficient R^2 = 0.9926; after heating at 45 °C, measured at 25 °C: y = 14.73x + 14.80, R^2 = 0.9913, x: concentration (ng/ml), y: emission at 510 nm).

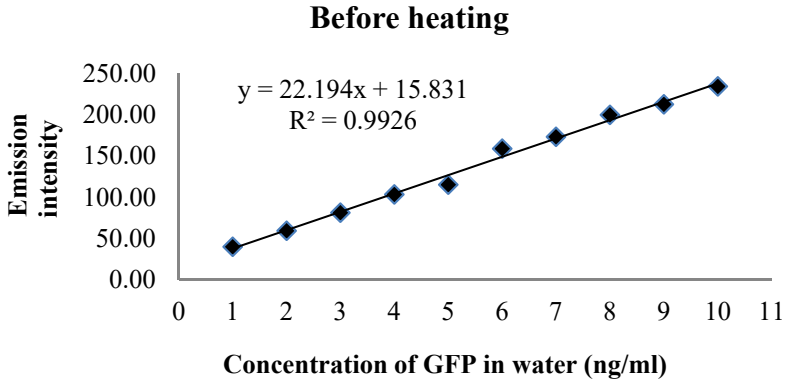

Figure 26. Calibration curve calculated from the emission at wave length 510 nm as a function of the concentration of green fluorescence protein.

It is known that the intensity of GFP and Rhodamine B is dependent on temperature. Therefore a water bath was used to heat up the GFP and Rhodamine B solution to simulate the heating condition as done by AMF. The correlation between fluorescence intensity and numbers of heating cycle is showed in Fig. 27. It was found that the fluorescence intensity decreased slightly to 92% after 5 heating cycles in the water bath. The fluorescence intensity of GFP and absorption of Rhodamine B in UV-Vis spectroscopy could be variable after heating as known the literatures.[126, 133] For this reason the results from water bath heating and AMF heating experiments were corrected by dividing 92%.

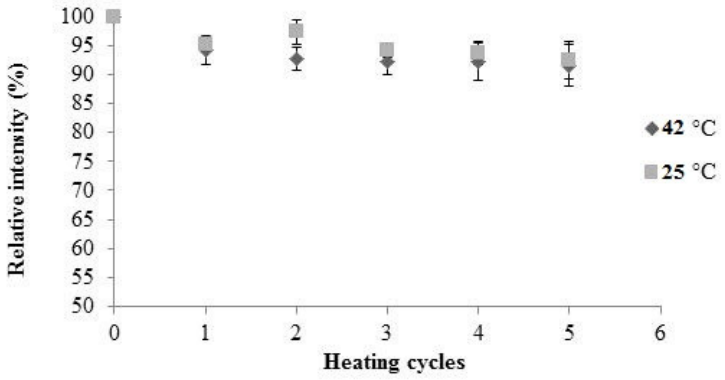

Figure 27. The correlation between fluorescence intensity of GFP and number of heating cycles

3.4.3. Demonstration of green fluorescent protein release

GFP was used as model drug with a large molecular weight compared to RhB. Moreover, GFP can be easily detected by fluorescence spectroscopy down to ng/mL. NBC containing GFP was obtained by the entrapment trapped in the NBC as dumpling-like structure without any external stimulus. It is different from a hydrogel formulation, where a drug release could be achieved by changing of water absorption resulting in a swelling/shrinking of matrix structure.[12]

A scheme of disk shape GFP loaded magnetic composite is depicted in the Fig. 28. Pulsatile release profiles of GFP were obtained from magnetic NBC (samples **R1-3**) induced by AMF compared to control samples (**R4-6**) shown in Fig. 29. There was no release of GFP at t_0 for both samples. For the samples stored at 25 °C, no GFP release was observed in the whole experiment. The GFP cannot penetrate the polymer layer due to its thickness of about 1 mm. This is a positive proof that the leaking of GPF can be avoided, which is a problem for the hydrogel materials in the application of controlled release.

After treating the sample by AMF for 12 min and for 48 min without AMF treatment, 5% of the GFP loaded was released from the NBC after 2 h. The release of the GFP was achieved after internal heating the NBC by AMF. After 3, 3.5, and 4 h total running time without additional exposure to AMF, a release of GFP could be observed (squares, Fig. 29) that was low compared to the amount released under exposure of AMF after 2 h. By applying repeated treatments with AMF, the amount of GFP released could be

increased (at 4.5 and 6.5 h). The dumpling-like structure was open after first melting process and GFP can diffuse into the medium.

Table 4. Samples of nanobiocomposites for controlled release studies (dextran myristate containing 1% magnetic nanoparticles)

Sample No.	Model drug	Heating source	Duration of release (h)	Duration of AMF within release time (min)
R1-R3	Rhodamine B	No	6	-
R4-R6	Rhodamine B	Water bath	6	-
R7-R9	Rhodamine B	AMF	6	36
R10-R12	Green fluorescent protein	No	8	-
R13-R15	Green fluorescent protein	AMF	8	36
R16-R18	Rhodamine B	No	1440	-
R19-R21	Rhodamine B	Water bath	1440	-
R22-R24	Rhodamine B	AMF	1440	72

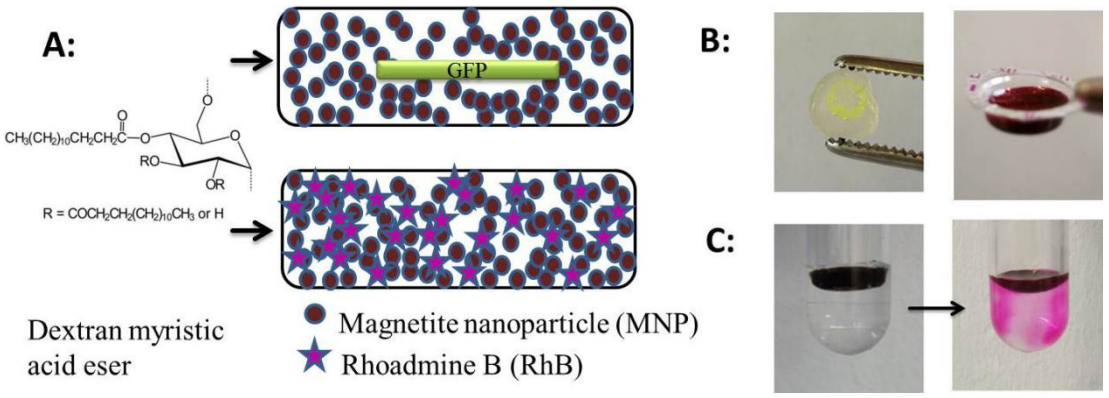

Figure 28. A: Scheme of magnetic biocomposite from magnetite nanoparticle and dextran myristic acid ester containing green fluorescence protein and rhodamine B, respectively. **B**: GFP composite without magnetic particle and RhB composite filled in a blister pack. **C**: Gradual heating generated with AC field resulting in release of RhB

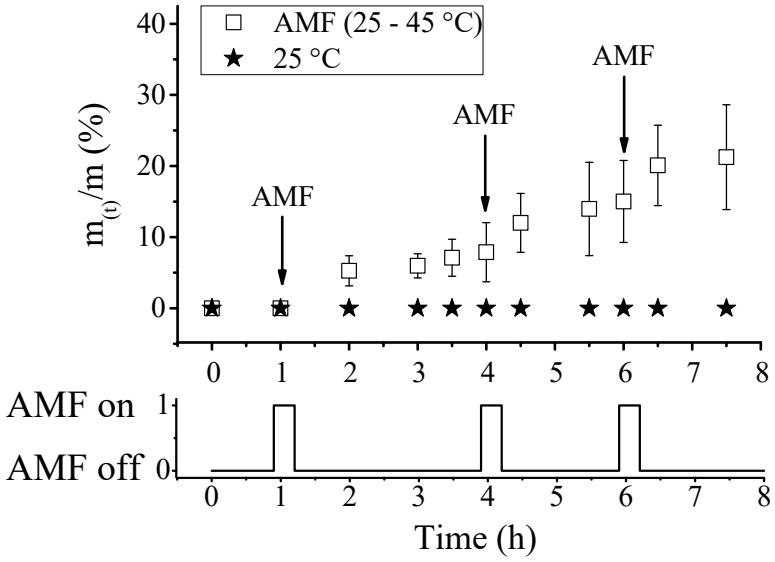

Figure 29. Cumulative release of GFP from nanobiocomposite (released mass at time t over the total mass of GFP, m_t/m) placed in phosphate buffered saline (PBS) solution (samples **R1-R3**). The samples were heated applying water bath (42 °C) or by alternating magnetic field (AMF) for 12 min interval.

3.4.4. Demonstration of Rhodamine B release

Disks of the NBC containing RhB prepared by the casting method as discussed were treated by AMF or by external heating using a water bath applying same duration and cycles of heating (samples R4-6, R7-9, R19-21, R22-24, see Table 4). The design of RhB containing NBC is different from GFP containing NBC as shown in Fig. 28. The RhB is loaded homogenously in the polymer matrix and it was to found out how is the

release behavior in this way. The amount of loaded RhB is 1 wt.% is fixed in this work, however, which can be variable.

The timings of the heating cycles in case of short term experiments (hours) are indicated in Fig. 30, for long term experiments (days) they are after 1, 2, 3, 7, 14, 30, and 60 days. It must be mentioned that different to the external heating in water bath, AMF generates a heating inside of the NBC. Release from the NBC containing RhB obtained under the different kind of heating shows a steady increase of released RhB at 42°C (temperature above melting) by external heating, on the one hand (Fig. 31). On the other hand, internal heating with AMF yield comparable amount of RhB released (about 2%) within two hours. Further AMF treatment yield an increased amount of RhB released. It turned out that externally heating using a water bath yields a slightly higher amount of RhB released of up to 6 wt.% compared to AMF. At 25°C a release of RhB was observed as well; after six hours about 2 wt.% are released.

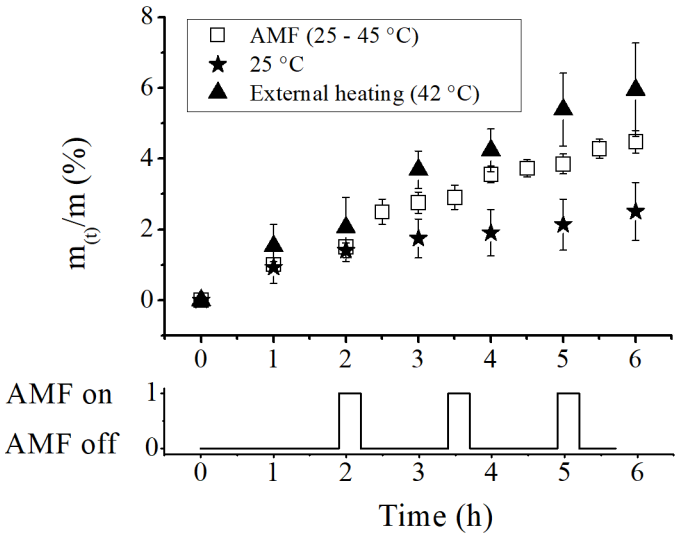

Figure 30. Cumulative released mass of Rhodamine B from composites over 6 hours (square, 1 wt.% MNP under exposure to alternating magnetic field for 12 min duration for one heating cycle), (triangle, 1 wt.% MNP, heated at 42 °C) and (star, 1 wt.% MNP, control sample at 25 °C) in phosphate buffered saline. m_t, represents cumulative mass released at time *t*. *m* represents the total mass loaded.

In long-term experiments, the cumulative RhB released is almost twice the amount compared to that of control samples treated at 25 °C after 60 days as shown in Fig. 31.

The amount of RhB released is comparable for samples stimulated by AMF and external heating by a water bath, considering the same heating cycles in both cases (12 min heating time per each cycle). However, the shorter effective time above the melting temperature in case of AMF heating. Comparing two release profile of RhB with two time span in Fig. 30 and Fig. 31, about 6 wt.% RhB was released after 6 hours, while in the long time release profile it could reach the same level only after 7 days. The reason for the higher percentage of released dye after 6 hours than that of 60 days is as following. The diffusion rate of dye from the NBC can be accelerated after new medium is added. During the 6 hours, 6 times new PBS solution was changed.

The release rates of both heated samples (AMF-25°C and Ex-25°C) were calculated as the difference of mass released between the sample (**R19-21**, **R22-24**) and the control sample (25°C, **R16-18**) over the cumulative heating time, which is considered as the effect of heating in Fig. 32. The release rates of the heated samples are higher than that of the control sample, which means that the heating increased the diffusion rate. The cumulative release rate of the control sample over the total time is given in Fig. 32 as well. Interestingly the rates of the heated samples differ for shorter release times, i.e. surface effects might be dominant. The local heat distribution in the samples might be different. Applying an external heating (water bath) the composites first start to melt on the surface or outer layers and thus the drug is released fast from these areas, whereas in AMF samples the melting temperature is first reached inside the sample and rather not at the surface layer due to heat dissipation into the aqueous medium assuming a homogeneous heating in samples with homogeneously distributed MNPs. Additionally, local fluctuations of the MNP concentration in the µm-scale can lead to temperature gradients. Local overheating over 42 °C near particle clusters can't be excluded. At long release times (60 days) the time intervals between the heating cycles are bigger and the heating comes less important that can be seen on the parallel curves in Fig. 31 and the similar release rates of both heated samples in Fig. 32.

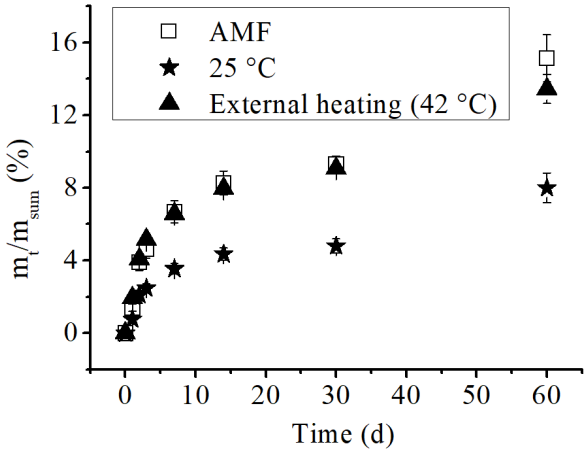

Figure 31. Cumulative mass released from Rhodamine B nanobiocomposite over 60 days (square, 1 wt.% MNP under exposure to alternating magnetic field for 12 min duration for one heating cycle), triangle, 1 wt.% MNP, heated externally at 42 °C and (star, 1 wt.% MNP, control sample at 25 °C) in phosphate buffered saline (pH 7.4). m_t, represents cumulative mass released at time t. m_{sum} represents the total mass loaded.

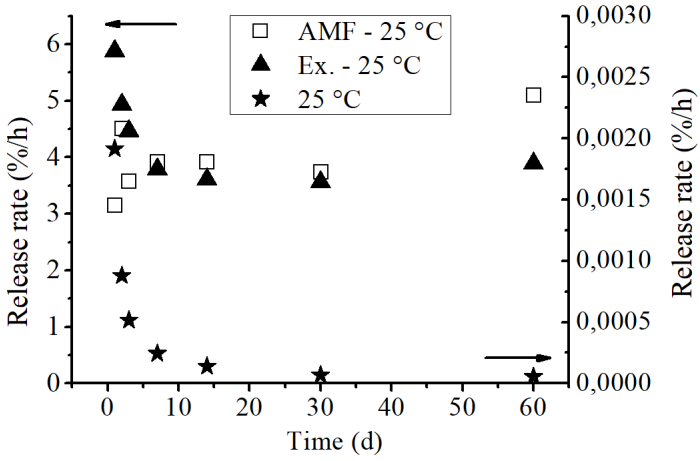

Figure 32. Release rate of (AMF-RT), calculated by difference of released mass between AMF sample and control sample over the cumulative heating time. Release rate of (Ex-25 °C), calculated by difference of released mass between external heating sample and control sample over the cumulative heating time.

3.5. Surface properties of meltable nanobiocomposites

Functional surfaces with controlled wetting properties, which can response to external stimuli, have attracted huge interest of the scientific community due to their wide range of potential applications, including microfluidic devices, controllable drug delivery and self-cleaning surfaces.[121] Superhydrophobic surface with contact angle bigger than 150 °C has self-cleaning effects, which have been used in the building and medical devices.

The techniques leading to the modification of wettability behavior on superhydrophobic surfaces can be realized under specific conditions: optical[134], magnetic[135], mechanical[136], chemical[120], thermal[137]. Hence it was studied if structuring of magnetic composite with magnetic field is possible. Three strategies were considered to influence the surface properties shown in Fig. 3. 32.

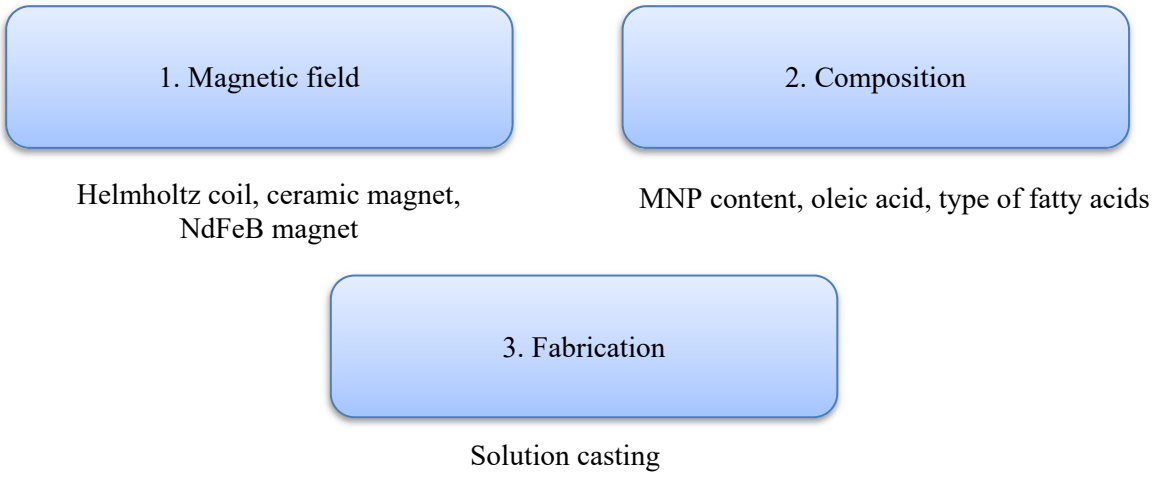

Figure 33. Overview of three strategies to influence the contact angle of water drop meltable nanobiocomposites. Different magnetic fields represent the magnetic strength to orient the magnetic particles. It indicates the influencing factors like MNP content, type of fatty acid used to esterification of dextran, oleic acid coating on the MNP in the block of composition. Solution casting is the method to fabricate the nanobiocomposites.

3.5.1. Structuring of magnetic nanobiocomposite in a static magnetic field

Three different kinds of magnetic field on the magnetic composite layers were applied separately, which was realized with Helmholtz coil, ceramic magnet, NdFeB magnet. Set-up of NdFeB magnetic system was displayed in the Fig. 34. It is composed of one NdFeB magnet and one ceramic magnet in order to have a strong magnetic field

gradient making possible to move the magnetic particle embedded in polymer matrix. Since magnetic field gradient of Helmholtz coil (0.016 T/m) was too weak to generate a mobility of MNP. In-between two ceramic magnets the magnetic field gradient can be reached to 20 T/m. A set-up of NdFeB magnet combined with ceramic magnet can lead the magnetic field gradient even to 90 T/m. Therefore, the permanent magnets with much higher magnet field strength were used. The composite layer was placed 1 mm near to the stronger magnet and 2 mm near to the weaker magnet. The correspondent magnetic field gradient is listed in the Table 5. It must be noted that the magnetic field gradient between the two magnets are not completely homogeneous. Different sample magnetic composite layers loading variable magnetic particle content were shown in the Table 6. The samples are named with T as prefix for the purpose of "texturing".

Table 5. Overview of magnetic field gradient with different set-up

	Helmholtz coil	Ceramic magnet combined with ceramic magnet	NdFeB magnet combined with ceramic magnet
Magnetic field gradient strength (T/m)	0.016	20	90

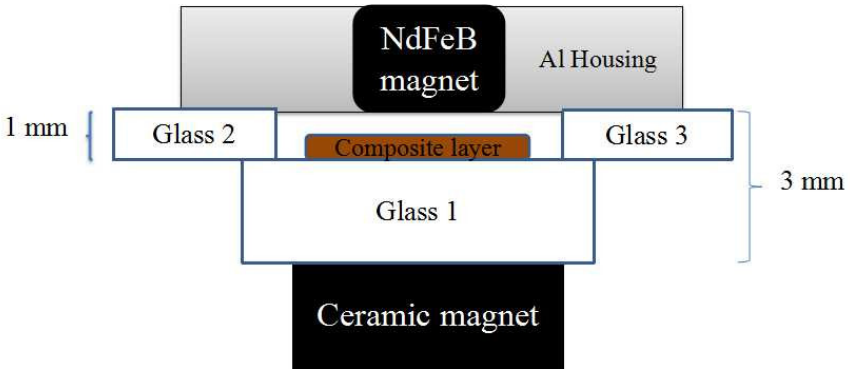

Figure 34. Set-up of magnetic structuring with NdFeB magnet (cross-section). NdFeB magnet can be replaced with ceramic magnet.

Table 6. Overview of samples for magnetic treatment. For each sample 10 points was measured on three layers with same composition.

Samples	Dextran ester/DS	MNP content (%)	Magnetic treatment
T1	Palmitate/2.69	0	No
T2	Myristate/2.56	0	No
T3	Palmitate/2.69	1	Helmholz coil
T4	Palmitate/2.69	1	Ceramic magnet
T5	Palmitate/2.69	1	NdFeB magnet
T6	Palmitate/2.69	2	NdFeB magnet
T7	Palmitate/2.69	5	NdFeB magnet
T8	Myristate/2.56	1	Ceramic magnet
T9	Myristate/2.56	1	NdFeB magnet
T10A[a]	Palmitate/2.69	1	NdFeB magnet

[a] no oleic acid coating)

3.5.2. Surface characterization of magnetic nanobiocomposite coating layer after treatment

Testing with goniometer is one method to characterize the surface property of composite layer, which is easy to handle, interpreting the hydrophilic state of the surface. The measuring principle is depicted in the Fig. 35. A defined volume of water drop is placed on the composite layer, recorded in real time by a camera. The contact angle " θ " was calculated analyzing software.

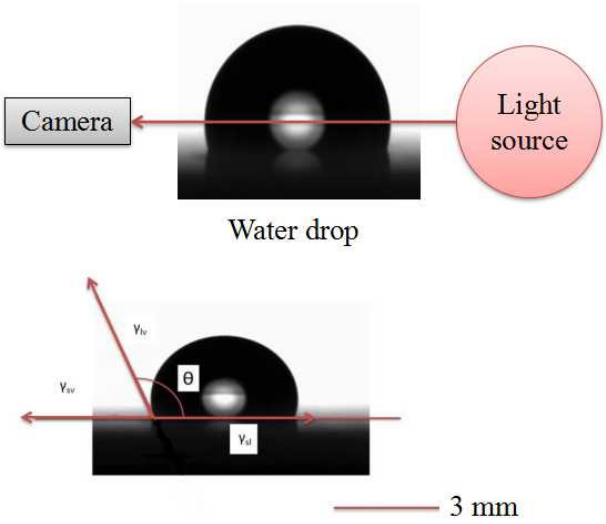

Figure 35. Schematic setup of the sessile drop method

It shows the influence of magnetic treatment on contact angle in the samples (T2 and T9) in Fig. 36. Pure myristate layers have an averaged contact angle of 107.2 ° showing a hydrophobic nature as expected. The myristate layers filled with 1% MNP without magnetic treatment have a very close value of 106.9 °. However, after magnetic treatment, a slight decrease of 2.4 ° of contact angle to 104.5 ° on the same samples was observed.

The arrangement of magnetic particle in the polymer was observed with SEM as shown in Fig. 37. The bright lines revealed by back scattering electrons consist of magnetic particles who arrange themselves in chain-like structure. The orientation of magnetic particle line is about 40° to the y-axis, which could be due to displacement of magnetic field. However, it is noticed that few particles can be found on the surface of composite. The similar observation was found in the literature [125], which shows the magnetic gel beads formed straight chain-like structures in uniform magnetic fields, while they aggregated in non-homogeneous fields.

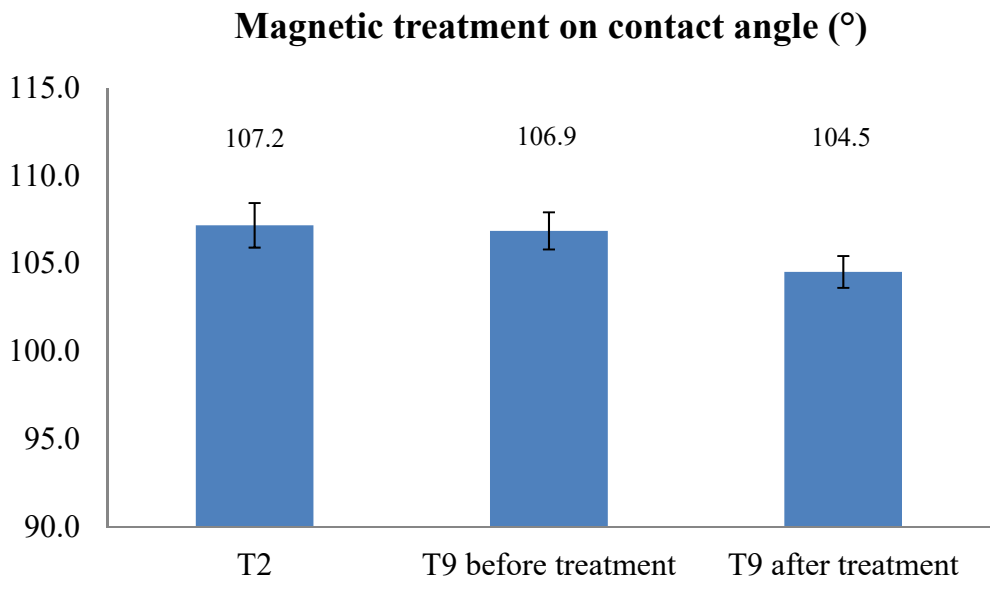

Figure 36. Dextran myristate (T2, T9): average contact angle slightly (2.4°) decreased after applying magnetic field (for each column totally 30 points measured)

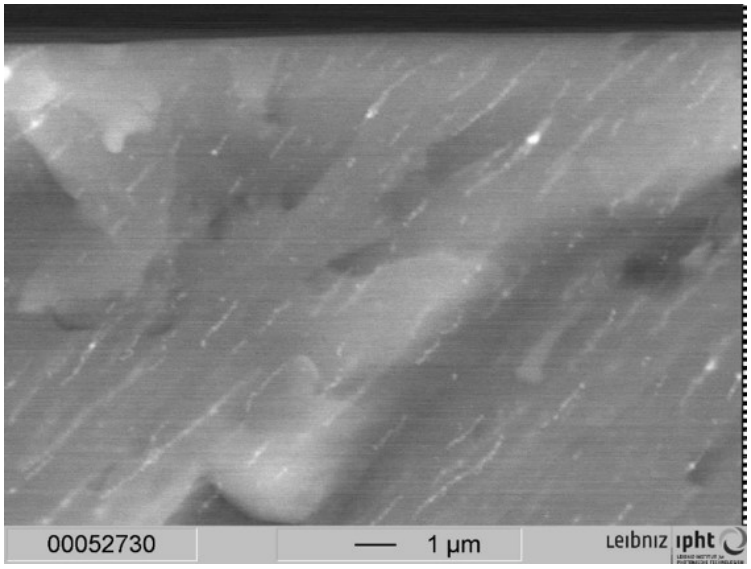

Figure 37. SEM picture of arrangement of magnetic particle in the myristate (T9) after applying magnetic field

However, the contact angle of water drop on the dextran palmitate samples (T5, T6, and T7) was not changed after the same magnetic treatment described for dextran myristate sample as shown in Fig. 38. The average contact angle on pure dextran palmitate coating layer was 109.3 °. The dextran palmitate was filled 1%, 2%, and 5% of MNP,

separately. The average contact angle was between 106.9 ° and 109.0 ° before magnetic treatment. After magnetic treatment, the average contact angle was between 107.5 ° and 107.8 °. Thus, no change on contact angle was found. A selected sample was analyzed with atomic force microscopy and scanning electron microscopy. However, no organized structure on the surface was found and no chain-like formation of MNP was observed.

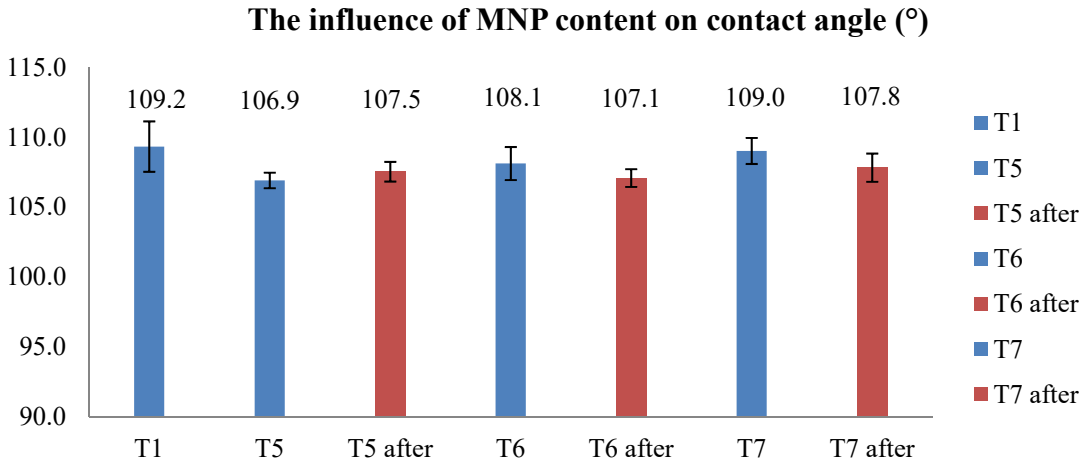

Figure 38. The influence of MNP content on contact angle (°) of samples (T1, T5, T6, T7) Sample without magnetic treatment (blue) and after magnetic treatment (red, for each column 30 points were measured)

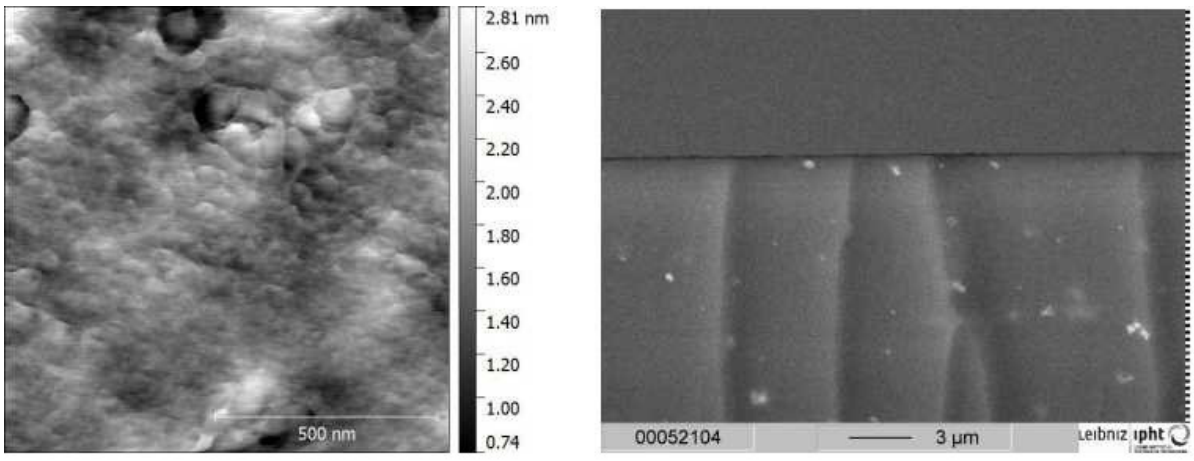

Figure 39. AFM (left) and SEM (right) picture of arrangement of magnetic particle in the palmitate (T5) after magnetic treatment

It shows that high magnetic field of NdFeB could induce the macroscopic accumulation of magnetic particles on the surface in Fig. 40. These magnetic particles align out of the coating layer. But no change was found with the contact angle measurement with water drop. One possible reason could be that the agglomeration of MNP is irregular under magnetic field.

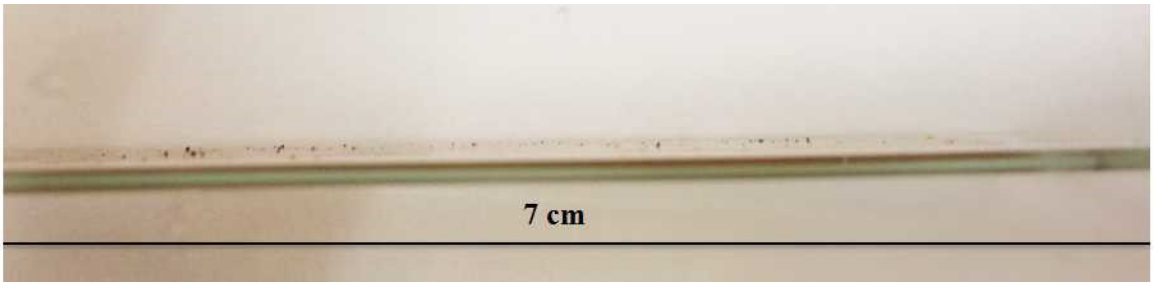

Figure 40. Macroscopic agglomerates of MNP can be found after treatment with NdFeB magnet.The bionanocomposite was coated on microscope slide

Oleic acid coated magnetic particles were embedded into the polymer matrix. MNPs without oleic acid represented as hydrophilic particles were embed into the polymer as well. CA is not changed with this component as shown in Fig. 41. One possible explanation can be that the hydrophilic uncoated MNPs are covered with hydrophobic polymer. The polymer determines the surface property of whole composite layer, which results in a unchanged contact angle.

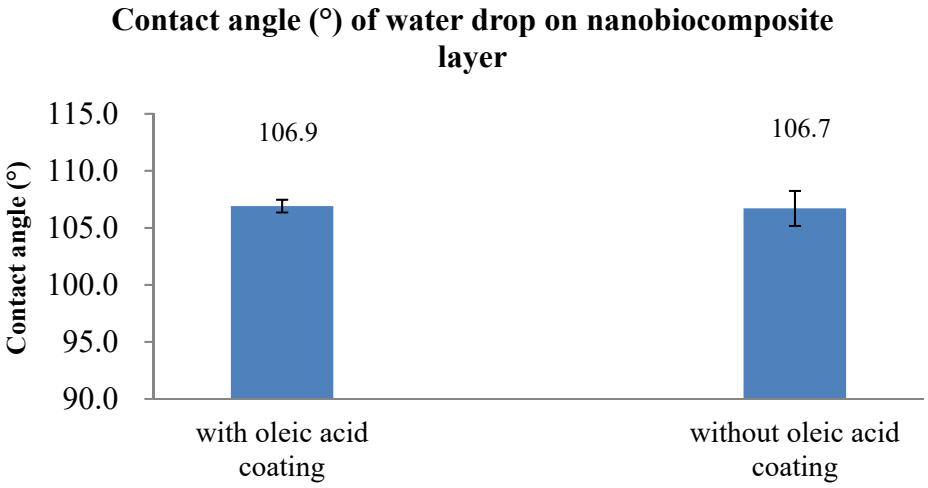

Figure 41. Average contact angle shows no obvious changes after applying magnetic field for the dextran palmitate (T5, T10) with and without oleic acid coating (for each column totally 30 points measured)

3.5.3. Biological study of magnetic nanobiocomposite coating layer after applying magnetic field

Composites with and without MNPs were prepared and treated to a magnetic field with a ceramic magnet or not resulting in four different kinds of samples (Table 7). Human umbilical vein endothelial cells (HUVECs) are primary cells derived from the endothelium of veins from the umbilical cord. [138] Cells line of human brain microvascular endothelial cells (HBMEC) that was used in the section 3.1 „for biocompatibility of composite" were taken into this part as well. Each sample was tested for cell attachment and growth for both HUVEC and HBMEC in three independent experiments. The background is the picture of composite layer coated on cover glasses but without cells under microscope (Fig. 42). It is shown that no fluorescence was observed. Therefore, the influence of autofluorescent effects caused by the composite itself was excluded based on background measurements of analogously stained composite samples not containing any cells.

Table 7. Overview of sample for biological study of magnetic nanobiocomposite coating layer after applying magnetic field

Type of cell	MNP content (%)	With magnet field exposure (pieces)	No magnet field exposure (pieces)
HUVEC	2	3	3
	0	3	3
HBMEC	2	3	3
	0	3	3
Background	2	2	2
	0	2	2

It shows the good cellular attachment/growth of HBMEC on composites In the Fig. 42. Microscopic investigations of fluorescently stained cells reveal that HBMEC attached to the composite surface in a well-distributed manner and show a regular cellular growth. Phalloidin-based staining of F-actin indicates that the cell morphology is not influenced and cell-cell contacts do not appear disrupted in the presence of composite. Furthermore, similar numbers of cells recovered from the dextran-coated surface exclude a composite-associated harmful effect on cell viability and proliferation as in section 3.1. However, no obvious difference between the sample with and without applying magnetic field was found. This gives the hint that the attachment/growth are irrespective of applying magnetic field . With respect to HUVEC, cellular attachment and growth on the surface of the composite was strongly diminished irrespectively from the presence of MNPs or surface texturing with applying magnetic field. A reason for this observation might be found in the elevated sensitivity of these primary cells towards the pronounced hydrophobic surface of the dextran palmitate composite. In general HUVECs are definitely more sensitive as they are primary cells. In all, no effects of magnetic surface texturing on cell growth are detectable.

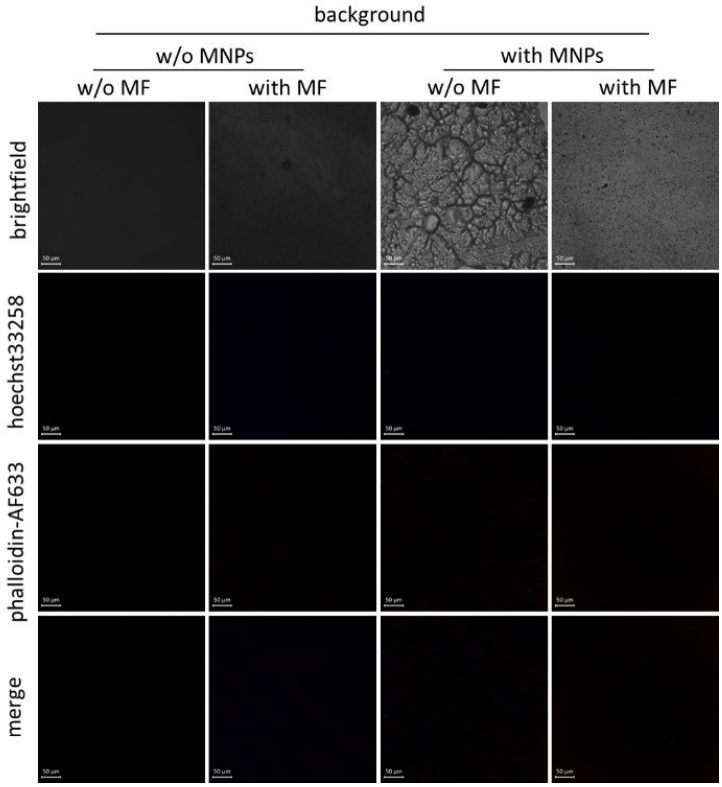

Figure 42. Photographic image of bionanocomposite without cells in the fluorescence microscope. “w/o MNP” means the sample without MNP. MF means the magnetic field

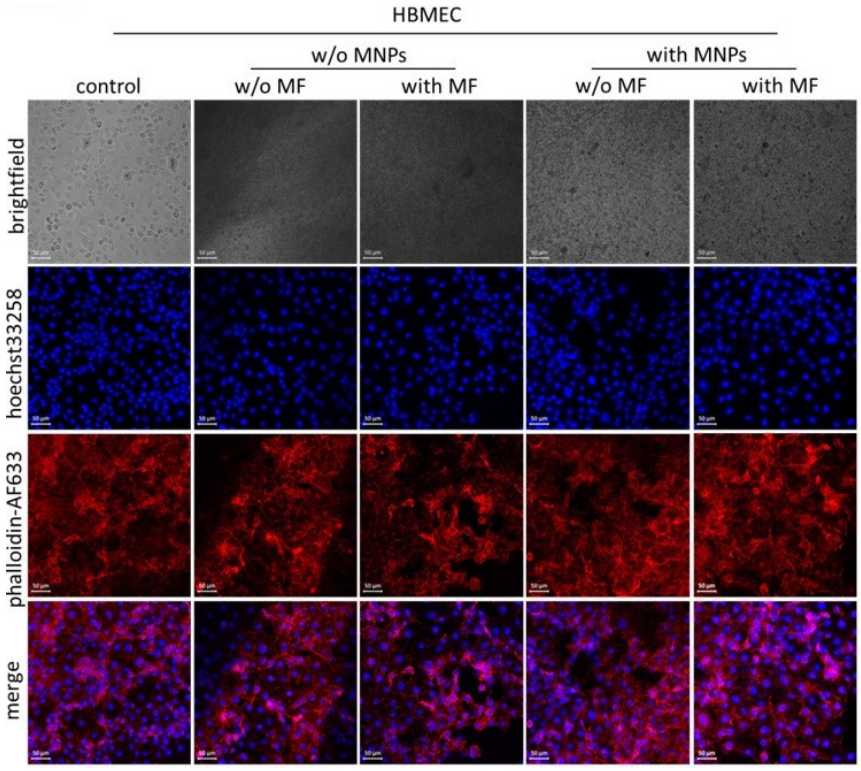

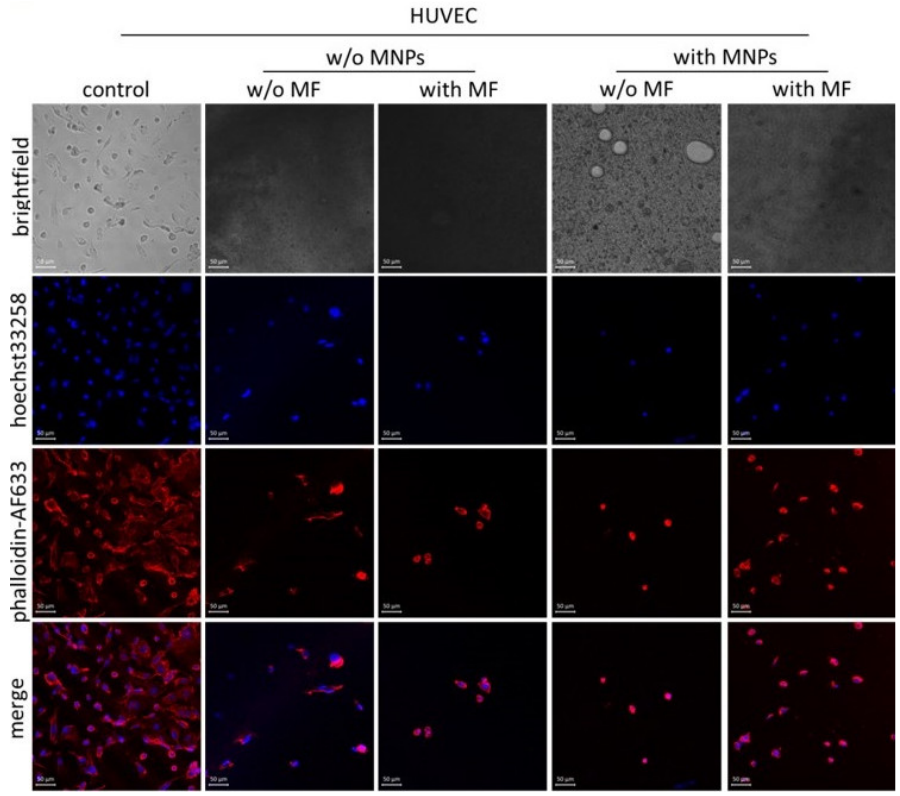

Figure 43. HBMEC (above) and HUVEC (below) seeded on dextran palmitate (**DE9**) containing magnetic particle concentrations of 2.0% immobilized on glass cover slips. Stained samples were analyzed by confocal laser scanning microscopy with 400-fold magnification. The nuclei and F-actin of HUVEC cell were not well distributed on the matrix compare that of HBMEC cell. Scale bars indicate 50µm.

4. Experimental part

4.1. Materials

Oxalyl chloride, *N, N*-dimethylacetamide (DMAc), and *N, N*-dimethylformamide (DMF) were obtained from Arcos Organics, Geel, Belgium. $FeCl_3$ x $6H_2O$ and $FeCl_2$ x $4H_2O$, tetrahydrofuran (THF), and oleic acid were obtained from Merck, Darmstadt, Germany. Palmitic acid (PA), myristic acid (MA), and lauric acid (LA) were purchased from Carl Roth GmbH, Karlsruhe, Germany. Dextran from *Leuconostoc mesenteroides* ssp. (M_w 6,000 g/mol, 15,000 g/mol, and 60,000 g/mol from Sigma Aldrich (Steinheim, Germany) was dried in vacuum at 100 °C for 24 h prior to use. Lithium chloride was supplied by Sigma Aldrich (Steinheim, Germany) and was treated in vacuum for 48 h at 100 °C. Rhodamine B (RhB) was obtained from Sigma-Aldrich. Green fluorescent protein (GFP) was supplied by University of Applied Sciences of Jena (Jena, Germany, concentration=1 mg/mL). Phosphate buffered saline was purchased by life technologies in UK (PBS, pH=7.4). High-performance liquid chromatography (HPLC) grade water was purchased by VWR international.

4.2. Synthesis

4.2.1. Synthesis of dextran fatty acid ester

Dextran fatty acid esters were prepared by *in situ* activation of the fatty acids (lauric acid, myristic acid, and palmitic acid) with iminium chloride. In a typical example (**DE9**), 5.0 g of dextran 6,000 was dissolved in 150 mL DMAc containing 5.0 g LiCl by heating the mixture to 100 °C for 1 h under stirring. A solution of fatty acid iminium chloride was formed by reacting 13.5 mL oxalyl chloride with 200 ml DMF at -20 °C and subsequent reaction with 39.5 g palmitic acid at -20 °C for 30 min. The solution was added into the dextran solution and allowed to react for 16 h at 60 °C. The dextran fatty acid esters were precipitated into 600 mL isopropanol and washed 3 times with 200 mL isopropanol to remove the remaining fatty acids, dried in vacuum at room temperature for 2 days. The product **DE9** is soluble in $CHCl_3$, THF, and toluene. Yield: 25.3 g (88.0 %); Degree of substitution (determined by ^{1}H NMR spectroscopy after peracetylation): 2.69; FTIR (KBr: cm^{-1}): 3480 *v* (OH), 2921, 2851 *v*(C-H alkyl), 1746 *v*(C=O ester), 1221 *v*(C-O-C ester)

4.2.2. Peracetylation of dextran palmitate (DE9), typical example

To determine the DS of the dextran esters by means of ^{1}H-NMR spectroscopy, perpropionylation was carried out. 0.3 g dextran palmitate ester was added into a mixture of 6 mL pyridine, 6 mL acetic acid anhydride, and 50 mg 4-(dimethylamino)pyridine as catalyst. After 24 h at 80 °C, the reaction mixture was cooled to room temperature and precipitated into 50 mL isopropanol. The product was washed three times with 50 mL isopropanol and dried in vacuum at room temperature for 2 days.

Yield: 0.31 g (86.1 %); FTIR (KBr: cm^{-1}): no ν(OH), 2920, 2851 ν(C-H), 1746 ν(C=O ester), 1222 ν(C-O ester); ^{1}H NMR ($CDCl_3$): δ (ppm) = 3.49-5.48 (H_{AGU}), 2.04 ($CH_{3\text{-acetate}}$), 0.77-1.93, 2.12-2.24 (CH_3 and $CH_{2\text{-palmitate}}$). $DS_{palmitate}$ = 2.69, DS_{acetyl} = 0.31.

4.2.3. Preparation of magnetic nanoparticles

The preparation of magnetic nanoparticles was performed by following a modification of a method described by S. Dutz.[139] A solution of 1M $NaHCO_3$ (32 mL) was slowly added to 10 mL $FeCl_2/FeCl_3$ solution (Fe^{3+}/Fe^{2+}: 4.2M/3.3M; 0.084 mol/0.066 mol) with a rate of 2 mL/min under permanent stirring up to pH 7-7.5, leading to the formation of a brownish precipitate. The solution was boiled for 10 min to form an almost black precipitate. After cooling, the suspension was washed with distilled water 3 times and dried. About 0.8 g magnetic nanoparticles obtained were coated with oleic acid as followed. 1.7 mL oleic acid and 2.58 mL 4.8M KOH were mixed with 1.62 mL of the particles aqueous suspension to promote the surfactant in the form of oleate to adhere to the particle surface. The oleate was converted into oleic acid by adding 0.37 mL 65 % HNO_3 nitric acid. The mixing steps were done in a ball mill (pulverisette 5, Fritsch, Germany) for 2 hours and 150 rpm in order to destroy large agglomerates. The product was washed with acetone and hot water alternately. After sedimentation in acetone, supernatant liquid was removed and the substance was dried. About 0.8 g MNP modified with oleic acid was obtained.

4.2.4. Preparation of magnetic bionanocomposite

Method a, extrusion: A Dynisco Laboratory Mixing Extruder was applied. In a typical example, 12.0 g dextran ester **DE09** and 0.120 g oleic acid coated MNP were premixed with a stirrer rod in a glass beaker. The mixture was added into the hopper and was

extruded at 70 °C twice. The extruded strands were granulated and coated by a lab applicator.

Method b, spin coating: Composite suspension (19.6 mg/mL dextran ester **DE09**, 0.04 mg/mL MNP in THF) was prepared and spin coated by DELTA 10TT (Süss MicroTec Lithography GmbH) on cover glass at 1000 rpm for 30 seconds.

Method c, solution casting: 1.96 g dextran ester **DE09** was dissolved in 10 mL THF and 0.04 g oleic acid coated MNPs were suspended in this solution. The suspension was treated in an ultrasonic bath (Elma Transsonic 460/H, 35 kHz) for 20 min. The suspension was poured into a petri dish and formed nanocomposite film (thickness < 1mm) under air flow. The nanocomposite was collected in form of granulates and dried in vacuum 2 days to remove the residual THF. Films of defined thickness were prepared from this material with a lab applicator after melting.

4.3. Measuring methods

4.3.1 Fourier transform infrared spectroscopy (FTIR) and nuclear magnetic resonance (NMR) spectroscopy

FTIR spectra were recorded on a Nicolet Protégé 460 spectrometer with 64 scans and a resolution of 4 cm^{-1}. The KBr tablets were dried at 100 °C for 2 h to remove moisture prior to the measurement.

NMR spectra were acquired on a Bruker AMX 250 spectrometer at room temperature with 16 scans for ^{1}H NMR, 10,240 scans for ^{13}C NMR measurements, and $^{1}H/^{13}C$ Heteronuclear Single Quantum Coherence (HSQC) spectra (40 mg sample/mL in $CDCl_3$). The degree of substitution (DS), the average number of functional groups per anhydroglucose repeating unit, was calculated from the ^{1}H NMR spectra of peracetylated samples, $DS_{\text{fatty acid}} = 3 - (7 \times I_{H,\text{acetyl}})/ (3 \times I_{H,\text{AGU}})$.

4.3.2. Gel permeation chromatography and elemental analysis The molecular weight was measured by gel permeation chromatography (GPC, Schimadzu, Japan, calibrated with polystyrene, 370–128,000 g/mol). The samples were dissolved in chloroform/isopropanol/triethylamine (94/2/4) and measured with a flow rate of 1 mL/min at 40 °C.

Elemental analyses were performed by CHNS 932 Analyzer (Leco, Germany) with combustion analysis.

4.3.3. Determination of melting temperature with hot stage microscope

The melting range was also determined with hot stage microscope (VEB Analytik Dresden). It consists of mainly three components, which are an electric heating table, a thermometer and an optical microscope. The set temperature of heating table is between the room temperature and 300 °C and the heating rate is approximately 0.5 °C/s. The measurement was done by adding about 10 mg testing sample in-between two cover glasses and by observing the onset of melting and clarification temperature of testing sample with the microscope. The temperature between the onset of melting and clarification of temperature is defined as melting temperature of polymer.

4.3.4. Determination of melting temperature by differential scanning calorimetry (DSC)

DSC experiments were carried out with a Netzsch DSC 204 F1 Phoenix equipment using 10 mg samples in an aluminum pan under nitrogen environment. The heating rate was 10 K/min and cooling rate was 20 K/min. The sample was first cooled to -50 °C and heated up to 200 °C. The heating/cooling cycle was carried out twice.

4.3.5. Scanning electron microscopy (SEM)

A scanning electron microscope is a type of electron microscope that produces images of a sample by scanning the surface with a focused beam of electrons, which is thermionically emitted from an electron gun fitted with a tungsten filament cathode. The energy exchange between the electron beam and the sample results in the reflection of high-energy electrons by elastic scattering, emission of secondary electrons by inelastic scattering and the emission of electromagnetic radiation. It scans in a raster fashion over a rectangular area of the sample surface. The morphology and distribution of MNPs in the polymer matrix were investigated by field emission scanning electron microscope (sputtered with graphite, 15kV, FE-SEM JSM 6300F, JEOL, back scattering electron contrast). Sample with 2 wt. % MNP was split into 2 parts by cryogenic break under liquid nitrogen to observe the nanocomposite morphology in the cross-sectional area.

4.3.6. Viscosity measurements

Viscosity of the composites in the melted state has been measured using the Anton Paar MCR301 rheometer. In the experiment a cone-plate measuring geometry and Peltier hood was utilized, which provides a virtually gradient-free sample temperature. Each sample was melted, tempered at T=100 °C at least during 15 minutes and the shear rate of 100 1/s was applied in order to homogenize the melt and provide reproducible initial conditions. Flow curves and viscosity curves were obtained at the constant temperature of T=100 °C in the shear rate range of 20-200 1/s. Further, a temperature sweep from 100 °C to 40 °C was done at the shear rate of 100 1/s and the cooling rate of ~0.025 °C/s.

4.3.7. Static magnetic measurements

Static magnetic measurements were carried out with a Vibrating Sample Magnetometer (VSM) MicroMag^{TM} 3900 (Princeton Measurements Corp., USA). A sample is placed inside a uniform magnetic field to magnetize the sample. The sample is then physically vibrated sinusoidally, typically through the use of a piezoelectric material. Magnetization curves $M_{(H)}$ for determining the specific saturation magnetization and coercivity were measured on the unmodified magnetic particles (to study the magnetic phase after preparation), on oleic acid coated particles, and on the composites for determination of the particle content.

4.3.8. Biocompatibility

Human brain microvascular endothelial cells (HBMEC) representing the human blood-brain barrier were used for testing biocompatibility of the dextran ester and their coating (50 μm) *in vitro*. HBMEC were cultured at 37 °C and 5% CO_2 in Roswell Park Memorial Institute (RPMI) 1640 medium and GlutaMAX™ (Invitrogen, Karlsruhe, Germany) supplemented with 10% heat-inactivated fetal calf serum (Biochrom-Seromed, Berlin, Germany) in a humidified atmosphere. GlutaMAX™ media is a standard cell culture media that contains a stabilized form of L-glutamine, L-alanyl-L-glutamine, preventing degradation and ammonia build-up even during long-term cultures. Dextran esters immobilized on circular glass cover slips (12 mm diameter, Menzel, Braunschweig, Germany) were sterilized by treating with 70%

ethanol for 30 min before 10^5 cells were seeded on the dextran ester-coated cover slips within 24 well plates (Greiner Bio-One) and cultured for 48h.

Immunosfluorescent Staining and Confocal Microscopy: For microscopic investigation of cell viability, adherent cells were washed three times with phosphate buffered saline and fixed in 10% neutral buffered formalin (Sigma-Aldrich Chemie, Steinheim, Germany) for 15 min. Subsequently, the cell membrane was permeabilized in 0.1% Triton X 100 (Sigma-Aldrich Chemie, Steinheim, Germany) for 15 min. For visualization and microscopic characterization of cells, both F-actin and nuclei were stained simultaneously with Alexa Fluor® 633 Phalloidin and Hoechst33258 (both Invitrogen, Karlsruhe, Germany) for 60 min at 37 °C. Fluorescence was analyzed using the confocal laser scanning microscope LSM 510 META (Carl Zeiss Microscopy GmbH, Jena, Germany).

4.3.9. Alternating current (AC)-Susceptometry

AC susceptibility (ACS) measurements probe the magnetization of a sample under the application of a sinusoidal AC magnetic field. The field amplitude is selected to be small enough to probe only the linear dynamic magnetization response of the MNP ensemble. The dynamic magnetic response is recorded as a function of the excitation frequency. It is described by two components, one that is in-phase with the excitation field (real part), and one which is out-of-phase (90-degree phase shift, the imaginary part).

The magnetic AC-susceptibility of 1wt% MNPs in dextran myristic ester based biopolymer was measured using a Quantum Design MPMS-5S with an integrated AC-option in the frequency range of 10^{-2} – 10^3 Hz at temperatures of 20 - 120 °C. For the measurement, about 50 mg of the biopolymer composite material were placed in an airtight sealed PCR-tube. The applied AC magnetic field had amplitude of 4 Oe.

4.3.10. Mössbauer spectroscopy

Mössbauer spectra of dextran myristate and palmitate ester based composites with a particle concentration of 1wt% were recorded in transmission geometry at temperatures of 20-110°C using a custom-built setup. A 40mCi ^{57}Co (Rh) source was used in constant acceleration mode. To provide sufficient absorption signal, a composite sample thickness of 9mm was used, corresponding to about 9 mg of nanoparticle powder per

cm^2. Mössbauer spectra at 4.3K were measured using an l-He bath-cryostat containing a superconducting magnet in split-coil geometry to provide a uniform magnetic field of up to 5 T along the γ-ray propagation direction.

4.3.11. Heating behavior in alternating magnetic field

Films of the magnetic nanocomposites with different MNP concentrations were coated on object glasses by lab applicator into about 30 mm x 20 mm square with thickness of 600 ± 20 µm, 50 ± 3 µm and 5 ± 1 µm (Table. 3). Nanocomposite coatings on object glass and disk shape samples were placed in the middle of a coil (3 turns and 5.5 cm diameter, water cooled) in air at room temperature and subjected to an alternating magnetic field with amplitude of 20 kA/m and frequency 400 kHz for 5 min. The object glasses were clamped into the coil. The disks were placed on a thin polymer blister on a porous polystyrene holder. The deviation of the field amplitude in the relevant area inside the coil was measured as smaller than 10%. The surface temperature of film and disk-shape samples in one second interval was monitored by IR thermography using a thermal camera (NEC Avio infrared Technology) 20 seconds before the start of magnetic induction for 5 min and analyzed by InfReC Analyzer NS9500 Standard (frame rate: 1 fps). The results were averaged over three points on the IR thermography. The spatial resolution of the camera combined with the arrangement of the experiment (distance between camera-sample) is about 0.3 mm. The initial temperature before switching on the field is always measured in order to see (and take into account) any drift.

The specific absorption rate (SAR) of the nanocomposite (2 wt. % MNP) was determined by measuring the initial heating rate with a fiberoptical sensor (OPTOcon, Dresden, Germany) on a bulk shaped sample of 0.10 g nanocomposite (granules < 1 mm, see 4.2.5, method c) evenly dispersed by hand in 0.90 g gelatin gel and filled in a 5 ml polystyrene round bottom tube. The tube is placed in an isolating polymer foam container inside the coil in order to suppress air convection (see Fig. 18). For the calculation of the SAR we used the equation $SAR = c \times m_f/m_c \times \Delta T/\Delta t$ with c as the specific sample's heat capacity (value of water), m_c the mass of nanocomposite, m_f the fluid mass, and $\Delta T/\Delta t$ the maximum value of the linear slope of the heating curve after subjecting the sample into an AMF (20 kA/m, 400 KHz).

4.3.12. Treatment of composite with an external static magnet to alter the heating ability

A static magnetic field with NdFeB magnet (field gradient about 20 T/m) was placed 1 cm close to magnetic composite to attract the magnetic particles, when the matrix is in melted state. Two possibilities to heat up the polymer, one is the external heating by using Peltier-element and another one is using the alternating magnetic field.

4.4. Controlled release of model drugs from magnetic dextran composite

4.4.1. Calibration of model drugs concentration with spectrometer in stock solution

In order to calibrate the GFP concentration with fluorescent intensity, ten of stock solutions were diluted with HPLC grade water. Their concentration of each GFP solution is between 1 ng/mL and 10 ng/mL. Samples were filled in a 10 mm path-length quartz curvette (Helma 111-QS, Germany). The excitation maximum for GFP was 400.0 nm and the wavelength of emission at λ = 510.0 nm of GFP in water was measured with fluorescent spectrometer (Perkin Elmer LS50-B, UK). Fluorescent intensity can be therefore correlated with the concentration of PBS solution. The PBS solution aliquot from controlled release experiment was taken out at each defined set time sampling points and diluted with HPLC grade water to the concentration range of calibration stock solution (1 ng/mL – 10 ng/mL).

10 stock solutions of Rhodamine B were diluted with HPLC grade water to a concentration between 0.5 and 5 x 10^{-6} mol/L and measured in a 10 mm path-length disposable plastic cuvette. The amount of Rhodamine B was determined with spectrophotometry (Lambda 950 UV/Vis/NIR spectrometer, Perkin Elmer) by calculating the wavelength of maximum absorbance at 544 nm.

Table 8. Condition of measurement of fluorescent spectrometer LS50-B (Perkin Elmer)

Parameters	Value
Cuvette	Helma 111-QS curvette
Modus	Emission
Excitation wavelength	400 nm
Excitation slit	15 nm

Emission slit	15 nm
Start	450 nm
End	600 nm
Scan speed	1000 nm/min.

4.4.2. Preparation of model drug composites and model drug magnetic composites

50 mg magnetic dextran myristic ester was filled into a mold with radius of 3 mm and thickness of 4 mm and the temperature was increased to 50 °C for 20 min in an oven forming a composite disk after solidification. 20 µL GFP solution was dropped on the composite with micropipette. The GFP solution was allowed to dry under air for 2 h to form a layer on the composite surface. Subsequently another 50 mg magnetic dextran myristic ester was added on the GFP layer and the temperature was increased to 50 °C for 20 min in an oven. After cooling down, a disk shape GFP loaded magnetic composite was formed. GFP control composites were prepared as described above. The disk samples have radius of 3 mm and thickness of 4 mm.

1.96 g dextran ester and 0.02 g Rhodamine B were dissolved in 10 mL tetrahydrofuran (THF) and 0.02 g oleic acid coated MNPs were suspended in this solution. The suspension was treated in an ultrasonic bath (Elma Transsonic 460/H, 35 kHz) for 30 min. It was poured into a petri dish and afterwards a film (thickness < 1mm) was formed under air flow. The Rhodamine B nanocomposite was collected in form of granulates and dried in vacuum 2 days. 50 mg Rhodamine B nanocomposite was filled into a blister pack with a radius of 3 mm and thickness of 4 mm and the temperature was increased to 50 °C for 20 min in an oven forming a composite disk after solidification.

4.4.3. Temperature measurement inside the composite

The temperature of the composite was determined with a fiber optical sensor (OPTOcon TS5, Dresden, Germany). The fiber sensor was embedded inside the composite disk (1 wt.% MNP) surrounded by 0.5 mL water.

4.4.4. Enclosement of GFP in the matrix before melting

To proof the sealability, a disk of GFP loaded magnetic composite was placed in a falcon tube containing 3 ml PBS solution in a water bath at 25 °C for 24 hours. The

aliquots were taken out and refilled after 1, 2, 3, 4 and 24 hours. At 24 hour, the temperature in the water bath was increased to 42°C. The aliquots were taken out and refilled again at 26th and 28th hour and measured with fluorescence spectrometer. The cumulative release was quantified as mass released at time t, M_t, over the total mass loaded, M_{sum}.

4.4.5. Composite treated externally in water bath and internally with alternating magnetic field

For the external treatment in the water bath, the composite disks filled in the blister pack, (samples R4 - R6, see Table 4), were placed in a 15 mL falcon tube containing 3 mL PBS solution. The falcon tube was heated in a water bath for 12 min. After 1 h the PBS solution was completely taken out and diluted with HPLC grade water into the linear fitting concentration range of calibration curve. New PBS solution was filled again into the tube and it was heated in a water bath for 12 min. Magnetic composites (samples R7 - R9 and R13 - R15) loaded with model drugs were put in the falcon tubes containing 0.5 mL PBS solution and placed in the middle of coil in AMF (3 turns, 5.5 cm diameter, water cooling). AMF was turned on for 12 min for each exposure (strength of 20 kA/m and frequency of 400 kHz). After 48 min PBS solution was completely taken out and later diluted with HPLC grade water. New PBS was filled again into the tube and next AMF was applied for 12 min. In 60 days RhB release experiment (R19 - R21), the tube was heated for 12 min at 42 °C externally in the water bath in each cycle, in order to have same heating time with the samples heated with AMF (R22 - R24). The sample was taken out for analyzing 4 hours after the treatment. Magnetic stirring was applied during the storage. Control samples (R1 - R3, R10 - R12 and R16 - R18) were placed in the same falcon tubes containing 3 mL PBS solution at 25 °C without any heat treatment. Cumulative release was quantified as mass released at time t, M_t, over the total mass loaded, M_{sum}

4.5. Structuring of magnetic composite

4.5.1. Fabrication of sample for magnetic structuring

Composite films containing magnetic particle were obtained by coating of the composite with a lab applicator on a microscope slide at 100 °C with a heating plate. The thickness of film was thickness between 30 - 50 μm, measuring with a micrometer.

4.5.2. Applying magnetic field on composite for structuring

Set-up of magnetic field is illustrated in the Fig. 34 the microscope slide containing composite layer was placed on a ceramic magnet, then two microscope slides (glass 2 and 3) were put on the part of side on glass 1 without contact to composite layer. Another magnet was placed on the part of glass (2 and 3). Therefore a defined distance between the two magnets was available. The magnetic field strength was measured with Gaussmeter (Dr. Steingroever GmbH) by inserting a Hall sensor between the two magnets. One ceramic magnet can be replaced with a NdFeB magnet.

4.5.3. Contact angle measurement

The contact angle was measured by a sessile drop method (OCA 25, DataPhysics Instrument GmbH, Filderstadt, Germany). A water droplet (sessile drop, 3 μL) was sat on a solid and subsequently was analyzed at room temperature with software (SCA 20, DataPhysics Instrument GmbH, Filderstadt, Germany). The base-line is defined by evaluating the grey scale values of the recorded image. To determine the right and left contact angle is to apply tangents at the intersections of the drop outline and the baseline. 10 water drops on the surface was measured at RT. The contact angle was averaged by three repeated samples.

5. Summary

Different properties of meltable magnetic bionanocomposites based on dextran fatty acid ester were systematically studied in this work, namely the heating behavior under alternating magnetic field, release behavior of loaded model drug, and the surface hydrophilic/hydrophobic property after applying alternating magnetic field.

The mobility of magnetic particles was investigated with static gradient magnetic field. Different to ferrofluid and magnetic hydrogel system, in this thermoplastic composite system the magnetic particles could only move slowly in the matrix due to high viscosity of polymer melts. The slow relaxation behavior of magnetic particles was observed at 120 °C with 0.05Hz in AC susceptometry.

The heating behavior of meltable nanobiocomposites with high frequency alternating magnetic field was studied and an optimal condition (> 1% magnetic particle content and > 1 mm thickness) for preparing NBC samples was worked out. In the molten state of the matrix a “magnetic texturing” of particles can be built by means of a static external magnetic field which could strengthen the heating ability of the composite material at certain spot.

Furthermore, meltable polysaccharide-based biopolymers can be applied to design magnetically remote controlled drug release system. An advantage of this NBC compared with hydrogel is that compounds of rather high molar mass，i.e. GFP, can be immobilized inside without leaking when no external thermal stimulus is applied. Increasing of temperature by AMF has accelerated diffusion of model drugs (GFP and RhB) compared with samples without heat treatment. The increased amount of released model drug is close to each other for AMF and external heating methods. After 60 days 16 wt.% of RhB is released by applying AMF. The immobilization of drug and their controlled release *in vivo* by applying magnetic field of this meltable and bio-based magnetic composite still need further investigation. This work is the first study on the heating ability and release behavior of this magnetic composite.

Applying magnetic field generated (2°) decrease of contact angle on the dextran myristate composites layers. Applying the same magnetic field on dextran palmitate samples has no effect on the contact angle. Furthermore, increasing concentration of MNP from 1% to 5% (dextran palmitate samples) brings no change on the contact angle.

The surface of composite layers embedded with hydrophilic magnetic particles (no oleic acid coating) keep their hydrophobic behavior of the matrix. No topographic change on the surface was revealed by SEM and AFM for all samples, though chain-like formation of magnetic particle was observed. With up to 5% MNP the surface morphology is not able to be modified to realize a change in contact angle. The cellular attachment and growth behavior of endothelial cell line HBMEC (human brain microvascular endothelial cell) on the surface of NBC was not changed after applying magnetic field. The reason could be that the energy given by magnetic field is not enough to generate a topographic change on the surface, compared to other methods, such as light and mechanical methods.

Zusammenfassung

Verschiedene Eigenschaften von schmelzbaren magnetischen Nanobiokompositen (NBC), die auf Dextranfettsäureestern basieren, werden in dieser Arbeit studiert. Es wurden die Heizbarkeit unter einem magnetischen Wechselfeld (MWF), das Freisetzungsverhalten von im Nanobiokompositen enthaltenen Modellwirkstoffen und die Hydrophobie/Hydrophilie-Balance der Oberflächen bei der Anwendung einens magnetischen Wechselfelds. Die Mobilität von magnetischen Partikeln wurde mit Gleichmagnetfeldgradient untersucht. Im Unterschied zu Ferrofluid- und magnetischen Hydrogel-Systemen, können sich die magnetischen Partikel wegen der hohen Viskosität in den thermoplastischen Kompositen nur langsam bewegen. Das Relaxationsverhalten von magnetischen Partikeln wurde mit AC-Suszeptometrie studiert. Das Maximum des imaginären ACS-Signals bei 120°C wurde bei 0.05 Hz gemessen.

Das Heizverhalten von schmelzbaren NBC im magnetischen Wechselfeld mit hoher Frequenz wurde studiert. Ein optimales Verfahren (> 1 wt.% magnetische Partikel und 1 mm Dicke) für die Herstellung der NBC Proben wurde ausgearbeitet. Im geschmolzenen Zustand kann eine “magnetische Textierung” aufgebaut werden, was die Heizfähigkeit in spezifischen Bereichen verstärken kann.

Weiterhin können die magnetischen NBC mit magnetischerm Wechselfeld ferngesteuert werden. Diese NBC haben im Vergleich zu Hydrogelen den Vorteil, dass Komponenten mit relativer hoher Molekülmasse darin mit verminderten Leaking immobilisiert werden können, wenn keine externe thermische Anregung vorhanden ist. Bei Proben kann unter magnetischer Behandlung durch den daraus resultierenden Anstieg von Temperatur die Diffusion von Modellwirkstoffen (GFP und RhB) erhöht werden. Das Freisetzungsverhalten von Modellwirkstoffen ist ähnlich für beide Methode von MWF und externe Heizung. Nach 60 Tagen werden 16 wt.% RhB bei Anwendung einens MWF freigesetzt.. Die Immobilisierung und Freisetzung von Modellwirkstoffen bei Anwendung von MWF *in vivo* wurden in dieser Arbeit nicht untersucht.

Der Kontaktwinkel von Wasser auf der Oberfläche von magnetischen Dextranmyristatkompositen wurde durch die Anwendung von MWF um 2° abgesenkt, was keiner signifikanten Veränderung des Kontaktwinkel entspricht. Ein weiterer Anstieg des Gehalt der magnetischen Partikel bis zu 5 wt.% (Dextranpalmitate) hat kein

Einfluss auf den Kontaktwinkel von Wasser. Die Oberfläche der NBC, in die hydrophile magnetische Partikel (keine Ölsäurebeschichtung) eingebettet worden sind, haben ebenfalls keine hydrophile Eigenschaft. Eine Ketten-förmige Struktur von MNP wurde mit SEM herausgefunden. Es wurde aber keine topographische Veränderung auf der Oberfläche durch AFM und SEM beobachtet. Die Erhöhung des MNP-Gehalts bis zu 5 wt.% führt zu keiner Veränderung der Oberflächenmorphologie. Die Anwendung von MWF zeigt ebenfalls keinen Einfluss auf das Aufwachsen von Zellsystemen. Ein möglicher Grund dafür ist, dass die Energie nicht für eine topographische Veränderung reicht, im Vergleich zu anderen Methoden, z.B. Licht und mechanische Kräfte.

Literatures:

1. Gupta, A. K.; Gupta, M., Synthesis and surface engineering of iron oxide nanoparticles for biomedical applications. *Biomaterials* **2005,** *26* (18), 3995-4021.
2. Sadhukha, T.; Wiedmann, T. S.; Panyam, J., Inhalable magnetic nanoparticles for targeted hyperthermia in lung cancer therapy. *Biomaterials* **2013,** *34* (21), 5163-5171.
3. Sadhukha, T.; Wiedmann, T. S.; Panyam, J., Enhancing therapeutic efficacy through designed aggregation of nanoparticles. *Biomaterials* **2014,** *35* (27), 7860-7869.
4. Satarkar, N. S.; Zhang, W.; Eitel, R. E.; Hilt, J. Z., Magnetic hydrogel nanocomposites as remote controlled microfluidic valves. *Lab Chip* **2009,** *9* (12), 1773-1779.
5. Wilson, S. A.; Jourdain, R. P. J.; Zhang, Q.; Dorey, R. A.; Bowen, C. R.; Willander, M.; Wahab, Q. U.; Willander, M.; Al-hilli, S. M.; Nur, O.; Quandt, E.; Johansson, C.; Pagounis, E.; Kohl, M.; Matovic, J.; Samel, B.; van der Wijngaart, W.; Jager, E. W. H.; Carlsson, D.; Djinovic, Z.; Wegener, M.; Moldovan, C.; Iosub, R.; Abad, E.; Wendlandt, M.; Rusu, C.; Persson, K., New materials for micro-scale sensors and actuators. *Materials Science and Engineering: R: Reports* **2007,** *56* (1-6), 1-129.
6. Satarkar, N. S.; Biswal, D.; Hilt, J. Z., Hydrogel nanocomposites: a review of applications as remote controlled biomaterials. *Soft Matter* **2010,** *6* (11), 2364-2371.
7. Satarkar, N. S.; Hilt, J. Z., Magnetic hydrogel nanocomposites for remote controlled pulsatile drug release. *Journal of Controlled Release* **2008,** *130* (3), 246-251.
8. Thevenot, J.; Oliveira, H.; Sandre, O.; Lecommandoux, S., Magnetic responsive polymer composite materials. *Chemical Society Reviews* **2013,** *42* (17), 7099-7116.
9. Mura, S.; Nicolas, J.; Couvreur, P., Stimuli-responsive nanocarriers for drug delivery. *Nature Materials* **2013,** *12* (11), 991-1003.
10. Qiu, Y. P., K. , *Advanced Drug Delivery Reviews* **2001,** *53*, 321-339.
11. Choi, S. W.; Zhang, Y.; Xia, Y., A temperature-sensitive drug release system based on phase-change materials. *Angewandte Chemie International Edition* **2010,** *49* (43), 7904-8.
12. Campbell, S. B.; Patenaude, M.; Hoare, T., Injectable superparamagnets: highly elastic and degradable poly(N-isopropylacrylamide)-superparamagnetic iron oxide nanoparticle (SPION) composite hydrogels. *Biomacromolecules* **2013,** *14* (3), 644-653.
13. Satarkar, N. S.; Zach Hilt, J., Hydrogel nanocomposites as remote-controlled biomaterials. *Acta Biomaterialia* **2008,** *4* (1), 11-16.
14. Dionigi, C.; Piñeiro, Y.; Riminucci, A.; Bañobre, M.; Rivas, J.; Dediu, V., Regulating the thermal response of PNIPAM hydrogels by controlling the adsorption of magnetite nanoparticles. *Applied Physics A* **2013,** *114* (2), 585-590.

15. Liebert, T.; Wotschadlo, J.; Laudeley, P.; Heinze, T., Meltable Dextran Esters As Biocompatible and Functional Coating Materials. *Biomacromolecules* **2011,** *12* (8), 3107-3113.
16. Heinze, T.; Liebert, T.; Heublein, B.; Hornig, S., *Advances in Polymer Science* **2006,** *205*, 199-291.
17. Klemm, D.; Schmauder, H.; Heinze, T.; Cellulose. In: De Baets S, V. E., Steinbüchel A (eds) Biopolymers: polysaccharides 2, vol 5. Wiley, Weinheim **2002**, 275-320.
18. Klemm D., H. B., Fink H.-P., Bohn A., Cellulose: Fascinating biopolymer and sustainable raw material, Angewandte Chemie, International Edition **2005,** *44* 3358-3393.
19. Klemm, D.; Heublein, B.; Fink, H. P.; Bohn, A., Cellulose: Fascinating Biopolymer and Sustainable Raw Material. *Angewandte Chemie International Edition* **2005,** *44* (22), 3358-3393.
20. Tang, W. J.; Fernandez, Javier G.; Sohn, Joel J.; Amemiya, Chris T., Chitin Is Endogenously Produced in Vertebrates. *Current Biology 25* (7), 897-900.
21. Jane, J.-l., Chapter 6 - Structural Features of Starch Granules II. In *Starch (Third Edition)*, Academic Press: San Diego, 2009; pp 193-236.
22. Heinze, T.; Liebert, T.; Koschella, A., Esterification of Polysaccharides. Springer-Verlag: Berlin Heidelberg, Germany, 2006
23. Philipp, B., Organic Solvents for Cellulose as a Biodegradable Polymer and Their Applicability for Cellulose Spinning and Derivatization. *Journal of Macromolecular Science, Part A* **1993,** *30* (9-10), 703-714.
24. Wanrosli, W. D.; Rohaizu, R.; Ghazali, A., Synthesis and characterization of cellulose phosphate from oil palm empty fruit bunches microcrystalline cellulose. *Carbohydrate Polymers* **2011,** *84* (1), 262-267.
25. Balser, K.; Hoppe, L.; Eicher, T.; Wandel, M.; Astheimer, H.; Steinmeier, H.; Allen, J. M., Cellulose Esters. In *Ullmann's Encyclopedia of Industrial Chemistry*, 2004.
26. Won, C.-Y.; Chu, C.-C., Inulin polysaccharide having pendant amino acids: Synthesis and characterization. *Journal of Applied Polymer Science* **1998,** *70* (5), 953-963.
27. Liebert, T. F.; Heinze, T., Tailored Cellulose Esters: Synthesis and Structure Determination. *Biomacromolecules* **2005,** *6* (1), 333-340.
28. Jandura, P.; Riedl, B.; Kokta, B. V., Thermal degradation behavior of cellulose fibers partially esterified with some long chain organic acids. *Polymer Degradation and Stability* **2000,** *70* (3), 387-394.
29. Vaca-Garcia, C.; Borredon, M. E.; Gaset, A., Method for making a cellulose or starch fatty ester by esterification or transesterification. Google Patents: **2000**.
30. Lino, F.; Ana, R.; Meriem, L.; A., B. M.; H., G. M.; S., C. A. M.; S., D. J., Biocompatibility of chemoenzymatically derived dextran-acrylate hydrogels. *Journal of Biomedical Materials Research Part A* **2004,** *68A* (3), 584-596.

31. Cao, X.; Sun, S.; Peng, X.; Zhong, L.; Sun, R.; Jiang, D., Rapid Synthesis of Cellulose Esters by Transesterification of Cellulose with Vinyl Esters under the Catalysis of NaOH or KOH in DMSO. *Journal of Agricultural and Food Chemistry* **2013,** *61* (10), 2489-2495.

32. Nafchi, A. M.; Moradpour, M.; Saeidi, M.; Alias, A. K., Thermoplastic starches: Properties, challenges, and prospects. *Starch/Stärke* **2013,** *65*, 61–72.

33. Forssell, P.; Mikkilä, J.; Suortti, T.; Seppälä, J.; Poutanen, K., Plasticization of Barley Starch with Glycerol and Water. *Journal of Macromolecular Science, Part A* **1996,** *33* (5), 703-715.

34. Averousa, L.; Moroa, L.; Doleb, P.; Fringant, C., Properties of thermoplastic blends: starch–polycaprolatone. *Polymer* **2000,** *41* 4157-4167.

35. Simon, J.; Müller, H. P.; Koch, R.; Müller, V., Thermoplastic and biodegradable polymers of cellulose. *Polymer Degradation and Stability* **1998,** *59* 107-115.

36. Edgar, K. J.; Buchanan, C. M.; Debenham, J. S.; Rundquist, P. A.; Seiler, B. D.; Shelton, M. C.; Tindall, D., Advances in cellulose ester performance and application. *Progress in Polymer Science* **2001,** *26* (9), 1605-1688.

37. Teramoto, Y., Functional Thermoplastic Materials from Derivatives of Cellulose and Related Structural Polysaccharides. *Molecules* **2015,** *20* (4), 5487.

38. Heinze, T.; Liebert, T., *Polymer Science: A Comprehensive Reference, Celluloses and Polyoses/Hemicelluloses*. Elsevier, Amsterdam: 2012; Vol. 10 p83-152.

39. Vaca-Garcia, C.; Gozzelino, G.; Glasser, W. G.; Borredon, M. E., Dynamic mechanical thermal analysis transitions of partially and fully substituted cellulose fatty esters. *Journal of Polymer Science Part B: Polymer Physics* **2003,** *41* (3), 281-288.

40. Aburto, J.; Alric, I.; Borredon, E., Preparation of Long-chain Esters of Starch Using Fatty Acid Chlorides in the Absence of an Organic Solvent. *Starch - Stärke* **1999,** *51* (4), 132-135.

41. Liebert, T.; Nagel, M. C. V.; Jordan, T.; Heft, A.; Grunler, B.; Heinze, T., Pure, Transparent-Melting Starch Esters: Synthesis and Characterization. *Macromolecular Rapid Communications* **2011,** *32* (17), 1312-1318.

42. Winkler, H.; Vorwerg, W.; Wetzel, H., Synthesis and properties of fatty acid starch esters. *Carbohydrate Polymers* **2013,** *98* (1), 208-216.

43. http://www.makeitfrom.com/material-properties/Polyetheretherketone-PEEK.

44. *IDEMITSU Kosan Co., Ltd.*

45. http://www.dupont.com/.

46. Seyednejad, H.; Vermonden, T.; Fedorovich, N. E.; van Eijk, R.; van Steenbergen, M. J.; Dhert, W. J. A.; van Nostrum, C. F.; Hennink, W. E., Synthesis and Characterization of Hydroxyl-Functionalized Caprolactone Copolymers and Their Effect on Adhesion, Proliferation,

and Differentiation of Human Mesenchymal Stem Cells. *Biomacromolecules* **2009,** *10* (11), 3048-3054.

47. Yan, B.; Gu, S.; Zhang, Y., Polylactide-based thermoplastic shape memory polymer nanocomposites. *European Polymer Journal* **2013,** *49* (2), 366-378.

48. Morooka, T.; Norimoto, M.; Yamada, T.; Shiraishi, N., Dielectric properties of cellulose acylates. *Journal of Applied Polymer Science* **1984,** *29* (12), 3981-3990.

49. Novak, L. J.; Tyree, J. T., **1960**, US Patent 2954372.

50. Grote, C.; Heinze, T., Starch Derivatives of High Degree of Functionalization 11: Studies on Alternative Acylation of Starch with Long-chain Fatty Acids Homogeneously in N,N-dimethyl acetamide/LiCl. *Cellulose* **2005,** *12* (4), 435-444.

51. Scheibler C, Investigation on the nature of the gelatinous excretion (so-called frog's spawn) which is observed in production of beet-sugar juices. *Zeitschrift des Vereins der Deutschen Zuckerindustrie* **1874,** *24*, 309-335.

52. Taylor C., C. N., Walker GJ., *Carbohydrate Research* **1985,** *137:1*.

53. M Naessens, A. C., W Soetaert, EJ Vandamme, *Journal of Chemical Technology & Biotechnology* **2005,** *80*, 845-860.

54. Van Cleve, J. W., Schaefer, W. C., Rist, C. E. , *Journal of the American Chemical Society* **1956,** *78*, 4435-4438.

55. Naessens, M.; Cerdobbel, A.; Soetaert, W.; Vandamme, E. J., Leuconostoc dextransucrase and dextran: production, properties and applications. *Journal of Chemical Technology & Biotechnology* **2005,** *80* (8), 845-860.

56. Tassa, C.; Shaw, S. Y.; Weissleder, R., Dextran-Coated Iron Oxide Nanoparticles: A Versatile Platform for Targeted Molecular Imaging, Molecular Diagnostics, and Therapy. *Accounts of Chemical Research* **2011,** *44* (10), 842-852.

57. Cadée, J. A.; Luyn, M. J. A. v.; Brouwer, L. A.; Plantinga, J. A.; Wachem, P. B. v.; Groot, C. J. d.; Otter, W. d.; Hennink, W. E., In vivo biocompatibility of dextran-based hydrogels. *Journal of Biomedical Materials Research* **2000,** *50* (3), 397-404.

58. Wahl, G. M.; Stern, M.; Stark, G. R., Efficient transfer of large DNA fragments from agarose gels to diazobenzyloxymethyl-paper and rapid hybridization by using dextran sulfate. *Proceedings of the National Academy of Sciences of the United States of America* **1979,** *76* (8), 3683-3687.

59. Han, G.-C.; Ouyang, Y.; Long, X.-Y.; Zhou, Y.; Li, M.; Liu, Y.-N.; Kraatz, H.-B., (Carboxymethyl–Dextran)-Modified Magnetic Nanoparticles Conjugated to Octreotide for MRI Applications. *European Journal of Inorganic Chemistry* **2010,** *2010* (34), 5455-5461.

60. Wotschadlo, J.; Liebert, T.; Clement, J. H.; Anspach, N.; Höppener, S.; Rudolph, T.; Müller, R.; Schacher, F. H.; Schubert, U. S.; Heinze, T., Biocompatible Multishell Architecture for Iron Oxide Nanoparticles. *Macromolecular Bioscience* **2013,** *13* (1), 93-105.

61. Elschner, T.; Wondraczek, H.; Heinze, T., Syntheses and detailed structure characterization of dextran carbonates. *Carbohydrate Polymers* **2013,** *93* (1), 216-223.

62. Cohen, J. L.; Schubert, S.; Wich, P. R.; Cui, L.; Cohen, J. A.; Mynar, J. L.; Fréchet, J. M. J., Acid-Degradable Cationic Dextran Particles for the Delivery of siRNA Therapeutics. *Bioconjugate Chemistry* **2011,** *22* (6), 1056-1065.

63. Beesh M., M. P., Vandamme Th. F, Synthesis and characterization of dextran esters as coating or matrix systems for oral delivery of drugs targeted to the colon. *International Journal of Drug Delivery* **2010,** *2*, 22-31.

64. Nichifor, M.; Carpov, A., Bile acids covalently bound to polysaccharides 1. Esters of bile acids with dextran. *European Polymer Journal* **1999,** *35* (12), 2125-2129.

65. van Dijk-Wolthuls, W. N. E.; Tsang, S. K. Y.; Kettenes-van den BoschW.E. Hennink, J. J., A new class of polymerizable dextrans with hydrolyzable groups: hydroxyethyl methacrylated dextran with and without oligolactate spacer. *Polymer* **1997,** *38* (25), 6235-6242.

66. Hornig, S.; Bunjes, H.; Heinze, T., Preparation and characterization of nanoparticles based on dextran–drug conjugates. *Journal of Colloid and Interface Science* **2009,** *338* (1), 56-62.

67. Behrens, S.; Appel, I., Magnetic nanocomposites. *Curr Opin Biotechnol* **2016,** *39*, 89-96.

68. Lee, C. S.; Lee, H.; Westervelt, R. M., Microelectromagnets for the control of magnetic nanoparticles. *Applied Physics Letters* **2001,** *79* (20), 3308-3310.

69. E., S. C.; Karen, B.-S.; Maj, H.; Christer, J., Magnetic characterization of iron oxides for magnetic resonance imaging. *Magnetic Resonance in Medicine* **1994,** *31* (3), 268-272.

70. Goya, G. F.; Berquó, T. S.; Fonseca, F. C.; Morales, M. P., Static and dynamic magnetic properties of spherical magnetite nanoparticles. *Journal of Applied Physics* **2003,** *94* (5), 3520-3528.

71. Müller, R.; Dutz, S.; Neeb, A.; Cato, A. C. B.; Zeisberger, M., Magnetic heating effect of nanoparticles with different sizes and size distributions. *Journal of magnetism and magnetic materials* **2013,** *328*, 80-85.

72. Chen, J.-K.; Chang, C.-J., Fabrications and Applications of Stimulus-Responsive Polymer Films and Patterns on Surfaces: A Review. *Materials* **2014,** *7* (2), 805-875.

73. de Vicente, J.; Klingenberg, D. J.; Hidalgo-Alvarez, R., Magnetorheological fluids: a review. *Soft Matter* **2011,** *7* (8), 3701.

74. Yancheng, L.; Jianchun, L.; Weihua, L.; Haiping, D., A state-of-the-art review on magnetorheological elastomer devices. *Smart Materials and Structures* **2014,** *23* (12), 123001.

75. Wisotzki, E. I.; Eberbeck, D.; Kratz, H.; Mayr, S. G., Magnetic response of gelatin ferrogels across the sol-gel transition: the influence of high energy crosslinking on thermal stability. *Soft Matter* **2016,** *12* (17), 3908-3918.

76. Na, H. B.; Song, I. C.; Hyeon, T., Inorganic Nanoparticles for MRI Contrast Agents. *Advanced Materials* **2009,** *21* (21), 2133-2148.

77. Pankhurst, Q. A.; Connolly, J.; Jones, S. K.; Dobson, J., Applications of magnetic nanoparticles in biomedicine. *Journal of Physics D: Applied Physics* **2003,** *36* (13), R167.

78. Shokrollahi, H.; Janghorban, K., Soft magnetic composite materials (SMCs). *Journal of Materials Processing Technology* **2007,** *189* (1), 1-12.

79. Heinze, T.; Siebert, M.; Berlin, P.; Koschella, A., Biofunctional Materials Based on Amino Cellulose Derivatives – A Nanobiotechnological Concept. *Macromolecular Bioscience* **2016,** *16* (1), 10-42.

80. Uthaman, S.; Lee, S.; Cherukula, K.; Cho, C.; Park, I.-K., Polysaccharide-Coated Magnetic Nanoparticles for Imaging and Gene Therapy. *BioMed Research International* **2015,** *2015*, 1-14.

81. Nypelo, T.; Rodriguez-Abreu, C.; Rivas, J.; Dickey, M. D.; Rojas, O. J., Magneto-responsive hybrid materials based on cellulose nanocrystals. *Cellulose* **2014,** *21* (4), 2557-2566.

82. Chang, P. R.; Yu, J.; Ma, X.; Anderson, D. P., Polysaccharides as stabilizers for the synthesis of magnetic nanoparticles. *Carbohydrate Polymers* **2011,** *83* (2), 640-644.

83. Liang, Y. Y.; Zhang, L. M.; Jiang, W.; Li, W., Embedding magnetic nanoparticles into polysaccharide-based hydrogels for magnetically assisted bioseparation. *Chemphyschem* **2007,** *8* (16), 2367-2372.

84. Edlund, U.; Albertsson, A.-C., Degradable Polymer Microspheres for Controlled Drug Delivery. In *Degradable Aliphatic Polyesters*, Springer Berlin Heidelberg: Berlin, Heidelberg, 2002; pp 67-112.

85. Burgess, D. J.; Hussain, A. S.; Ingallinera, T. S.; Chen, M.-L., Assuring quality and performance of sustained and controlled release parenterals: Workshop report. *AAPS PharmSciTech* **2002,** *4* (2), 13-23.

86. Shi, Y.; Li, L., Current advances in sustained-release systems for parenteral drug delivery. *Expert Opinion on Drug Delivery* **2005,** *2* (6), 1039-1058.

87. Burgess, D. J.; Crommelin, D. J. A.; Hussain, A. S.; Chen, M.-L., Assuring quality and performance of sustained and controlled release parenterals: EUFEPS workshop report. *AAPS PharmSciTech* **2004,** *6* (1), 100-111.

88. Bromberg, L. E.; Ron, E. S., Temperature-responsive gels and thermogelling polymer matrices for protein and peptide delivery. *Advanced Drug Delivery Reviews* **1998,** *31* (3), 197-221.

89. Rapoport, N. Y.; Kennedy, A. M.; Shea, J. E.; Scaife, C. L.; Nam, K.-H., Controlled and targeted tumor chemotherapy by ultrasound-activated nanoemulsions/microbubbles. *Journal of controlled release : official journal of the Controlled Release Society* **2009,** *138* (3), 268-276.

90. Sershen, S.; West, J., Implantable, polymeric systems for modulated drug delivery. *Advanced Drug Delivery Reviews* **2002,** *54* (9), 1225-1235.

91. Yuan, Q.; Zhang, Y.; Chen, T.; Lu, D.; Zhao, Z.; Zhang, X.; Li, Z.; Yan, C.-H.; Tan, W., Photon-Manipulated Drug Release from a Mesoporous Nanocontainer Controlled by Azobenzene-Modified Nucleic Acid. *ACS Nano* **2012,** *6* (7), 6337-6344.

92. Deng, Z.; Zhen, Z.; Hu, X.; Wu, S.; Xu, Z.; Chu, P. K., Hollow chitosan–silica nanospheres as pH-sensitive targeted delivery carriers in breast cancer therapy. *Biomaterials* **2011,** *32* (21), 4976-4986.

93. Singh, N.; Karambelkar, A.; Gu, L.; Lin, K.; Miller, J. S.; Chen, C. S.; Sailor, M. J.; Bhatia, S. N., Bioresponsive Mesoporous Silica Nanoparticles for Triggered Drug Release. *Journal of the American Chemical Society* **2011,** *133* (49), 19582-19585.

94. Derfus, A. M.; von Maltzahn, G.; Harris, T. J.; Duza, T.; Vecchio, K. S.; Ruoslahti, E.; Bhatia, S. N., Remotely Triggered Release from Magnetic Nanoparticles. *Advanced Materials* **2007,** *19* (22), 3932-3936.

95. Andrä, W.; Häfeli, U., In *Magnetism in Medicine: A Handbook, Second Edition*, **2007** pp 63-73.

96. Hu, S.-H.; Chen, S.-Y.; Gao, X., Multifunctional Nanocapsules for Simultaneous Encapsulation of Hydrophilic and Hydrophobic Compounds and On-Demand Release. *ACS Nano* **2012,** *6* (3), 2558-2565.

97. Bonini, M.; Berti, D.; Baglioni, P., Nanostructures for magnetically triggered release of drugs and biomolecules. *Current Opinion in Colloid & Interface Science* **2013,** *18* (5), 459-467.

98. Atle, B.; Lars, J., The utility of superparamagnetic contrast agents in MRI: theoretical consideration and applications in the cardiovascular system. *NMR in Biomedicine* **2004,** *17* (7), 465-477.

99. Ludwig, R.; Stapf, M.; Dutz, S.; Müller, R.; Teichgräber, U.; Hilger, I., Structural properties of magnetic nanoparticles determine their heating behavior - an estimation of the in vivo heating potential. *Nanoscale Research Letters* **2014,** *9* (1), 602.

100. Tiwari, S. B.; Murthy, T. K.; Raveendra Pai, M.; Mehta, P. R.; Chowdary, P. B., Controlled release formulation of tramadol hydrochloride using hydrophilic and hydrophobic matrix system. *AAPS PharmSciTech* **2003,** *4* (3), 18-23.

101. Chithaluru, K.; Tadikonda, R.; Gollapudi, R.; Kandula, K. K. K., *Formulation and invitro evaluation of sustained release matrix tablets of losartan potassium*. 2011; Vol. 4, p 18-22.
102. Giani, G.; Fedi, S.; Barbucci, R., Hybrid Magnetic Hydrogel: A Potential System for Controlled Drug Delivery by Means of Alternating Magnetic Fields. *Polymers* **2012,** *4* (2), 1157.
103. Hua, M.-Y.; Liu, H.-L.; Yang, H.-W.; Chen, P.-Y.; Tsai, R.-Y.; Huang, C.-Y.; Tseng, I. C.; Lyu, L.-A.; Ma, C.-C.; Tang, H.-J.; Yen, T.-C.; Wei, K.-C., The effectiveness of a magnetic nanoparticle-based delivery system for BCNU in the treatment of gliomas. *Biomaterials* **2011,** *32* (2), 516-527.
104. Vincent, P.; Claire, W.; Véronique, M.; Christine, M.; Florence, G.; Jack-Michel, R.; Sylviane, L., Anti-Estrogen-Loaded Superparamagnetic Liposomes for Intracellular Magnetic Targeting and Treatment of Breast Cancer Tumors. *Advanced Functional Materials* **2011,** *21* (1), 83-92.
105. Mark, B.; Christine, G.; Adrian, S.; Philip, B.; H., C. J.; Silvio, D.; Steffen, W.; H., S. F., Macromol. Rapid Commun. 4/2017. *Macromolecular Rapid Communications* **2017,** *38* (4).
106. Zhang, F.; Braun, G. B.; Pallaoro, A.; Zhang, Y.; Shi, Y.; Cui, D.; Moskovits, M.; Zhao, D.; Stucky, G. D., Mesoporous Multifunctional Upconversion Luminescent and Magnetic "Nanorattle" Materials for Targeted Chemotherapy. *Nano Letters* **2012,** *12* (1), 61-67.
107. Meng, F.; Zhong, Z.; Feijen, J., Stimuli-Responsive Polymersomes for Programmed Drug Delivery. *Biomacromolecules* **2009,** *10* (2), 197-209.
108. Mahmoudi, M.; Simchi, A.; Imani, M.; Häfeli, U. O., Superparamagnetic Iron Oxide Nanoparticles with Rigid Cross-linked Polyethylene Glycol Fumarate Coating for Application in Imaging and Drug Delivery. *The Journal of Physical Chemistry C* **2009,** *113* (19), 8124-8131.
109. Schild, H. G., Poly(N-isopropylacrylamide): experiment, theory and application. *Progress in Polymer Science* **1992,** *17* (2), 163-249.
110. Mengesha, A. E.; Wydra, R. J.; Hilt, J. Z.; Bummer, P. M., Binary Blend of Glyceryl Monooleate and Glyceryl Monostearate for Magnetically Induced Thermo-Responsive Local Drug Delivery System. *Pharmaceutical Research* **2013,** *30* (12), 3214-3224.
111. Rovers, S. A.; Hoogenboom, R.; Kemmere, M. F.; Keurentjes, J. T. F., Repetitive on-demand drug release by magnetic heating of iron oxide containing polymeric implants. *Soft Matter* **2012,** *8* (5), 1623-1627.
112. Yin, H.; Yu, S.; Casey, P. S.; Chow, G. M., Synthesis and properties of poly(d,l-lactide) drug carrier with maghemite nanoparticles. *Materials Science and Engineering: C* **2010,** *30* (4), 618-623.

113. Kluin, O. S.; van der Mei, H. C.; Busscher, H. J.; Neut, D., Biodegradable vs non-biodegradable antibiotic delivery devices in the treatment of osteomyelitis. *Expert Opinion on Drug Delivery* **2013,** *10* (3), 341-351.
114. Lyu, S.; Untereker, D., Degradability of Polymers for Implantable Biomedical Devices. *International Journal of Molecular Sciences* **2009,** *10* (9), 4033-4065.
115. Guilhem, G.; Thierry, D.; Frédéric, G., Switchable surfaces from highly hydrophobic to highly hydrophilic using covalent imine bonds. *Journal of Applied Polymer Science* **2016,** *133* (11).
116. Sun, T.; Feng, L.; Gao, X.; Jiang, L., Bioinspired Surfaces with Special Wettability. *Accounts of Chemical Research* **2005,** *38* (8), 644-652.
117. Reinhardt, M.; Dzubiella, J.; Trapp, M.; Gutfreund, P.; Kreuzer, M.; Gröschel, A. H.; Müller, A. H. E.; Ballauff, M.; Steitz, R., Fine-Tuning the Structure of Stimuli-Responsive Polymer Films by Hydrostatic Pressure and Temperature. *Macromolecules* **2013,** *46* (16), 6541-6547.
118. Yu, Y.; Ikeda, T., Photodeformable Polymers: A New Kind of Promising Smart Material for Micro- and Nano-Applications. *Macromol Chem Phys* **2005,** *206* (17), 1705-1708.
119. Chen, T.-H.; Chuang, Y.-J.; Chieng, C.-C.; Tseng, F.-G., A wettability switchable surface by microscale surface morphology change. *Journal of Micromechanics and Microengineering* **2007,** *17* (3), 489.
120. Zhou, F.; Huck, W. T. S., Three-stage switching of surface wetting using phosphate-bearing polymer brushes. *Chemical Communications* **2005,** (48), 5999-6001.
121. Verplanck, N.; Coffinier, Y.; Thomy, V.; Boukherroub, R., Wettability Switching Techniques on Superhydrophobic Surfaces. *Nanoscale Research Letters* **2007,** *2* (12), 577.
122. Katz, E.; Sheeney-Haj-Ichia, L.; Basnar, B.; Felner, I.; Willner, I., Magnetoswitchable Controlled Hydrophilicity/Hydrophobicity of Electrode Surfaces Using Alkyl-Chain-Functionalized Magnetic Particles: Application for Switchable Electrochemistry. *Langmuir* **2004,** *20* (22), 9714-9719.
123. Cheng, Z.; Feng, L.; Jiang, L., Tunable Adhesive Superhydrophobic Surfaces for Superparamagnetic Microdroplets. *Advanced Functional Materials* **2008,** *18* (20), 3219-3225.
124. Drotlef, D.-M.; Blümler, P.; Papadopoulos, P.; del Campo, A., Magnetically Actuated Micropatterns for Switchable Wettability. *ACS Applied Materials & Interfaces* **2014,** *6* (11), 8702-8707.
125. Zhang, J. L.; Srivastava, R. S.; Misra, R. D. K., Core−Shell Magnetite Nanoparticles Surface Encapsulated with Smart Stimuli-Responsive Polymer: Synthesis, Characterization, and LCST of Viable Drug-Targeting Delivery System. *Langmuir* **2007,** *23* (11), 6342-6351.

126. Sagar, D. M.; Aoudjane, S.; Gaudet, M.; Aeppli, G.; Dalby, P. A., Optically Induced Thermal Gradients for Protein Characterization in Nanolitre-scale Samples in Microfluidic Devices. *Scientific Reports* **2013,** *3*, 2130.
127. Gräfe, C.; Slabu, I.; Wiekhorst, F.; Bergemann, C.; Eggeling, F. v.; Hochhaus, A.; Trahms, L.; Clement, J. H., Magnetic particle spectroscopy allows precise quantification of nanoparticles after passage through human brain microvascular endothelial cells. *Physics in Medicine & Biology* **2016,** *61* (11), 3986.
128. Odenbach, S., *Colloidal magnetic fluids*. Springer: 2009.
129. Landers, J.; Salamon, S.; Remmer, H.; Ludwig, F.; Wende, H., Simultaneous Study of Brownian and Néel Relaxation Phenomena in Ferrofluids by Mössbauer Spectroscopy. *Nano Letters* **2016,** *16* (2), 1150-1155.
130. Landers, J.; Roeder, L.; Salamon, S.; Schmidt, A. M.; Wende, H., Particle–Matrix Interaction in Cross-Linked PAAm-Hydrogels Analyzed by Mössbauer Spectroscopy. *The Journal of Physical Chemistry C* **2015,** *119* (35), 20642-20648.
131. Laurent, S.; Dutz, S.; Häfeli, U. O.; Mahmoudi, M., Magnetic fluid hyperthermia: Focus on superparamagnetic iron oxide nanoparticles. *Advances in Colloid and Interface Science* **2011,** *166* (1), 8-23.
132. Gonzales-Weimuller, M.; Zeisberger, M.; Krishnan, K. M., Size-dependant heating rates of iron oxide nanoparticles for magnetic fluid hyperthermia. *Journal of magnetism and magnetic materials* **2009,** *321* (13), 1947-1950.
133. Cao, A.; Ye, Z.; Cai, Z.; Dong, E.; Yang, X.; Liu, G.; Deng, X.; Wang, Y.; Yang, S.-T.; Wang, H.; Wu, M.; Liu, Y., A Facile Method To Encapsulate Proteins in Silica Nanoparticles: Encapsulated Green Fluorescent Protein as a Robust Fluorescence Probe. *Angewandte Chemie International Edition* **2010,** *49* (17), 3022-3025.
134. Athanassiou, A.; Lygeraki, M. I.; Pisignano, D.; Lakiotaki, K.; Varda, M.; Mele, E.; Fotakis, C.; Cingolani, R.; Anastasiadis, S. H., Photocontrolled Variations in the Wetting Capability of Photochromic Polymers Enhanced by Surface Nanostructuring. *Langmuir* **2006,** *22* (5), 2329-2333.
135. Jin, M.; Feng, X.; Feng, L.; Sun, T.; Zhai, J.; Li, T.; Jiang, L., Superhydrophobic Aligned Polystyrene Nanotube Films with High Adhesive Force. *Advanced Materials* **2005,** *17* (16), 1977-1981.
136. Junghoon, L.; Bo, H.; Neelesh, A. P., A roughness-based wettability switching membrane device for hydrophobic surfaces. *Journal of Micromechanics and Microengineering* **2005,** *15* (3), 591.

137. Sun, T.; Wang, G.; Feng, L.; Liu, B.; Ma, Y.; Jiang, L.; Zhu, D., Reversible Switching between Superhydrophilicity and Superhydrophobicity. *Angewandte Chemie International Edition* **2004,** *43* (3), 357-360.
138. Park, H.-J.; Zhang, Y.; Georgescu, S. P.; Johnson, K. L.; Kong, D.; Galper, J. B., Human umbilical vein endothelial cells and human dermal microvascular endothelial cells offer new insights into the relationship between lipid metabolism and angiogenesis. *Stem Cell Reviews* **2006,** *2* (2), 93-101.
139. Dutz, S.; Andrä, W.; Hergt, R.; Müller, R.; Oestreich, C.; Schmidt, C.; Töpfer, J.; Zeisberger, M.; Bellemann, M. E., Influence of dextran coating on the magnetic behaviour of iron oxide nanoparticles. *Journal of magnetism and magnetic materials* **2007,** *311* (1), 51-54.

Publication list

- M. Zhou, T. Liebert, R. Müller, A. Dellith, C. Gräfe, J.H. Clement, T. Heinze*, "Magnetic Biocomposites for Remote Melting", Biomacromolecules, 2015, 16, 2308-2315.

- R. Müller, M. Zhou, T. Liebert, J. Landers, S. Salamon, S. Webers, A. Dellith, D. Borin, T. Heinze*, H. Wende, "Mobility Investigations of Magnetic Nanoparticles in Biocomposites", Materials Chemistry and Physics, 2017, 193, 364–370.

- R. Müller, M. Zhou, A. Dellith, T. Liebert, T. Heinze, "Meltable Magnetic Biocomposites for Controlled Release", Journal of Magnetism and Magnetic Materials 2017, 431, 289-293.

- Z. Samuel, M. Zhou, M. A., R. Müller, T. Liebert, T. Heinze, and H. Hamaguchi*, "Determination of Percent Crystallinity of Side-Chain Crystallized Alkylated-Dextran Derivatives with Raman Spectroscopy and Multivariate Curve Resolution", Anal. Chem. 2016, 88, 4644−4650.

- T. Heinze, R. Müller, M. Zhou, M. Rabel, P. Warncke, D. Fischer, "Studies on the Controlled Release of Drugs from Magnetic Nanobiocomposites", Indonesian Journal of Fundamental and Applied Chemistry, 2019, submitted.

Resume

Name:	Mengbo Zhou
Date and place of birth:	4. May 1986 in Guiyang, PR China
Address:	Hohe Str. 34, 01187, Dresden, Germany
Mobile:	0049 152-3734-1759
E-Mail:	zhoumengbo@gmail.com

Working Experience

6/2018 – Now **JIN DUN industrial GmbH**
Sales Manager in EU area

11/2012 – 05/2013 **DELO Industrielle Klebstoffe GmbH & Co. KG**
Technical Trainee in Engneering department

- Technical support on Chinese market with feasibility analysis and implementation of project

07/2010 – 09/2010 **Lohmann GmbH & Co. KG**
Student apprentice in R&D department:

- Modification on an adhesive with thermal conductive fillers for electronics

Education

10/2013 – 12/2017 **Friedrich-Schiller-University Jena**
Ph.D. student in Center of Excellence for Polysaccharide Research

Doctoral thesis: Development and application of a meltable biopolymer based magnetic composite for controlled release of drug.

- Cooperation with 5 partners
- Supervision on a bachelor student
- Talk in European Polysaccharide Network of Excellence 2017 annual Conference, 20-24 August 2017, Jena.

10/2010 – 11/2011 **University of Saarland**
2. years – Joint European Master Program in Advanced Material Science and Engineering
Master thesis: Measurement of crosslinking state on the breakage surface of a PU adhesive

09/2009 – 06/2010 **Luleå University of Technology**
1 year – Joint European Master Program in AMASE.

09/2004 – 06/2008 **Beijing University of Chemical Technology**
Bachelor of Engineering in Polymer Science
Title: Synthesis and analyze of novel polyurethane acrylates for high hardness coating (excellent thesis)

Social Work

08/2015 – 12/2017 Chinese-German Chemical Association (CGCA)

Committee member and local chairman of CGCA east

- Contact with sponsoring parterners (EVONIK, Suzhou Nanopolis, JINDUN Chemical)
- Organisation of conference in 2016 und 2017. (100 participants)

Others

EDP-skills Microsoft Office
Language skill Chinese (Mandarin): native speaker
German: fluent in speaking and writing
English: fluent in speaking and writing

German driving license B and Chinese driving license

Acknowledgement

In the first place I am indebted to my supervisor Prof. Dr. Thomas Heinze for the possibility to prepare my Ph.D. thesis in his group for his constant support, the discussions, and providing good laboratory conditions to make the current work possible.

Moreover, special thanks to Tim Liebert and Peggy Laudeley for the support and I am indebted to Robert Müller from Leibniz Institute of Photonic Technology for the efficient cooperation.

Î appreciated all coworkers of the Center of Excellence for Polysaccharide Research at the Friedrich Schiller University of Jena for the good working atmosphere, german-learning atmosphere and the general support.

For the financial support of my Ph.D. work, I thank the German Science Foundation SPP1681, contracts HE2054/14-1 and HE2054/14-2). Moreover, I thank the European Polysaccharide Network of Excellence (EPNOE) for financing the participation at different international conferences. Special thanks I would like to dedicate to the cooperation partners Joachim Landers and Heiko Wende (University of Duisburg-Essen), Joachim H. Clement and his coworker Christine Gräfe (Jena University Hospital), for the inspiring cooperation and the insights into new methods and scientific fields.

Many thanks also to the employees of the Institute of Organic Chemistry and Macromolecular Chemistry of the Friedrich Schiller University of Jena and Andrea Dellith from Leibniz Institute of Photonic Technology for measuring my samples.

I sincerely thank Prof. Schacher for the preparation of the second review for this Ph.D. thesis.

Last but not least I thank my friends, my family, in particular my wife Fei Xiang for their support also beyond the Ph.D. work.

Selbständigkeitserklärung

Ich erkläre, dass ich die vorliegende Arbeit selbstständig und unter Verwendung der angegebenen Hilfsmittel, persönlichen Mitteilungen und Quellen angefertigt habe. Sie wurde weder im Ganzen noch in Teilen an dieser oder einer anderen Universität zur Erlangung des akademischen Grades Doktor-rerum naturalium (Dr. rer. nat.) vorgelegt.

Jena, den

Unterschrift